



**HSB**  
Hochschule Bremen  
City University of Applied Sciences



Fakultät 2 - Architektur, Bau und Umwelt  
Zukunftsfähige Energie- und Umweltsysteme M.Eng.

Master's Thesis

# GIS-based workflow for identifying renewable heat potentials and an optimal strategy for LowEx district heating

Summer Semester 2024

First examiner and supervisor:	Prof. Dr. Jürgen Knies
Second examiner:	Prof. Dr. Thomas Kumm
Submitted by:	Novi Vania Sari Pujianto
Mat. Number:	5015385
Date of Submission:	25 May 2024

## Declaration of independent preparation of work

I hereby certify that I have written this thesis independently and have not used any sources or aids other than those indicated. The passages in the work that have been taken from other works in terms of wording or meaning are indicated by the source.

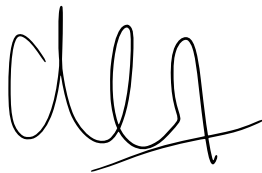
This declaration also applies to graphics, sketches and illustrations contained in the thesis as well as to sources from the Internet.

I have not yet submitted the work in the same or similar form, even in part, as part of an examination or course assignment.

I certify that the submitted electronic version of the work is completely consistent with the print version.

Novi Pujiyanto

5015385

A handwritten signature in black ink, appearing to read 'Novi Pujiyanto', with a horizontal line underneath the final part of the signature.

Bremen, 25 May 2024

## Abstract

To reach climate protection goals, Germany aims to significantly reduce emissions through the heat transition. Providing renewable heat sources in urban areas presents one of the greatest challenges due to the limited space, yet high energy demand. This thesis addresses the issue by creating a workflow based on GIS (Geographic Information Systems) to quickly identify so-called “sub-areas” where low temperature (LowEx) district heating could be suitable. The heating concept shall connect sources of shallow geothermal energy within an observed area and enable a more effective distribution of heat. Photovoltaics (PV) on roofs as well as parking lots shall counter the increased power demand of the decentralized heat pumps. The workflow involves estimations of annual technical potentials and the identification of sub-areas using ArcGIS Pro, Polysun, and Earth Energy Designer. This was created based on and applied to the district of Neu-Schwachhausen, Bremen. Scenarios (S) of 2022, 2030, 2038-a, and 2038-b were observed, varying the availability of the selected technologies (borehole heat exchanger and PV) and the level of heat demand for space and water heating. The sub-areas were evaluated regarding overall quality based on selected criteria. Results show that such a concept of LowEx DH is the ideal heating strategy for the district if the circumstances in S-2038-b can be achieved. Most neighborhoods would be technically suitable, especially due to the 300 m deep boreholes and heat demand reductions. Considering the cumulated values, the required power for heat pumps could be covered by PV alone in many of the areas, underlining the necessity of efficient energy storage in reality. Solar parking lots have a less substantial impact overall compared to roof potentials, though a detailed feasibility study is recommended to confirm this. This thesis also shows the importance of sharing local sources between neighborhoods, in addition to using large sports fields, to efficiently maximize area usage. Prioritizing these elements would lead to higher energy self-sufficiency in the sub-areas. In further research, the workflow can be extended by adding an economic parameter, seasonal fluctuations, and improved automation.

## Zusammenfassung

Um die Klimaschutzziele zu erreichen, will Deutschland die Emissionen durch die Wärmewende weitgehend reduzieren. Die Bereitstellung erneuerbarer Wärmequellen stellt in städtischen Gebieten aufgrund des begrenzten Raums, aber des hohen Energiebedarfs, eine der größten Herausforderungen dar. In dieser Arbeit wird ein auf GIS (Geographische Informationssysteme) basierender Workflow zur schnellen Ermittlung von sogenannten „Sub-Areas“ (Teilgebiete) entwickelt, in welchen Niedertemperaturnetze (LowEx) geeignet sein könnten. Das Wärmekonzept soll Quellen oberflächennaher Geothermie innerhalb eines betrachteten Gebietes verbinden und eine effektivere Verteilung der Wärme ermöglichen. Photovoltaik (PV) auf Dächern und Parkplätzen soll dem erhöhten Strombedarf der dezentralen Wärmepumpen entgegenwirken. Der Workflow umfasst Abschätzungen der jährlichen technischen Potenziale und die Bestimmung von Sub-Areas mit ArcGIS Pro, Polysun und Earth Energy Designer. Dieser wurde auf Basis des Quartiers Neu-Schwachhausen in Bremen erstellt und angewendet. Es wurden die Szenarien (S) 2022, 2030, 2038-a und 2038-b betrachtet, in denen die Verfügbarkeit der ausgewählten Technologien (Erdwärmesonden und PV) und der Wärmebedarf für Raumheizung und Warmwasser variiert wurden. Die Teilgebiete wurden hinsichtlich der Gesamtqualität anhand ausgewählter Kriterien bewertet. Die Ergebnisse zeigen, dass ein solches LowEx-Wärmenetzkonzept für das Quartier die ideale Heizstrategie ist, wenn die Bedingungen in S-2038-b erreicht werden können. Die meisten Gebiete wären dafür technisch geeignet, insbesondere aufgrund der 300 m tiefen Bohrungen und der Wärmebedarfsreduzierung. Betrachtet man die kumulierten Werte, so könnte die erforderliche Leistung für Wärmepumpen in vielen Gebieten allein durch PV gedeckt werden, was bedeutet, dass eine effiziente Energiespeicherung in der Realität unerlässlich wäre. PV-Parkplätze haben generell im Vergleich zu bestehenden Dächern einen wesentlich geringeren Einfluss. Eine detaillierte Machbarkeitsstudie wird jedoch empfohlen, um dies zu bestätigen. Zudem zeigt diese Arbeit, wie relevant die gemeinsame Nutzung lokaler Wärmequellen und zusätzlich die Verwendung großer Sportplätze ist, damit Flächen möglichst effektiv genutzt werden. Die Priorisierung dieser würde zu einer höheren Energieautarkie in den Sub-Areas führen. In weiteren Forschungsarbeiten kann der Workflow durch Hinzufügen eines wirtschaftlichen Parameters, saisonaler Schwankungen und einer verbesserten Automatisierung erweitert werden.

## Table of Contents

<b>1. Introduction.....</b>	<b>1</b>
1.1. <i>Background.....</i>	1
1.2. <i>Study Purpose and Objectives.....</i>	2
<b>2. State of the Art.....</b>	<b>3</b>
2.1. <i>Shallow Geothermal Energy.....</i>	3
2.2. <i>Photovoltaics.....</i>	6
2.3. <i>District Heating.....</i>	8
2.4. <i>Related Works.....</i>	11
<b>3. Description of the Study Area.....</b>	<b>12</b>
<b>4. Methodology.....</b>	<b>14</b>
4.1. <i>Geodata collection.....</i>	16
4.2. <i>Processing Heat Demand Data.....</i>	17
4.3. <i>Potential Analysis of Shallow Geothermal Energy.....</i>	18
4.3.1. <i>Potential Area Scan using ModelBuilder.....</i>	18
4.3.2. <i>Soil Thermal Conductivity.....</i>	20
4.3.3. <i>EED Simulation.....</i>	22
4.3.4. <i>Potential Estimation and Applicability Test.....</i>	23
4.4. <i>Potential Analysis of Solar Energy.....</i>	24
4.4.1. <i>Classifying Potential Roofs.....</i>	24
4.4.2. <i>Potential of Solar Parking Lots.....</i>	26
4.4.3. <i>Polysun Simulation and Grouped Calculations.....</i>	27
4.5. <i>Creation of Sub-Areas.....</i>	29
4.6. <i>Evaluation of Sub-Areas.....</i>	31
<b>5. Results.....</b>	<b>33</b>
5.1. <i>Shallow Geothermal Energy Potential.....</i>	33
5.2. <i>Solar Energy Potential.....</i>	42
5.3. <i>Scenario Outcomes.....</i>	47
5.3.1. <i>Heat and Power Demand.....</i>	47
5.3.2. <i>Energy Potential and Demand Gap.....</i>	49

5.3.3. Sub-Areas for LowEx District Heating .....	53
5.3.4. Evaluation.....	56
<b>6. Discussion .....</b>	<b>57</b>
6.1. <i>LowEx District Heating Strategy</i> .....	57
6.2. <i>Workflow Assessment</i> .....	63
<b>7. Conclusion and Outlook .....</b>	<b>67</b>
<b>References.....</b>	<b>68</b>
<b>List of Appendices .....</b>	<b>72</b>

## List of Figures

Figure 1: An example of shallow geothermal energy use in a single-family home. 1A- closed-loop probe (BHE); 1B- Horizontal collector; 1C- open-loop probe; 2- Heat pump; 3- Heat sink e. g. floor heating and shower. (Hajto et al., 2019) .....	4
Figure 2: Solar energy orientation chart of Germany (SAENA GmbH, 2023) .....	7
Figure 3: Difference between district heating with centralized and decentralized heat pumps (LowEx) (BWP, 2022) .....	9
Figure 4: View of Neuschwachhausen with seven characteristic areas (Map: DOP10, © GeoBasis-DE / Landesamt GeoInformation Bremen 2023) .....	12
Figure 5: The workflow created and applied to identify possible LowEx sub-areas .....	14
Figure 6: Close-up view of heat demand data (DBI) stored in building-specific points as an example.....	17
Figure 7: A view of the first section of “GeothermalPot” in ModelBuilder, which identifies the exclusion zones and potential areas for BHEs.....	19
Figure 8: A view of the second section of “GeothermalPot” in ModelBuilder, which excludes small polygons of potential areas and generates random points as boreholes .....	20
Figure 9: The distribution of mean soil thermal conductivity across Neu-Schwachhausen at 100 m depth according to GdFB .....	21
Figure 10: Close-up view of the displayed solar cadastre as an example .....	25
Figure 11: Identified potential sites for solar parking lots in A, B, C, and D. (Map: DOP10, © GeoBasis-DE / Landesamt GeoInformation Bremen 2023) .....	27
Figure 12: Example of an observed grid cell (G), its direct neighbors (N), and its non-direct neighbors (here: yellow hatched cells).....	30
Figure 13: Example of the identification process of sub-areas (here: outlined blue) – Heat suppliers (G1, G2, and G3) shall distribute heat to suitable heat receivers among direct neighbors (N) (here: flow is marked with arrows).....	30
Figure 14: Potential areas for BHEs in Neu-Schwachhausen.....	34
Figure 15: Close-up view of several of the defined exclusion zones for BHEsn (Map: DOP10, © GeoBasis-DE / Landesamt GeoInformation Bremen 2023) .....	34
Figure 16: Comparison of possible borehole locations with 100 m depth (left) and 300 m depth (right).....	35

Figure 17: Technical potential of shallow geothermal energy in the scenarios S-2022 (top) and S-2030 (bottom) clustered in grid cells.....	38
Figure 18: Technical potential of shallow geothermal energy in the scenarios S-2038-a (top) and S-2038-b (bottom) clustered in grid cells .....	39
Figure 19: Statistical distribution of BHEs per grid cell in 100 m and 300 m depth.....	40
Figure 20: Deviation in sampled grid cells in terms of heat potential and BHE number .....	41
Figure 21: Proportions of PV sub-categories in the total technical potential .....	44
Figure 22: Technical potential of solar energy in S-2022 (top) and S-2030 (bottom) clustered in grid cells .....	45
Figure 23: Technical potential of solar energy in S-2038-a and S-2038-b clustered in grid cells .....	46
Figure 24: Heat demand distribution in S-2022 (top) and S-2030 (bottom) clustered in grid cells .....	48
Figure 25: Heat demand distribution in S-2038-a and -b .....	49
Figure 26: Geothermal potential and heat demand in comparison to solar energy potential and power demand in S-2022 (top) and S-2030 (bottom) clustered in grid cells .....	51
Figure 27: Geothermal potential and heat demand in comparison to solar energy potential and power demand in S-2038-a (top) and S-2038-b (bottom) clustered in grid cells.....	52
Figure 28: LowEx sub-areas in S-2022 (top) and S-2030 (bottom) ranked by their suitability .....	54
Figure 29: LowEx sub-areas in S-2038-a (top) and S-2038-b (bottom) ranked by their suitability .....	55
Figure 30: Comparison between densely (left) and sparsely built neighborhoods (right) .....	59
Figure 31: Effect of PV installation on ESE-oriented roofs on the power gap as observed from S-2022 (left) to S-2030 (right) .....	60



## List of Tables

Table 1: Overview of the four scenarios with the defined settings for heat generation and demand .....	15
Table 2: List of used geodata .....	16
Table 3: Excluded areas for BHEs and the source of the geodata.....	19
Table 4: Estimation of mean soil thermal conductivity (STC) at 100 m and 300 m based on the sampling report from the GDfB .....	21
Table 5: Fixed parameters of ground data, borehole properties, and U-pipe properties applied in all four simulations.....	22
Table 6: Exemplary set of simulations to be conducted in EED for one scenario to estimate the geothermal heat generation. ....	23
Table 7: Subcategories for pitched and flat roofs based on the aspect and slope .....	26
Table 8: Additional subcategories for solar parking lots based on the aspect values. ....	26
Table 9: PV module configuration chosen in all simulations .....	27
Table 10: Classification of LowEx suitability levels (SL) applied to “heat suppliers” and “heat receivers” .....	31
Table 11: Summary of the selected criteria and their weighting factors .....	32
Table 12: Simulation results from EED for the scenarios S 2022, S 2030, S 2038-a (depth 100 m) and S 2038-b (depth 300 m). ....	36
Table 13: Summary of the total technical potential of shallow geothermal energy.....	37
Table 14: Results of the plausibility check compared to the estimated max. potentials in 100 m depth .....	40
Table 15: Simulation results from Polysun .....	42
Table 16: Summary of the total technical potential of solar energy.....	43
Table 17: Overview of the observed heat and power demand in all scenarios .....	47
Table 18: Number of grid cells with heat and power surplus out of the observed 84 in all scenarios.....	49
Table 19: Numbers for the quantitative evaluation of the sub-areas and the results .....	56
Table 20: Evaluation of the sub-areas in all scenarios using a scale of 1 (very low) to 5 (very high) .....	56

## List of Legal and Regulatory Frameworks

### Technical Standards

VDI 4640 Part 1:2010-06 Thermal use of the underground; Fundamentals, approvals, environmental aspects. Berlin: Beuth Verlag

VDI 4640 Part 2:2019-06 Thermal use of the underground; Ground source heat pump systems. Berlin: Beuth Verlag

### International Treaties

Doha Amendment to the Kyoto Protocol, December 21, 2012

Kyoto Protocol to the United Nations Framework Convention on Climate Change, December 10, 1997

### Federal and Regional Laws

*Bremische Landesbauordnung* (Bremen State Building Code) in the revised version of October 18, 2022 (Brem.GBl. p. 603) – BremLBO –

*Bremisches Denkmalschutzgesetz* (Bremen Monument Protection Act) in the revised version of December 18, 2018 (Brem.GBl. 2018, p. 631) – BremDSchG –

*Bremisches Solargesetz* (Bremen Solar Energy Act) of May 2, 2023 (Brem.GBl. I No. 71) – BremSolarG –

*Bremisches Wassergesetz* (Bremen Water Act) of April 12, 2011 (Brem.GBl. p. 262), last amended by Article 6 No. 5 of the Act of November 24, 2020 (Brem.GBl. pp. 1486, 1581) – BremWG –

*Bundes-Klimaschutzgesetz* (Federal Climate Protection Act) of December 12, 2019 (BGBl. I p. 2513), amended by Article 1 of the Act of August 18, 2021 (BGBl. I p. 3905) – KSG –

*Bundesberggesetz* (Federal Mining Act) of August 13, 1980 (BGBl. I p. 1310), last amended by Article 4 of the Act of March 22, 2023 (BGBl. 2023 I No. 88) – BBergG –

*Gebäudeenergiegesetz* (Building Energy Act) of August 8, 2020 (BGBl. I p. 1728), last amended by Article 1 of the Act of October 16, 2023 (BGBl. 2023 I No. 280) – GEG –

*Standortauswahlgesetz* (Repository Site Selection Act) of May 5, 2017 (BGBl. I p. 1074), last amended by Article 8 of the Act of March 22, 2023 (BGBl. 2023 I No. 88) – StandAG –

*Wärmeplanungsgesetz* (Heat Planning Act) of December 20, 2023 (BGBl. 2023 I No. 394) – WPG –

*Wasserhaushaltsgesetz* (Federal Water Act) of July 31, 2009 (BGBl. I p. 2585), last amended by Article 7 of the Act of December 22, 2023 (BGBl. 2023 I No. 409) – WHG –

## List of Abbreviations

ALKIS	<i>Amtliches Liegenschaftskatasterinformationssystem</i>
AGFW	<i>Arbeitsgemeinschaft Fernwärme</i>
BbergG	<i>Bundesberggesetz (Federal Mining Act)</i>
BDEW	<i>Bundesverband der Energie- und Wasserwirtschaft e.V.</i>
BEG	<i>Bundesförderung für effiziente Gebäude</i>
BEW	<i>Bundesförderung für effiziente Wärmenetze</i>
BHE	borehole heat exchanger
BKG	<i>Bundesamt für Kartographie und Geodäsie</i>
BMWK	<i>Bundesministerium für Wirtschaft und Klimaschutz</i>
BremDSchG	<i>Bremisches Denkmalschutzgesetz (Bremen Monument Protection Act)</i>
BremLBO	<i>Bremische Landesbauordnung (Bremen State Building Code)</i>
BremSolarG	<i>Bremisches Solargesetz (Bremen Solar Energy Act)</i>
BremWG	<i>Bremisches Wassergesetz (Bremen Water Law)</i>
CO <sub>2</sub>	carbon dioxide
DBI GUT	DBI Gas- und Umweltechnik GmbH
DH	district heating
DOP	Digital Orthophoto
DWD	<i>Deutscher Wetterdienst</i>
EC	European Commission
EED	Earth Energy Designer
ESE	East-South-East
FR	flat roof
GDfB	<i>Geologischer Dienst für Bremen (Geological Survey of Bremen)</i>
GEG	<i>Gebäudeenergiegesetz (Building Energy Act)</i>
GHG	greenhouse gas
GIS	geographic information system

GWp	giga watt peak
KSG	<i>Bundes-Klimaschutzgesetz (Federal Climate Change Act)</i>
kWp	kilowatt peak
LfU	<i>Bayerisches Landesamt für Umwelt</i>
MWp	megawatt peak
PL NE	parking lot, North-East
PL SW	parking lot, South-West
PV	photovoltaic
S	scenario
SL	suitability level
SLB	<i>Statistisches Landesamt Bremen</i>
SPF	seasonal performance factor
SSE	South-South-East
SSW	South-South-West
StandAG	<i>Standortauswahlgesetz (Repository Site Selection Act)</i>
STC	soil thermal conductivity
SUKW	<i>Senatorin für Umwelt Klima und Wissenschaft</i>
UBA	<i>Umweltbundesamt</i>
UBB	<i>Umweltbetrieb Bremen</i>
UMBW	<i>Umweltministerium Baden-Württemberg</i>
VBA	Visual Basic for Application
VDI	<i>Verein Deutscher Ingenieure e. V.</i>
WHG	<i>Wasserhaushaltsgesetz (Federal Water Act)</i>
WMS	Web Map Service
Wp	watt peak
WPG	<i>Wärmeplanungsgesetz (Heat Planning Act)</i>
WSW	West-South-West
WWNW	WärmewendeNordwest

## 1. Introduction

One of the greatest challenges facing humanity today is to transform modern societies in the way of life and to facilitate them with essential infrastructure in order to mitigate climate change. The reduction of greenhouse gas (GHG) emissions is considered a promising measure for long-term climate protection and has been set as a goal for industrialized nations including the European Union. With the nationwide “heat transition” (German: *Wärmewende*), Germany prepares to take its responsibility to a high level.

### 1.1. Background

The commitment made in the Kyoto Protocol was to reduce carbon dioxide (CO<sub>2</sub>) along with other GHG emissions by at least 5% and 18% compared to the pre-1990 level by 2012 and 2020, respectively (Article 3 of the Kyoto Protocol 1997; Article 1 of the Doha Amendment 2012). The EU then agreed to further decrease its emissions by at least 55% by 2030 to meet the target set in the Paris Agreement of 2016 (EC, 2020). With the Federal Climate Change Act (*Bundes-Klimaschutzgesetz*, “KSG”), Germany has specified its goal of transforming towards a carbon-free nation by 2045 with the energy transition (§ 3 KSG). As a city-state, the Free Hanseatic City of Bremen has shortened its target with the more ambitious Climate Protection Strategy 2038 (*Bremen Klimaschutzstrategie 2038*) amid the intensifying climate and energy crises.

Germany’s GHG emissions are predominantly caused by fossil fuel combustion for energy and transportation (UBA, 2024b). The trend of using renewable energy sources has been positive in recent years with electricity, measured by the final energy consumption, reaching a significant proportion at 51.8% in 2023, marking a big leap of above 5% from 2022. However, for heating the fraction is still much lower at 18.8%, which is dominated by biomass (UBA, 2024a). This matter leaves a high improvement potential in producing sustainable thermal energy for a successful heat transition, especially in urban areas in which a tight competition for land and resources exists. In accordance, several national laws have recently become effective, including the Building Energy Act (*Gebäudeenergiegesetz*, “GEG”), which regulates the implementation of emission-free heating and cooling technologies (e.g. shallow geothermal energy, air source heat pump, solar thermal energy) as well as standards for building insulation, and the Heat Planning Act (*Wärmeplanungsgesetz*, “WPG”), which aims to ensure that climate neutrality in district heating is achieved by 2045. The dynamic political circumstances are highly relevant for energy suppliers, consumers, local planning authorities, and research groups in the search for better heating solutions with renewable sources.

## 1.2. Study Purpose and Objectives

The presented study is conducted with the assistance of Research Area 5 (*Forschungsfeld 5*) of the group WärmewendeNordwest (WWNW), which addresses the challenges of the heat transition by developing modern solutions for district heat grids. This thesis intends to contribute with an adequate workflow that shall ease in creating a sustainable heating strategy for urban areas. The strategy should prioritize the use of local renewable energy potentials for heating and any power supplement.

The focus here is placed on the concept of low-temperature (LowEx) district heating. Shallow geothermal energy shall be investigated as the potential heat source and solar energy as the power source, due to their abundance and accessibility in a typical urban environment. Finding a possible way for sustainable power generation is essential since such systems involve heightened electricity demand. To provide a clear direction for the workflow and limit the extent of this research, only the combination of the two technologies is explored. The district Neu-Schwachhausen in Bremen, Germany, is selected as the study area.

Therefore, the following questions shall be investigated:

### **1<sup>st</sup> Research Question**

How can geothermal and solar energy potentials in a selected urban district be identified and estimated to provide a foundation for detailed planning?

### **2<sup>nd</sup> Research Question**

Which heat supply strategies are adequate for the district Neu-Schwachhausen, Bremen, differentiated spatially and temporally considering the development of energy efficiency in buildings and local renewable heat sources?

To properly clarify these questions, a workflow using geographic information systems (GIS) is developed, that should ideally be applicable in other urban areas as well. It begins with identifying shallow geothermal and solar energy potentials within the study area. Scenarios of district heating are created, considering the availability of the technologies and presumed heat demand in the current and future state until 2038, in which climate neutrality in Bremen should be achieved. Suitable areas for the defined concept of district heating are identified and assessed using an evaluation method. Finally, an optimal heating strategy for Neu-Schwachhausen is proposed. Both the suggested workflow and heating strategy shall provide a new perspective, widen the spectrum of possibilities, and ultimately serve their purpose of guiding further research and technical planning procedures on a district level.

## 2. State of the Art

To address the research problem, it is necessary to comprehend the technical and legal aspects of the examined technologies. This chapter covers the relevant technicalities and current standards and regulations regarding shallow geothermal energy, solar energy, and district heating (DH), regarding their usage in urban areas. Finally, several related works that influence the aim and methodology of the study are summarized.

### 2.1. Shallow Geothermal Energy

#### Technical Principles

Geothermal energy is an abundant resource that arises from the natural heat of the earth's core and absorbed solar radiation in the near-surface region. The exothermic reaction in the earth's core allows constant heat regeneration, making it an abundant and optimal source of renewable energy. The stored energy can be extracted directly for heating or electricity generation. Here, two main categories are distinguished based on the depth of the source and temperature range: "shallow geothermal energy" refers to the energy extraction from up to 400 m below ground surface, and "deep geothermal energy" exploits the heat at depths greater than 400 m, though often executed at more than 1000 m (Panteleit et al., 2022). Both forms differ in the purpose, technical implementation, and legal requirements. While its high thermal capacity makes deep geothermal energy optimal for large-scale DH and power generation, shallow geothermal energy's lower capacity range is unsuitable for this purpose but is much more technically and economically accessible (García Gil et al., 2022a). Therefore, the latter is ideal for providing space and water heating to both individual buildings and districts.

In shallow geothermal energy, the ground temperature usually does not exceed 25°C. The heat is extracted through loop collectors of various forms, which can be installed horizontally or vertically as geothermal probes (Stober & Bucher, 2020b). For all variants the efficiency of the system highly depends on the rock or soil type and, in the case of probes, the filling material between the collector and soil. Their thermal properties are fundamental, including the soil thermal conductivity (STC) (W/mK) and the volumetric heat capacity (J/Km<sup>3</sup>), which is based on the ground porosity (Dickinson et al., 2009). Generally, higher moisture content and material density result result in higher STC, ensuring greater energy transfer. Meanwhile, higher porosity leads to the opposite (García Gil et al., 2022c; Stober & Bucher, 2020c).

Horizontal ground collectors consist of up to a 100 m long heat exchanger and are typically inserted just around 1 - 2 m below the surface. These take advantage of the heat stored from solar radiation as well as ambient conditions (Stober & Bucher, 2020b). On the other hand,

geothermal probes can be inserted up to 400 m underground and make use of the stable temperature of 10 - 20°C in the rocks and aquifer. This is because in greater depths the heat largely depends on the energy released from the earth's core, also called the geothermal heat flux ( $W/m^2$ ). The phenomenon is defined as the geothermal gradient of 3 K per 100 m beginning at about 15 - 20 m below ground (Panteleit et al., 2022; Schiel et al., 2016). The probes can be realized in an open-loop system, which utilizes groundwater as the direct heat carrier, or a closed-loop system, also known as a borehole heat exchanger (BHE), in which a heat carrier fluid is pumped in a cycle. Two tubes are typically inserted in a BHE, forming a so-called "double U pipe" (García Gil et al., 2022b).

With either horizontal or vertical collectors, the heat exchanger leads to a heat pump that is typically connected to a storage tank in the target building, as illustrated in Figure 1. Electric heat pumps are required to achieve the target temperature, for example for space and domestic water heating. Efficiency is a crucial factor that is typically expressed in its seasonal performance factor (SPF), which is the average coefficient of performance over a heating period. Hence, this value indicates the mean ratio of heat output over electrical input. Ground source heat pumps with a minimum SPF of 4 are considered efficient and are usually recommended (Panteleit et al., 2022).

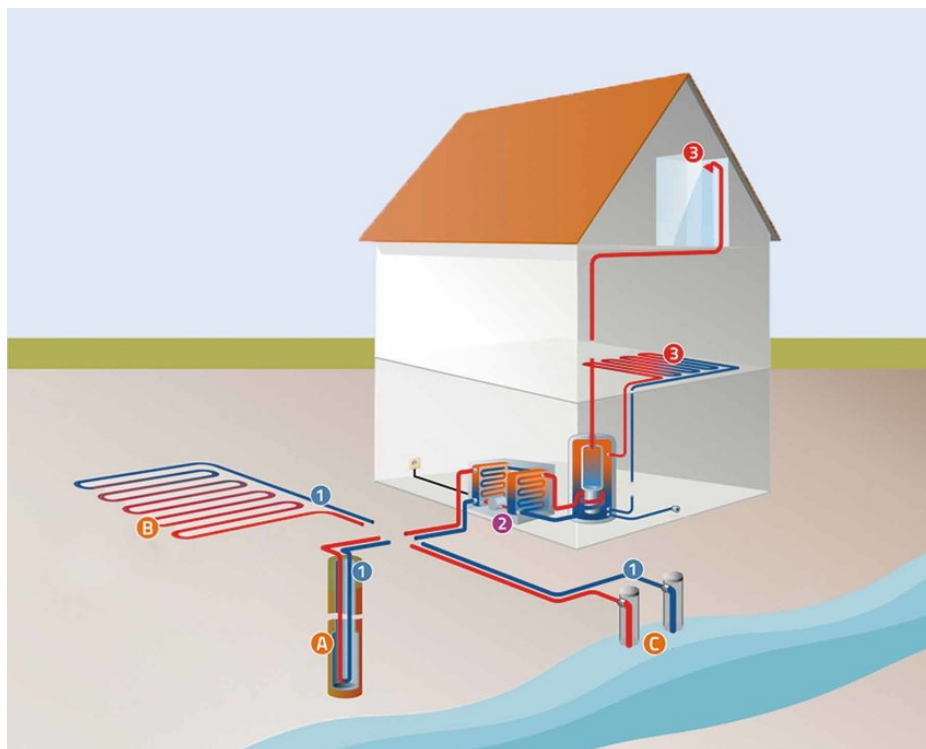


Figure 1: An example of shallow geothermal energy use in a single-family home. 1A- closed-loop probe (BHE); 1B- Horizontal collector; 1C- open-loop probe; 2- Heat pump; 3- Heat sink e. g. floor heating and shower. (Hajto et al., 2019)



Geothermal probes are the optimal technology for shallow geothermal energy in urban areas because of the efficient use of space. However, high initial investment costs for drilling and installation are expected, for example at around 70 €/m for BHEs (Bockelmann et al., 2019). Yet, in contrast to other renewables such as air source heat pumps or solar thermal energy, operational costs of geothermal energy are lower, making it seemingly attractive on the market (Hajto et al., 2019).

### Standards and Regulations

The installation of shallow geothermal energy in Germany is less complicated with horizontal collectors in terms of bureaucracy as it does not require a permit unless groundwater is affected. Geothermal probes are to be installed with approval according to local and federal water law and, if applicable, also mining law. In Bremen, provisions in the Federal Water Act (*Wasserhaushaltsgesetz*, “WHG”) and the Bremen Water Act (*Bremisches Wassergesetz*, “BremWG”) are to be compiled before and after installation. If an installation in a water protection area is planned, certain restrictions also apply according to the regulations of the protection area (Panteleit et al., 2022).

The Federal Mining Act (*Bundesberggesetz*, “BBergG”) regulates heat extraction from underground as it is stated that geothermal energy shall be treated as mineral resources (§ 3 (3) no. 2b BBergG). Therefore, approval for borehole depths of more than 100 m is necessary according to § 7 BBergG, and the procedure is to be notified to the regional mining authority and additional requirements might arise. Also, in case the drilling site was determined as a potential nuclear disposal site in the Repository Site Selection Act (*Standortauswahlgesetz*, “StandAG”), an additional approval process according to § 21 StandAG is required.

Relevant standards and technical guidelines for Germany regarding fundamentals, planning, approvals, and operation can be found in VDI (*Verein Deutscher Ingenieure e.V.*) 4640 Part 1 and 2. To obtain a permit, several conditions related to the site and operation must be met. Distance restrictions for probes include 2 m to buildings, 0.5 m to public streets, and 3 - 5 m to cadastral boundary for private usage. A specific distance to various underground pipelines (such as wastewater pipes, gas pipes, etc.) is to be held as well. The VDI suggests borehole spacing of at least 6 m for depths above 50 m to reduce geothermal interference between the probes. Grouting material in boreholes must also be 30 mm thick (LfU, 2012; Panteleit et al., 2022). Furthermore, the mean fluid temperature will decrease during its lifetime due to the gradual heat removal until it stabilizes. To prevent over-extraction of ground heat, a 50-year simulated prognosis of the fluid temperature must be submitted to guarantee that the return temperature ( $T_{\text{return}}$ ) is maintained above 0°C (VDI 4640 Section 2) on a monthly average and above -3°C at any time during its whole lifetime (Panteleit et al., 2022).

## 2.2. Photovoltaics

### Technical Principles

Photovoltaics (PV) convert solar energy to electricity by capturing sunlight in a solar cell, made of a combined (negative) n-type and (positive) p-type semiconductor. Once absorbed, the radiation excites electrons and forms electron-hole pairs in the material. The electrons (negatively charged) travel to the p-type side while their holes (positively charged) move to the n-type side, therefore creating an electric field (Boyle, 2012). These cells are connected to form a larger unit usually with an area of around 1.5 m<sup>2</sup>, referred to as a PV module. The electric power from the module is generated in direct current, so an inverter is vital to convert it to alternating current for electronic devices, battery storage, or grid integration (Kaushika et al., 2018a).

Several PV technologies are distinguishable by design, material, and purpose. The most popular type remains solar modules consisting of cells out of wafer-based crystalline silicon (Taylor & Jäger-Waldau, 2020). The typical efficiency of new modules in standardized conditions (1000 Wp/m<sup>2</sup>, solar irradiance at 25°C) currently reaches 21% (Wirth & ISE, 2023). Silicon-based PV is typically differentiated into monocrystalline and polycrystalline modules. The former has almost absolute silicon purity, which offers a higher efficiency at 5 - 7%, making it technically superior to polycrystalline, but therefore more expensive (Kaushika et al., 2018b). However, module prices in general have been plummeting since the emergence of the technology. The decrease from 2010 to 2020 was as much as 90%, and this trend is expected to continue in the long term provided that the production rate still increases with time (Wirth & ISE, 2023).

The power output is a function of solar irradiance and module area. Although diffuse rays contribute to energy generation, direct beams have a greater effect. Maximum system efficiency is gained by capturing as much direct beam as possible throughout the year. In Germany, this means positioning the modules towards the south at about a 30° - 40° tilt angle. The larger the deviation from the optimal aspect and inclination, the less energy yield is expected (SAENA GmbH, 2023). This also applies to the thermal output of solar thermal collectors, which are typically used for domestic hot water and space heating (Schabbach & Leibbrandt, 2021). Figure 2 shows a solar energy orientation chart, which gives an overview of the expected yield of various PV aspects and inclinations compared to the optimal position. Automated tracking systems are usually found in solar parks to maximize efficiency and boost annual production up to 30% (Wirth & ISE, 2023). A larger proportion of diffuse rays, for example by simple cloudy conditions, can also drastically reduce technical efficiency (Page, 2018). A result is that, with Germany's less optimal weather conditions, power production very

rarely reaches above 65% of the installed capacity. In Bremen, the annual sunshine duration is 1545 h/a (DWD, 2021) and the specific yield lies at 922 kWh/kWp (Wirth & ISE, 2023).

Modulneigung in Grad	Modulabweichung von Süden in Grad																		
	Süd				Südwest Südost				West Ost				Nordwest Nordost				Nord		
	0	10	20	30	40	50	60	70	80	90	100	110	120	130	140	150	160	170	180
0°	87%	87%	87%	87%	87%	87%	87%	87%	87%	87%	87%	87%	87%	87%	87%	87%	87%	87%	87%
10°	93%	93%	93%	92%	92%	91%	90%	89%	88%	86%	85%	84%	83%	81%	81%	80%	79%	79%	79%
20°	97%	97%	97%	96%	95%	93%	91%	89%	87%	85%	82%	80%	77%	75%	73%	71%	70%	70%	70%
30°	100%	99%	99%	97%	96%	94%	91%	88%	85%	82%	79%	75%	72%	69%	66%	64%	62%	61%	61%
40°	100%	99%	99%	97%	95%	93%	90%	86%	83%	79%	75%	71%	67%	63%	59%	56%	54%	52%	52%
50°	98%	97%	96%	95%	93%	90%	87%	83%	79%	75%	70%	66%	61%	56%	52%	48%	45%	44%	43%
60°	94%	93%	92%	91%	88%	85%	82%	78%	74%	70%	65%	60%	55%	50%	46%	41%	38%	36%	35%
70°	88%	87%	86%	85%	82%	79%	76%	72%	68%	63%	58%	54%	49%	44%	39%	35%	32%	29%	28%
80°	80%	79%	78%	77%	75%	72%	68%	65%	61%	56%	51%	47%	42%	37%	33%	29%	26%	24%	23%
90°	69%	69%	69%	67%	65%	63%	60%	56%	53%	48%	44%	40%	35%	31%	27%	24%	21%	19%	18%

Figure 2: Solar energy orientation chart of Germany (SAENA GmbH, 2023)

In 2022, PV contributed to 10.4% of Germany's gross electricity generation with 67.4 GWp of installed capacity (BDEW, 2023), of which the largest fraction is from common usage on roofs (Wirth & ISE, 2023). Integrated PV in urban areas will be enforced to contribute in the future, such as through so-called "solar parking lots". PV installation over parking lots takes advantage of available space, may offer vehicle protection, and generates electricity for electric vehicle charging stations. The layout should be individually configured to suit each parking lot, such as in form, inclination, and mounting system. Despite its increasing popularity in Europe, this strategy is still uncommon due to relatively high mounting costs and low self-consumption rate, which describes the energy consumed on-site relative to the total energy generated (Hochreutener et al., 2022). In Germany, most of its 59 GWp potential of solar parking lots is still untapped (Wirth & ISE, 2023).

### Standards and Regulations

In Bremen, the need to expand PV capacity on roofs is addressed with the Bremen Solar Energy Act (*Bremisches Solargesetz*, "BremSolarG") that recently became effective. Soon, using PV will be mandatory on new buildings as much as 50% of their gross roof area as well as buildings with retrofitted roofs. This can be exempted only under certain conditions (§ 2 BremSolarG). The installation itself is much less restricted than geothermal energy since it rarely invades natural resources and ecosystems. PV on roofs for public or private use is only subject to a few restrictions stated in the Bremen State Building Code (*Bremische Landesbauordnung*, "BremLBO") and Bremen Monument Protection Act (*Bremisches Denkmalschutzgesetz*, "BremDSchG") and does not require a permit (§ 61 para. 1 cl. 3 BremLBO) unless built on buildings listed under monument protection (§ 10 BremDSchG).

Between the module and neighboring firewall, a minimum spacing of 0.5 m is required (§ 32 para. 5 BremLBO).

In Germany, ground-mounted systems, such as solar parks, are typically regulated in the land-use planning of the county or town. In recent years, a growing number of towns has selected areas specifically for solar parks in their land-use plans. Though in dense cities such as Bremen, these are hardly feasible in terms of space availability. Furthermore, solar parking lots have been made mandatory under certain conditions in several federal states, such as Lower Saxony, Baden-Württemberg, and Nordrhein-Westfalen (Christner, 2022). With the Climate Protection Strategy 2038, Bremen aims to implement a similar regulation by 2030 for industrial areas, supermarkets, and new residential areas with at least 25 parking spaces. However, there is currently no statement regarding a funding program, unlike in Baden-Württemberg, in which subsidies can be applied for PV installation over existing parking lots (UMBW, 2024).

### 2.3. District Heating

#### Technical Principles

In a centralized heating system, also commonly known as district heating (DH), heat generation and consumption do not necessarily occur in the same place. The heat from one or more sources is extracted or recovered through heat carrier fluids, then distributed through underground insulated pipes to the end-users over a large area such as a neighborhood, district, or a whole city. DH initially used steam as a heat carrier when it first emerged (Lund et al., 2014). The next generations of DH began using hot water, further reducing the operating temperature with each evolutionary step to allow the coupling of more waste heat sources and to minimize heat loss during transport. The 4th generation DH introduced the idea of integrating renewable sources and electric heat pumps to reach the target temperature, which ideally favors the reduction of a building's heat demand for greater efficiency (Lund et al., 2021). The 5<sup>th</sup> generation DH does not differ significantly by definition, though it emphasizes the use of very low temperatures ranging from 10 to 40°C (Doubleday et al., 2019), bidirectional heat exchange ability, and the possibility of cooling (Lund et al., 2021). The term "LowEx district heating" is not officially defined and can describe both 4th and 5<sup>th</sup> generation DH. In this study, LowEx DH shall be understood as a broader term, simply characterized by renewable sources and a heat grid operated at a much lower temperature than conventional DH so that decentralized heat pumps are essential. In Germany, the energy for DH nowadays still mostly derives from combined heat and power plants (AGFW, 2023). DH currently only contributes 14.2% to domestic heating in Germany (BDEW, 2023).

Generally, when integrating ambient heat, there can be decentralized heat pumps located at each consumer or central heat pumps with higher thermal output that uplift the temperature before distribution, as illustrated in Figure 3. Decentralized heat pumps, as in LowEx heating systems, are more beneficial in some cases because the supplied heat can be individually raised to meet the target temperature at each consumer. Thus, transport heat loss is very low, especially in areas with low heat demand density. Yet in such areas, it is practically difficult to maintain the competitiveness of DH with ambient heat in general due to very low heat generation costs but high specific capital costs. In this case, an advantage of a large-scale heat pump is the greater cost-effectiveness compared to having many decentralized heat pumps (Averfalk et al., 2021).

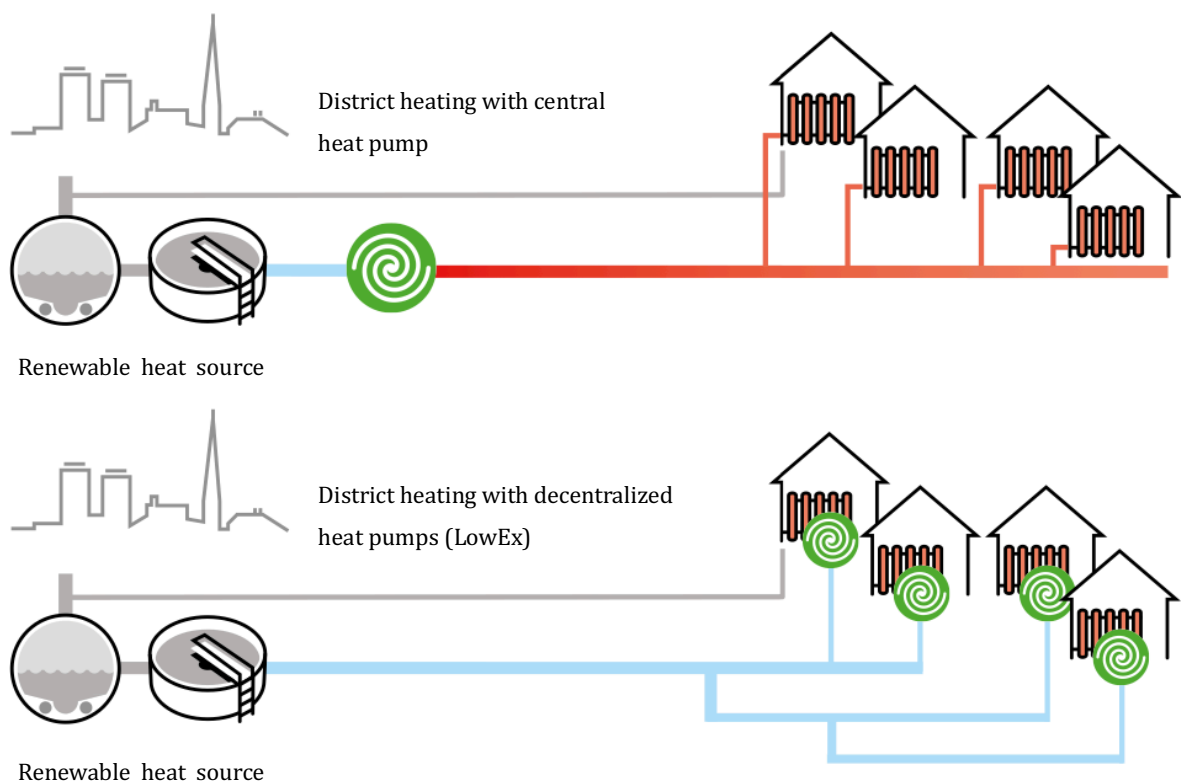


Figure 3: Difference between district heating with centralized and decentralized heat pumps (LowEx) (BWP, 2022)

### Practical Examples

Most LowEx DH systems are currently being planned, built, or were only recently finished so long-term results do not exist yet. Suitable renewable sources include solar thermal collectors, geothermal systems, water systems, and heat waste from data centers, which have been applied in several projects in Germany, the Netherlands, and Switzerland (Averfalk et al., 2021; dena, 2021). A local LowEx project in Bremen is underway, which will supply the Tabakquartier (a housing, office, and leisure complex of 20 ha) with recovered heat from wastewater and two

large-scale heat pumps with 1.2 MW total capacity (Justus Grosse, 2023). An ongoing project in a new residential area in Warendorf is an example of LowEx DH with exclusive geothermal energy use and decentralized heat pumps. BHEs at 150 m depth and a 5 km long trench collector are planned, which will provide full renewable heat and cooling to 500 residential units by 2026 (Bundesverband Geothermie, 2021; Wetter & Brüggling, 2023). In Bremen, the feasibility of LowEx DH with 300 m deep BHEs and decentralized heat pumps in the “Humboldt-Straße” was studied. An annual thermal output of 1.650 MWh/a can be expected from a total of 63 boreholes (energiekonsens GmbH, 2022).

Seasonal heat storage is crucial for an efficient LowEx heating system since the demand is concentrated in winter months, while ambient heat availability is not. The same applies to solar power availability, which can aid heat pump operation, as known in the LowEx heating grid in Wüstenrot (dena, 2021) which uses geothermal collectors. The consumer buildings are installed with PV, which can effectively provide about 50% of the required power for the heat pumps. This can generally be improved by aiming greater self-consumption rate and, thus, PV solar fraction, which describes how much of the energy demand is covered by the modules, through efficient energy storage technologies and better load management (SAENA, 2023). Building-integrated storage tanks are usually implemented, but also BHEs can be used to direct excess heat into the ground for seasonal storage using reversible heat pumps, simultaneously applying cooling. Its combination with solar thermal collectors is another way to support heat storage and regeneration of ground heat. Such systems are becoming increasingly popular in DH (Cruickshank & Baldwin, 2022).

### Standards and Regulations

DH networks in Germany, whether new or existing, shall be “decarbonized” following the Heat Planning Act (WPG). § 4 WPG obliges municipalities and cities to create heat planning strategies by 2026 or 2028 (depending on population size), which shall provide steps to reach climate neutrality by 2045 with the use of any non-fossil source (i.e. renewable source and/or unpreventable waste heat). Obligations for DH suppliers are stated in § 29 to § 32 WPG: while the proportion of non-fossil sources in existing networks must be at least 30% of the delivered heat until 2030 and 80% until 2040 (§ 29 para. 1 WPG), in new heat networks reaching at least 65% is mandatory by March 2025 (§ 30 para. 1 WPG). This corresponds to the mandatory integration of at least 65% of non-fossil sources for space and water heating in any new heating system (§ 71 para. 1 GEG). Both law passages indicate that the SPF of any installed heat pump shall be at least equal to 3 (electricity input = 1/3), considering that the power grid still consists of fossil-based energy. The government offers several funding options to support, such as the BEG program (*Bundesförderung für effiziente Gebäude*) with up to 20% bonus for

consumers for building retrofits and heat pump purchases. For heat grid operators, the BEW-Program (*Bundesförderung für effiziente Wärmenetze*) would aid with up to 40% of investment costs for green DH (BMWK, 2024).

#### 2.4. Related Works

Regarding the objectives of this thesis, the following studies have similarly aimed to identify LowEx DH potentials, geothermal energy, or solar energy for DH by using GIS. Some conceptual ideas, data, and missing aspects from these are implemented in the workflow.

A GIS-based concept was developed and tested for the city of Oldenburg (Germany) that aims to determine “suitability areas” in a city for different heat supply options including LowEx systems (Knies, 2018). The concept focuses on the so-called “linear heat density” as a primary factor for the economic viability of the possible supply options, as also investigated by Dochev et al. (2018). Furthermore, it pointed out the importance of integrating heat storage in network plans for the Winter period when heat demand peaks and solar energy is less abundant. This approach was recently tested again on Bremen with current and future heat demand estimated by the firm *DBI Gas- und Umwelttechnik GmbH* (DBI GUT) (Knies et al., 2024). However, the possible technologies and their heat potential were not explored in any of these studies.

Quick estimations of geothermal energy are challenging since the potential strongly depends on various geological factors that are site-specific (Bayer et al., 2019). Schiel et al. (2016) presented a GIS-based method to calculate the CO<sub>2</sub> reduction if geothermal energy were applied for space and water heating in Ludwigsburg. The study estimated the heat demand per building and the geothermal heat extraction potential in each cadastral parcel. The latter was calculated from given borehole data and values found in VDI 4640, so geothermal interference in that dimension is not fully considered. The number of boreholes was determined through random point placement, only considering the required spacing to buildings and cadastral boundaries. Thus, this method only gives a very rough estimation.

On the other hand, determining solar energy potential is much simpler as it primarily depends on roof properties, solar radiation, and module efficiency. The benefit of GIS-based methods here lies when estimating PV potential in large urban areas with complex heterogeneity of buildings (Mansouri Kouhestani et al., 2019). A solar cadastre for Bremen has been developed by Geoplex GIS GmbH and published for viewing by the state ministry *Senatorin für Umwelt Klima und Wissenschaft* (SUKW) on the website “*Solarkataster Bremen*” (SUKW, 2019). The compatibility and power output of an individual roof are roughly estimated and could be shown by interaction on the website, though it is only based on a simple calculation assuming an area of 7 m<sup>2</sup> per kWp (swb AG, n.d., accessed 07.05.2024).

### 3. Description of the Study Area

The district Neu-Schwachhausen is located centrally in the city of Bremen, Germany, just north-east of the old town, directly bordering the Bürgerpark to the west, which is the biggest park in Bremen. The investigated area for this study, presented in Figure 4, covers a great majority of the residential areas in Neu-Schwachhausen. In this thesis, the area will be referred to as the “district” itself for simplicity reasons.



Figure 4: View of Neuschwachhausen with seven characteristic areas (Map: DOP10, © GeoBasis-DE / Landesamt GeoInformation Bremen 2023)

Neu-Schwachhausen was created as an additional neighborhood in the 1960s to the already existing district Schwachhausen, offering new residential quarters in attached row houses and individual blocks (Bremen Online, n.d., accessed 05.05.2024). Today, it is considered as one of the preferred residential districts due to its proximity to the city center and the Bürgerpark.



There are 1,014 residential units (houses or apartments) in total, of which the majority were built between 1949 and 1978. Bremen shows a positive trend in terms of population growth in the last 10 years, and in Neu-Schwachhausen the population as of 2022 reached 6,104 with an average age of 45.2 which places it slightly above the city's average age of 43.4. All residential units within the district today largely consist of single households (updated census of 2011, accessed through *Statistisches Landesamt Bremen (SLB) (2024)*).

As shown above in Figure 4, seven areas (marked A to G) are noticeable:

- A. Densely built residential area with attached row houses, some with enclosed green areas, and a small supermarket
- B. Buildings with mixed functions including residences, a pharmacy, and a supermarket, as well as a parking lot for the supermarket
- C. Non-residential area containing a primary school, and a large sports club complex of "Bremen 1860" with indoor halls, a rugby field, several tennis fields, and parking lots
- D. Residential space with several attached apartment buildings (facing south-west and south-east) and large green areas in between
- E. Middle-sized attached row houses in three parallel streets (facing East-South-East and West-North-West)
- F. Detached houses with large gardens surrounding a kindergarten in the center
- G. Residential units of mixed styles including detached houses with large tree-dense gardens and apartment buildings of different sizes

Neu-Schwachhausen does not contain any natural or large artificial water bodies, nature conservation or water protection sites, or archeological monuments. The district still places a great value on environmental protection by maintaining a high tree density in many places and putting many of the trees under special protection, including some on private properties. The cutting of such trees and also any tree in public areas (such as streets) requires additional permission and replanting in another appropriate site (Mathes et al., 2020).

Currently, district heating serves for 15% of domestic heating in Bremen and largely derives from combined heat and power plants. The city's energy supplier, swb AG, plans to expand the heat grids that exist in three regions of Bremen by 68.8 MW thermal capacity, while also incorporating more climate-friendly alternatives to coal by 2035 and eventually reach climate neutrality by 2050 (swb, 2020). However, a plan to expand the grid or implement LowEx DH in Neu-Schwachhausen is yet unknown. Here, according to the latest census data of 2011, central heating was mostly applied for room and domestic hot water, while district heating only accounted for 11.8% of all residential units (SLB, 2024). The small heating grid is found in "Kulenkampallee" by the supermarket in characteristic area B.

## 4. Methodology

The chapter presents the created workflow and the methods used for each phase, which are geodata collection, heat demand examination and processing, potential analysis of geothermal and solar energy, and identification of neighborhoods that are suitable for a joint LowEx DH concept. Here, these are regarded as “sub-areas”. The energy potentials estimated refer to the “technical potential”, which is restricted by space availability, technology performance, and certain technical and/or legal regulations. The proposed sub-areas are identified and evaluated as the final step of the approach. An overview of the workflow is illustrated in Figure 5.

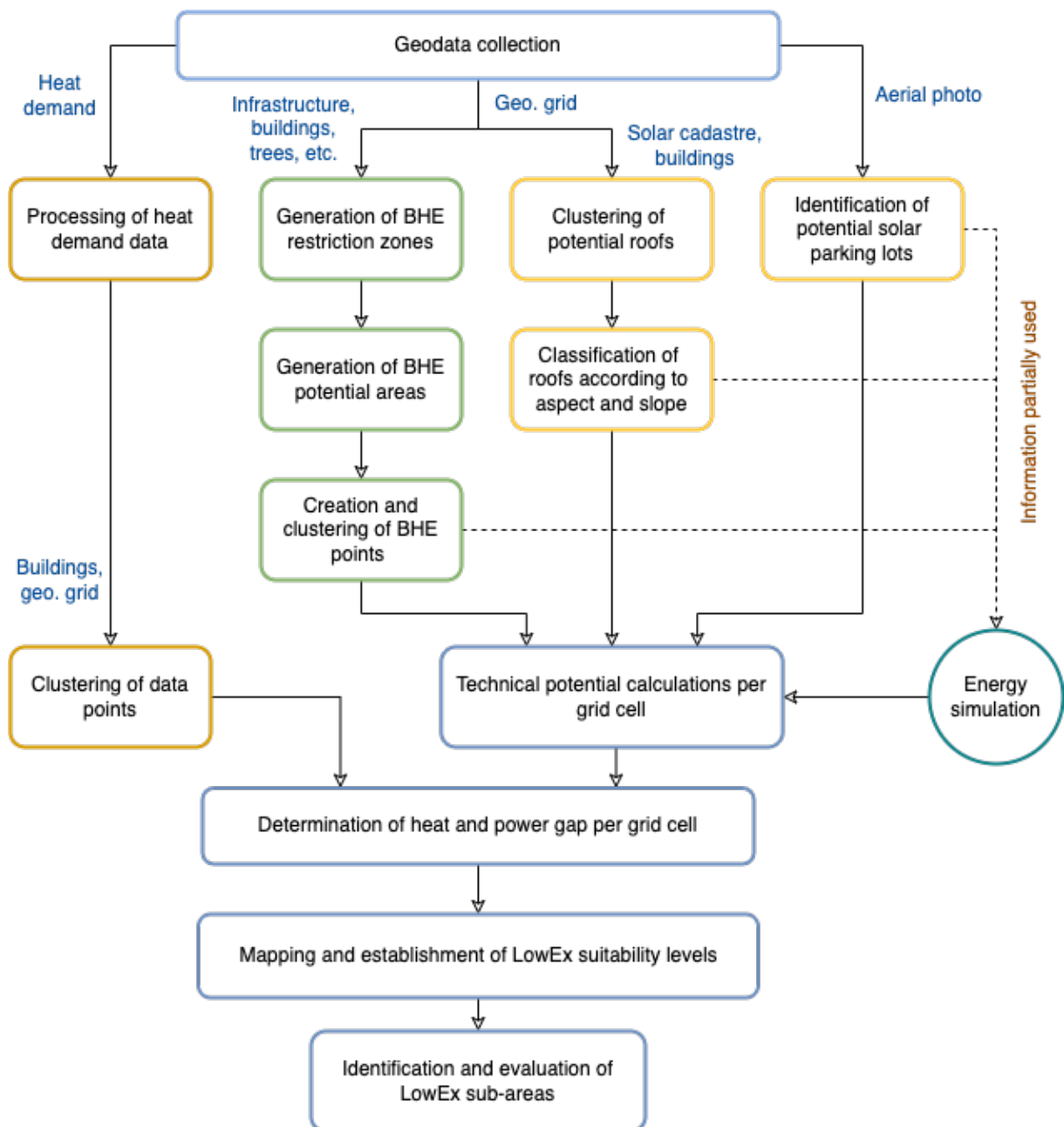


Figure 5: The workflow created and applied to identify possible LowEx sub-areas

The research questions of this study shall be investigated by applying the workflow to four scenarios (S): 2022, 2030, 2038-a, and 2038-b. The defined scenarios reflect the positive development of geothermal and solar energy installations as well reduction of heat demand, both of which are expected with time. It is assumed that investment costs of geothermal and solar energy will gradually decrease while the popularity and public acceptance will increase. Heat demand and consumption will decrease with growing awareness and political measures that reinforce necessary building retrofits. Available heat demand data describes the situation in 2022, therefore the first scenario S-2022 is assumed as the “status quo”. Scenarios S-2038-a and -b shall both illustrate the year 2038, in which climate neutrality in Bremen is expected, but differ from each other in geothermal energy extraction. Table 1 describes the different settings established for the four scenarios.

*Table 1: Overview of the four scenarios with the defined settings for heat generation and demand*

Scenario	Heat demand	Installed Technologies	
		Geothermal Energy	Solar Energy
S 2022	Status quo	Borehole depth 100 m 30% of max. available space	Roofs with PV adequacy level 1
S 2030	First reduction	Borehole depth 100 m 70% of max. available space	Roofs with PV adequacy level 1 and 2
S 2038-a	Second reduction	Borehole depth 100 m 100% of max. available space	Roofs with PV adequacy level 1 and 2 Solar parking lots
S 2038-b	Second reduction	Borehole depth 300 m 100% of max. available space	Roofs with PV adequacy level 1 and 2 Solar parking lots

The workflow contains manual and automated analyses using ArcGIS Pro, energy simulations on Polysun and Earth Energy Designer (EED), as well as additional calculations on Microsoft Excel. All the analyses required the geographical grid with 100 m resolution for the clustering of data. This was necessary since the scenario results can be easily compared to each other and building- and parcel-specific data can remain anonymous.

This approach does not inspect the viability that includes economic and social factors. Furthermore, it aims to give simplified cumulated results in a year, so daily or monthly potentials and demands are neither examined nor presented.

## 4.1. Geodata collection

Geodata are the foundation of spatial analyses. Mostly, these were provided through WWNW, though some were directly accessed online on the websites of the responsible institution. Table 2 lists all the geodata collected and used for this study along with the sources.

Table 2: List of used geodata

Geodata	Source	Data Currency
Buildings, other structures, and streets	Landesamt GeoInformation Bremen (GeoBremen) (pub.): ALKIS ( <i>Amtliches Liegenschaftskatasterinformationssystem</i> )	2023 Last accessed: 02.05.2023
Digital Orthophoto (DOP10)	Landesamt GeoInformation Bremen (pub.): True Orthophotos (TrueDOP), 10 cm ground resolution	05/2023 Last accessed: 20.12.2023
Geographical grid, 100 m resolution (in Lambert projection)	Bundesamt für Kartographie und Geodäsie (BKG) (pub.): <i>Geographische Gitter für Deutschland in Lambert-Projektion (GeoGitter Inspire)</i> . Accessible online (BKG, 2023)	12/2019 Last accessed: 05.12.2023
Heat demand (building-specific modelled data for Bremen, predicted for the years 2022, 2030, and 2045)	DBI Gas- und Umwelttechnik (DBI GUT) (creator)	2023 Last accessed: 11.03.2024
Public trees, location and crown size	Umweltbetrieb Bremen (UBB): <i>Straßenbäume mit Kronenradius Stadt Bremen</i> (WMS). Accessible online (UBB, 2023)	09/2023 Last accessed: 20.12.2023
Soil thermal conductivity (modelled for 40 m – 140 m ground depth)	Geological Survey of Bremen (GDfB) (pub.)	03/2018 Last accessed: 06.02.2024
Solar Cadastre of Bremen	Freie Hansestadt Bremen, Die Senatorin für Umwelt, Klima, und Wissenschaft (SUKW) (pub.), in cooperation with Geoplex GIS GmbH: <i>Solarkataster Bremen</i>	01/2020 Last accessed: 01.05.2023

All geodata were obtained in or converted to the projection system ETRS89 / UTM 32N (European Terrestrial Reference System 1989). If not specified otherwise, the basemap displayed in figures in this document is the “World Topographic Map” (© Esri).

## 4.2. Processing Heat Demand Data

To determine potential sub-areas for LowEx DH, it is necessary to gather the overall heat demand and its distribution in Neu-Schwachhausen. Building-specific modeled data by DBI GUT, which were also applied in the test run by Knies et al. (2024) (see Chapter 2.4), were used for this study. These contain precise coordinates of the buildings according to ALKIS (*amtliches Liegenschaftskatasterinformationssystem*) as shown in Figure 6. Here, the information refers to the demand for room heating and domestic hot water, and is presented in the annual cumulated amount.



Figure 6: Close-up view of heat demand data (DBI) stored in building-specific points as an example.

The heat demand was first modeled for 2022 and based mostly on 3D data of the buildings, which provide information regarding the function (e.g. residential, industrial, or communal) and specific data of the building (e.g. structure, dimension, usable area, and age). These were then further specified using characteristic values that correspond to the sector and region of each building, such as its retrofitting status and residents' data. Heat demand was also modeled for the years 2030 and 2045, essentially by extrapolating current statistics and taking into account multiple factors that will likely develop, especially climate, population, household size and number, and measures for building retrofits in the upcoming years. External data that was used

included regional and national statistics as well as prognoses. A complete explanation to obtaining the data can be found in the official report “*DBI-Ansatz zur Modellierung von Wärmebedarfen*” by Heinrich et al. (2023).

In this study, the heat demand is not differentiated into the various building types or functions. The values for the year 2038 were interpolated using the given data. Although the overall development from 2022 to 2045 resembled a non-linear progression, it was assumed that it did resemble a linear one from 2030 to 2045 due to the lack of accessible information.

Buildings with the point data for 2022, 2030, and 2038 were assigned to the grid cell, in which the center of the polygon lies, through its unique polygon ID (e.g. the field “rowid”). This allowed to determine the heat demand per grid cell, which would later be used for comparison with heat generation potential and the formation of sub-areas (see Chapter 4.5). Points that neither intersect a building nor are within 2 m from the outline were excluded, as with buildings without heat demand data. The process was automated using the ModelBuilder function on ArcGIS Pro.

### 4.3. Potential Analysis of Shallow Geothermal Energy

The technical potential of shallow geothermal energy within Neu-Schwachhausen is estimated at this stage. This shall be the main heat source for the LowEx heat network. In this study, geothermal probes were considered since these are most suitable in areas with many densely built neighborhoods. Borehole heat exchangers (BHE) were selected as the observed technology.

#### 4.3.1. Potential Area Scan using ModelBuilder

A GIS tool named “GeothermalPot” was created using ModelBuilder to automate the process of identifying potential areas and placing possible borehole locations. Firstly, available space for the probes was determined within the district border. This was carried out by taking the whole area of Neu-Schwachhausen and excluding the sites where the probes would either be impractical or legally prohibited. The remaining polygons were viewed as potential areas for BHEs. Figure 7 shows how the mentioned steps were implemented in the tool “GeothermalPot”.

The geodata for constructed objects (e. g. buildings and streets) originate from ALKIS while most public trees were registered by UBB and provided online as WMS. The polygon outline of the trees was extracted as vector data. Manual digitization based on orthophotos was also necessary since newer structures, some public trees as well as all private trees were missing from the data. Other vegetations such as bushes were not identified as a restriction. All

excluded objects, which are listed in Table 3, were set as variable parameters in the model. This shall avoid any limitation regarding the geodata source, so the input data can be selected freely. This study shall investigate a DH concept with joint heat grids that can share the extracted heat, so plot boundaries were omitted.

Table 3: Excluded areas for BHEs and the source of the geodata.

Areas excluded	Buffer zone	Applied Geodata
Streets	0.5 m	ALKIS
Buildings	2 m	ALKIS; manually digitized based on DOP 2023
Other structures	0.5 m	ALKIS; manually digitized based on DOP 2023
Underground spaces	2 m	ALKIS
Trees (crown radius)	3 m	UBB; manually digitized based on DOP 2023
Pools and ponds	2 m	manually digitized based on DOP 2023

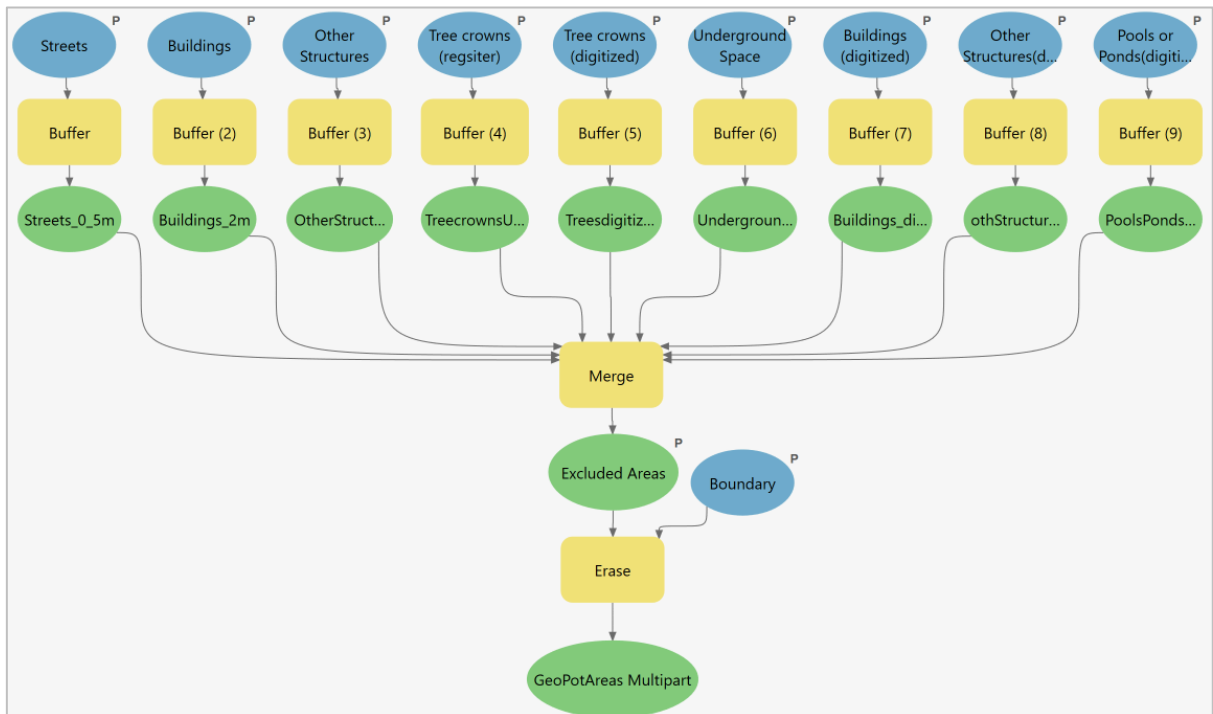


Figure 7: A view of the first section of “GeothermalPot” in ModelBuilder, which identifies the exclusion zones and potential areas for BHEs

Possible locations of boreholes were randomly placed with a point generator within the potential areas with a minimum of 6 m and 10 m distance between boreholes for the 100 m and 300 m borehole depth, respectively, as a technical restriction (see Chapter 2.1). In the tool

“GeothermalPot” this took place as the final step after removing several polygons of the potential area that had been generated but were deemed too small for a BHE installation, which was set as below 2 m<sup>2</sup> (see Figure 8). The extracted geothermal energy should be prioritized for surrounding consumers nearby and the location categorized for determining the suitable sub-areas (see Chapter 4.5). Therefore, the points were clustered in grid cells.

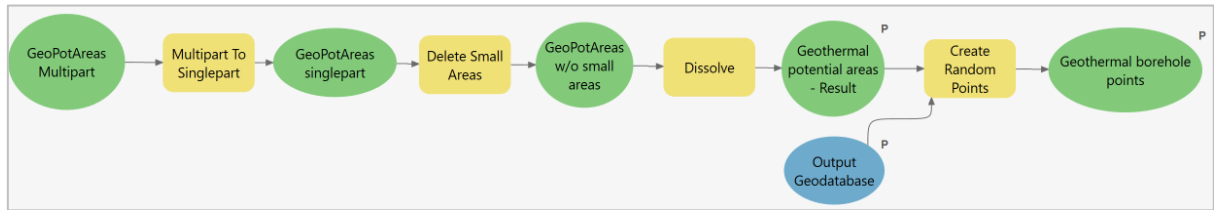


Figure 8: A view of the second section of “GeothermalPot” in ModelBuilder, which excludes small polygons of potential areas and generates random points as boreholes

#### 4.3.2. Soil Thermal Conductivity

The mean soil thermal conductivity (STC) in the observed ground layers was required for estimating the heat extraction. The values at 100 m depth were retrieved as vector data from the Geological Survey of Bremen (GDfB). The data was modeled through inter- and extrapolation of sampling results from diverse locations and depths across Bremen. Upon first observation, it was clear that the district was divided into five zones of mean STC values ranging between 1.2 and 1.6 W/mK in 0.1 steps, which were clustered in grid cells that differ from those provided by BKG (see Figure 9). The five values were returned to all the borehole points located within the different zones.

Modeled values for 300 m depth were not yet available due to the lack of drilling activities and sampling at such depths at the time of this study. Instead, actual sampling data from 100 m below ground, which was retrieved via E-Mail from the GDfB<sup>1</sup>, was used to estimate it. The mean STC at depths of 100 m and 300 m at the sampling site were 2.43 and 1.94 W/mK, respectively, based on an estimation using the given information (see Table 4). Thus, the STC at 300 m depth was roughly 80% of that at 100 m depth. Because the sampling site is found in the STC zone of 1.2 W/mK according to the modeled data, the value at 300 m depth was assumed to be 0.96 W/mK and was applied to all boreholes.

<sup>1</sup> Anonymized sampling report “Stellungnahme zu den Untergrundverhältnissen (Standortauskunft) zur Planung einer Erdwärmesondenanlage für ein Gebiet in Bremen, Ottilie-Hoffmann-Straße 1X” (created on April 27, 2023) sent via E-Mail from Dr. Björn Panteleit (GDfB) to Timmy Schwarz (WWNW), received on Feb. 06, 2024.



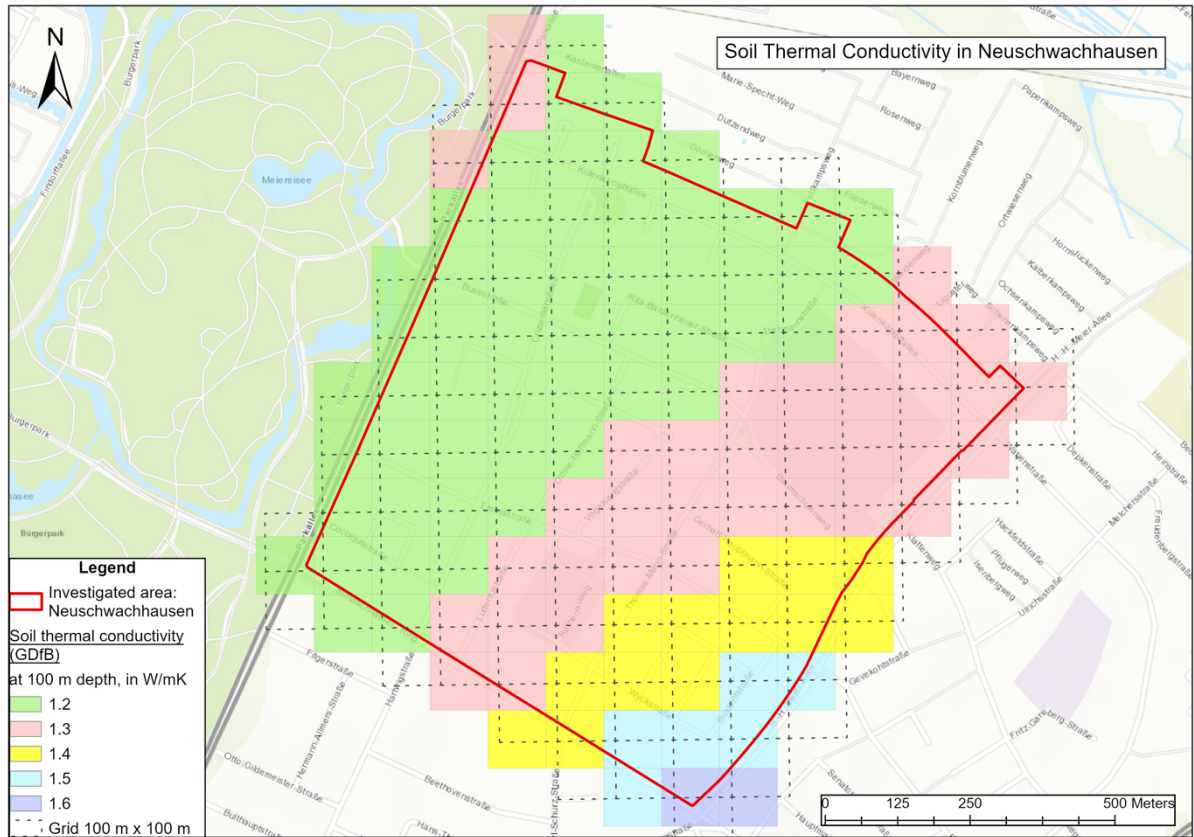


Figure 9: The distribution of mean soil thermal conductivity across Neu-Schwachhausen at 100 m depth according to GdFb

Table 4: Estimation of mean soil thermal conductivity (STC) at 100 m and 300 m based on the sampling report from the GdFb

	Ground layer range in m below ground	Layer thickness (m)	STC (W/mK)	Weighted STC in layer (W/mK)
<b>Sampling result</b>	0 to 3 m	3	0,6	0,02
	3 to 44 m	41	2,2	0,90
	44 to 52 m	8	2,8	0,22
	52 to 80 m	28	2,6	0,73
	80 to 100 m	20	2,8	0,56
	>100 m	100	1,7	1,70
<b>Estimation result</b>	0 to 100 m	100	-	2,43
	0 to 300 m	300	-	1,94

### 4.3.3. EED Simulation

Since a greater dimension of borehole fields was expected, a suitable simulation software, Earth Energy Designer (EED), was used. Several variations were simulated to estimate the maximum possible heat extraction, which differ in borehole depth, configuration, and STC. There are fixed parameters required in all simulations, including properties regarding the soil, borehole, U-pipe, and heat carrier fluid, as listed below in Table 5. These were chosen based on site-specific findings, guideline recommendations, and gathered knowledge (see Chapter 2.1). Several specific values were taken from the in-built guide of EED.

*Table 5: Fixed parameters of ground data, borehole properties, and U-pipe properties applied in all four simulations*

<b>Parameter</b>	<b>Value</b>	<b>Background (Source)</b>
<b>Ground data</b>		
Volumetric heat capacity	1.7 J/Km <sup>3</sup> (at 100 m depth); 1.6 J/Km <sup>3</sup> (at 300 m depth);	Sediment type “fine sand with silt elements” at 100 m and “silt or clay” at 300m depth (GDfB sampling report <sup>1</sup> ; EED)
Ground surface temperature	8.8°C	Site-specific (EED)
<b>Borehole properties</b>		
Type	Closed-loop system, Double-U	Common variant (García Gil et al., 2022b)
Diameter	170 mm	Recommended, with 30 mm of grouting material required (LfU, 2012; Panteleit et al., 2022)
Filling thermal conductivity	0.7 W/mK	Bentonite as standard grouting material (Stober & Bucher, 2020a)
<b>U-Pipe properties</b>		
Material and dimensions	PE DIN 32	Standard type (LfU, 2012; EED)
Shank spacing	78 mm	Recommended, with internal spacers (LfU, 2012)
Seasonal Performance Factor	3	A minimum of 65% of renewable energy in residential heating (§ 71 GEG)
Heat carrier fluid	Water + Ethanol 15%	Suitable, freezing point < -3°C (T <sub>return</sub> ) (Panteleit et al., 2022)

Table 6 illustrates an exemplary set of simulations and their input variables. Simulations no. 1 to 5 and simulation no. 6 would deliver results for S 2038-a and S 2038-b respectively. Each scenario was given a different STC and borehole configuration, determined by calculating the average number of borehole points per grid cell and selecting a rectangular BHE field (to reflect a grid cell) with the closest borehole number available from the in-built database of EED.

*Table 6: Exemplary set of simulations to be conducted in EED for one scenario to estimate the geothermal heat generation.*

<b>Simulation</b>	<b>Borehole depth (m)</b>	<b>Borehole spacing (m)</b>	<b>Configuration</b>	<b>Soil thermal conductivity (W/mK)</b>
<b>1</b>	100	6	X boreholes	1.2
<b>2</b>	100	6	X boreholes	1.3
<b>3</b>	100	6	X boreholes	1.4
<b>4</b>	100	6	X boreholes	1.5
<b>5</b>	100	6	X boreholes	1.6
<b>6</b>	300	10	Y boreholes	0.96

EED simulates the heat extraction based on a given heat demand base load and peak load, and presents the mean fluid temperature as the result. In addition to the mentioned input data, the base load was first set at the mean heat demand per grid cell, while peak load was omitted for greater simplicity and generalization. Regarding the min. monthly mean  $T_{\text{Return}} \geq 0^\circ\text{C}$  and an assumed average temperature spread of 3 K, the minimum mean fluid temperature at  $1.5^\circ\text{C}$  was set as criteria. Following the suggestion of a consulting engineer in Germany with EED-experience<sup>2</sup>, the base load was adjusted until it remained above this threshold throughout the expected lifetime of 50 years (see Chapter 2.1). The new heat demand was divided by the number of boreholes to obtain a value, which was considered the maximum heat extraction per borehole. The process was repeated for all simulations.

#### 4.3.4. Potential Estimation and Applicability Test

The geothermal potential in each grid cell ( $Q_G$ ) was estimated with the following equation:

$$Q_G = \sum_{i=1}^n B_i * QS_i \quad (\text{Eq. 1})$$

<sup>2</sup> Communication via E-Mail, sent from Kim Schwettmann (consultant of Ingenieurgesellschaft Heidt + Peters mbH) to Jan Pötzsch (consultant of IGIG Planungsgesellschaft mbH), received on Feb. 27, 2024

In which  $B$  and  $QS$  correspond to the number of boreholes and simulated heat extraction per borehole, respectively. The summation includes all considered STC values represented in  $i$  to  $n$ . The results of all grid cells were summed to obtain the total annual geothermal potential. This was repeated for all scenarios.

The applicability of the calculation was also tested since single simulation results may be less suitable for large-scale applications. For this, four grid cells were selected that contain different BHE numbers at max. potential in the 100 m variant, which corresponds to the scenario S-2038-a. For each of these, a test simulation was conducted on a specific borehole configuration based on the exact BHE number. The results were compared to the potentials estimated in S-2038-a. To gain a better understanding, the statistical distribution of BHE number per grid cell was also examined in the final two scenarios.

#### 4.4. Potential Analysis of Solar Energy

The solar energy potential of an investigated site essentially depends on the available area and solar irradiance. In this study, the roof area of all buildings (both residential and non-residential) within Neu-Schwachhausen are considered potential sites. Moreover, the possibility of solar parking lots is examined.

##### 4.4.1. Classifying Potential Roofs

The solar cadastre of Bremen (*Solarkataster Bremen*) holds all roofs of residential as well as non-residential buildings (e. g. office buildings, restaurants, kindergartens, and carports) with, among others, the following essential information: area, slope, orientation, and shade. Resulting of these factors, for each roof the so-called “PV-area” had been calculated and an adequacy level (German: “Eignung”) of 1 (very high), 2 (high), 3 (medium) or 6 (low) had been assigned (swb AG, n.d., accessed 07.05.2024) as displayed in Figure 10. The PV-area gives the effective area of solar modules after excluding shaded parts and other roof structures such as chimneys and windows. Roofs with an adequacy level of 3 and 6 were considered unviable due to adverse conditions and were, therefore, not observed in the analysis.

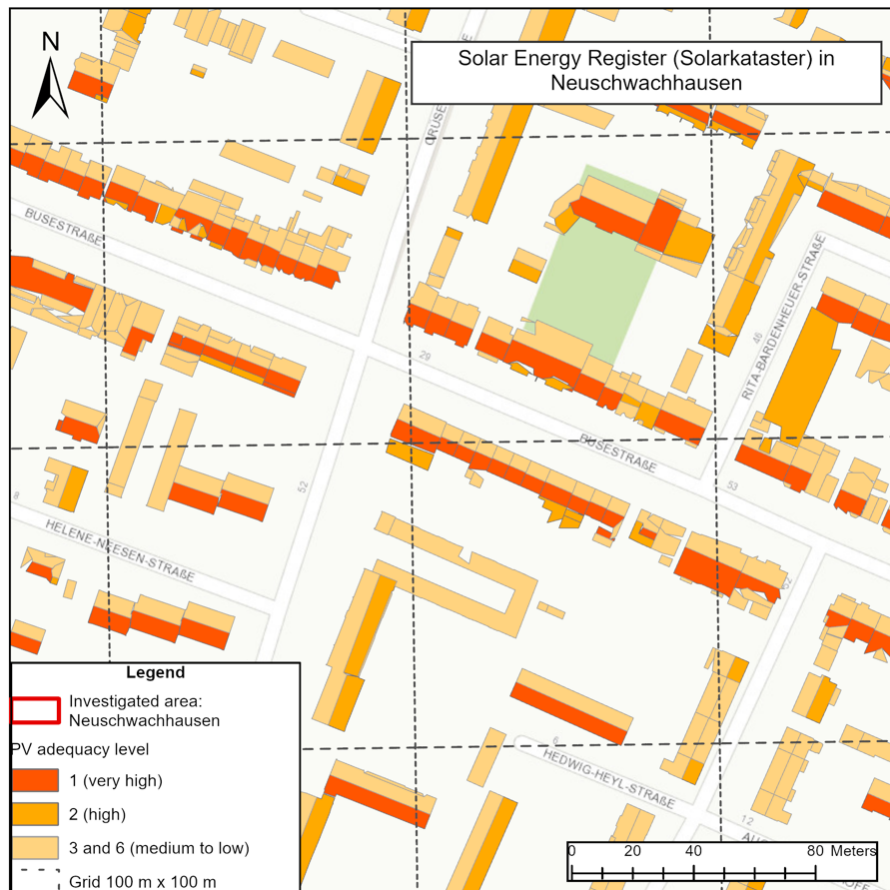


Figure 10: Close-up view of the displayed solar cadastre as an example

For the clustering, it was defined that a building was to be assigned to the grid cell in which its center is situated. Any roof on top of it or attached to it was assigned to that building and, therefore, to the same grid cell. The clustering was carried out using unique values of the objects (e.g.. “Object ID”).

Since the efficiency of a PV module highly depends on the roof properties, the roofs were classified into two main categories: flat or pitched. All roofs with a slope of less than  $10^\circ$  were defined as flat roofs, on which the modules require sub-structure to tilt them at an optimal angle. All pitched roofs were again classified based on the slope and orientation (aspect) into different subcategories. All roofs were classified using an Excel tool (originally named “*Excel\_Solarkataster\_Vorlage*”) which had been provided by WWNW. The tool was integrated into an automation process using VBA (Visual Basic for Application) for quick classification per grid cell. In total, nine subcategories, as listed in Table 7, were observed. The aspect is measured in degrees ( $0^\circ$  to  $360^\circ$ ) in a clockwise rotation:  $0^\circ$  = north,  $90^\circ$  = east,  $180^\circ$  = south, and  $270^\circ$  = west.

Table 7: Subcategories for pitched and flat roofs based on the aspect and slope

Roof type	Aspect	Slope	Subcategory
Pitched roof	East-South-East (ESE) (Aspect 90° - 135°)	10° - 50°	ESE 1
		50° - 90°	ESE 2
	South-South-East (SSE) (Aspect 135° - 180°)	10° - 50°	SSE 1
		50° - 90°	SSE 2
	South-South-West (SSW) (Aspect 180° - 225°)	10° - 50°	SSW 1
		50° - 90°	SSW 2
	West-South-West (WSW) (Aspect 225° - 270°)	10° - 50°	WSW 1
		50° - 90°	WSW 2
Flat roof	all aspects	<10°	FR

#### 4.4.2. Potential of Solar Parking Lots

Parking lots in public areas (including those of supermarkets) were considered potential sites for solar parking lots. Reliable geodata for this were not found, so these were identified using aerial images (DOP10, 2023) and digitized as polygons **A**, **B**, **C**, and **D** as seen in Figure 11 on the following page. All are located on the western side of Neu-Schwachhausen with one being directly at the border of the investigation area.

The full coverage of the parking lots with slightly tilted PV as roofs (slope = 5°) was assumed, so half of the parking area would be covered with modules of one aspect and the remaining half with modules of the opposite aspect. Due to the structure of the existing car slots, the aspect 220° (South-West) and its opposite aspect 40° (North-East) were considered most suitable and were, thus, selected for the power estimation. Given the irregular form of the areas that are possibly less ideal for usual PV configurations and other unexpected technical limitations, the technical potential was set to 80% of the identified parking lots. The parking lots were observed as further subcategories and simulations were conducted (see Table 8). Unlike the potential estimation on roofs, the generated energy is fed into the power grid. Assuming that the whole district would benefit from it, the total yield shall be divided equally among all grid cells.

Table 8: Additional subcategories for solar parking lots based on the aspect values.

Aspect	Slope	Subcategory name
South-West (Aspect 220°)	5°	PL SW
North-East (Aspect 40°)	5°	PL NE



Figure 11: Identified potential sites for solar parking lots in A, B, C, and D. (Map: DOP10, © GeoBasis-DE / Landesamt GeoInformation Bremen 2023)

#### 4.4.3. Polysun Simulation and Grouped Calculations

The 11 subcategories were each simulated in Polysun with 10 modules. A monocrystalline type was selected due to its efficiency and general popularity. The specific module and configuration were chosen from the in-built database in Polysun and are listed in Table 9. The varying input data in each simulation are the slope and aspect. Polysun receives input data for slope in the regular expression as mentioned, while aspect is expressed from +90° (East) to -90° (West), so that it was necessary to convert these values beforehand.

Table 9: PV module configuration chosen in all simulations

<b>Manufacturer</b>	Solarwatt
<b>Product</b>	ECO 120M-335, Monocrystalline
<b>Nominal capacity</b>	335 Wp
<b>Inverter</b>	Sunkid 3000 HF
<b>Cable loss</b>	2%
<b>Module gross area</b>	1.69 m <sup>2</sup>

For each pitched-roof subcategory, the mean slope and aspect in the district were calculated and inserted as input data in the corresponding simulation using the Excel tool mentioned previously in Chapter 4.4.1. As for the flat roof (FR) subcategory, the average aspect was determined and chosen for the simulation of all flat roofs. Here, it was assumed that the modules were installed on substructures at an optimal tilt angle. The value was selected using the solar energy orientation chart (see Figure 2 in Chapter 2.2).

Considering required space for the module frame, min. distance to neighboring walls for fire protection, and roof structures that had been overlooked during data gathering, the technical potential area was set as 80% of the PV-area for pitched roofs. On flat roofs, area-usage is less efficient due to the necessary tilting and larger row spacing to avoid shading, therefore, the technical potential area of a flat-roof with a sub-structure inclination at 35° was assumed to be 30% of the PV-area. The expected annual yield per grid cell ( $E_G$ ) was first calculated with the following equation:

$$E_G = \sum_{i=1}^n \frac{E_{SCi}}{A_{Sim}} * A_{SCi} \quad (\text{Eq. 2})$$

in which  $E_{SC}$  is the simulated yield of each subcategory,  $A_{SC}$  is the total roof area of the same subcategory, and  $A_{Sim}$  is the total gross module area in the simulation. The various simulations are represented here by  $i$  to  $n$ , depending on how many subcategories were observed. However, solar parking lots (subcategories “PL SW” and “PL NE”) were excluded from this calculation, as they required a different approach (see Chapter 4.4.2). The energy yield in all grid cells was summed to calculate the total annual yield in the district ( $E_{Total}$ ). The method was repeated for all scenarios.

The total installed capacity ( $P_{Total}$ ) in the district and the annual specific yield ( $E_s$ ) were then determined using the equations below:

$$P_{Total} = \frac{A_{Total}}{A_m} * \frac{1}{P_n} \quad (\text{Eq. 3})$$

$$E_s = \frac{E_{Total}}{P_{Total}} \quad (\text{Eq. 4})$$

in which  $A_{Total}$  is the technical potential area in total,  $A_m$  is the module area, and  $P_n$  is the module's nominal capacity.



#### 4.5. Creation of Sub-Areas

The suitable sub-areas for LowEx DH were determined after all previous steps had been completed. For this phase, the following conditions were defined:

- a) "Heat demand" is regarded as "heat consumption"
- b) Sub-areas shall only consume heat from geothermal energy
- c) All heat-consuming buildings and energy potentials belonging to the same grid cell are viewed as one inseparable "neighborhood"
- d) The energy self-sufficiency within a grid cell is prioritized
- e) Solar power is used entirely for the decentralized heat pumps within the same grid cell
- f) Only the required power should be generated, so power surplus is prevented
- g) Grid cells with geothermal heat surplus shall distribute the rest to adequate "neighbors" with heat deficit to form larger sub-areas

The required power to operate the decentralized heat pumps within a neighborhood corresponds proportionally to its heat demand, since the maximum power is consumed when the heat demand is fully met. Therefore, given the heat pumps' SPF of 3, the required power (here also referred to as "power demand") is defined as 1/3 of the heat demand.

The differences between geothermal potential and heat demand as well as solar energy potential and power demand were determined for each grid cell, which correspond to "heat gap" and "power gap", respectively. The power gap is expressed relative to the power demand (opposite of solar fraction): no solar utilization corresponds to power gap = -100%, full solar utilization corresponds to power gap = 0%, and power surplus corresponds to power gap > 0%.

Neighborhoods that can achieve energy self-sufficiency in terms of heating (heat gap  $\geq 0$  kWh/a) and at least 70% solar fraction (power gap  $\geq -30\%$ ) were identified as potential sub-areas. These should maximize BHE installation and distribute heat to certain "direct neighbors" that lack geothermal potential. In grid view, direct neighbors are other grid cells that directly touch the boundary of that grid cell either horizontally, vertically, or diagonally, as shown in Figure 12. Non-direct neighbors were not considered to limit transport heat losses. Hence, heat loss in the pipelines was assumed to be insignificant and was omitted in any calculation.

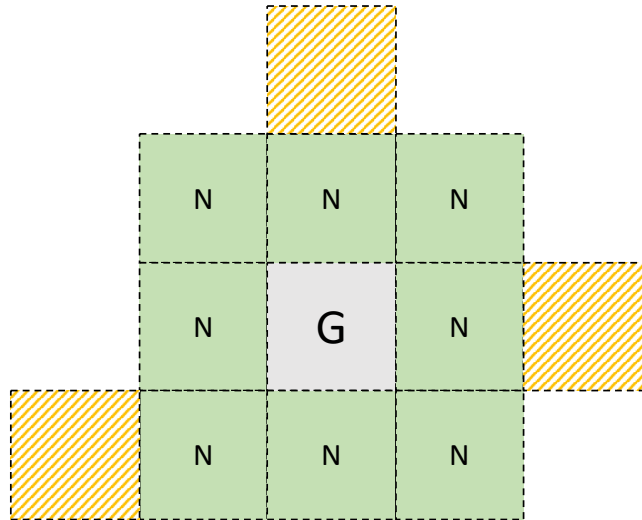


Figure 12: Example of an observed grid cell (G), its direct neighbors (N), and its non-direct neighbors (here: yellow hatched cells)

The heat gap (in kWh/a) was grouped into 5 classes of positive (heat surplus) and 5 classes of negative values (heat deficit). A grid cell can only deliver its heat surplus to direct neighbors with at least 70% solar fraction and belonging to the equivalent class or lower in the negative range – for example, a grid cell with medium surplus (class +2) can provide for neighbors with medium to low deficit (class -2 and -1), but not for those with large deficit (class -3). This was to ensure that all sub-areas should ideally achieve energy self-sufficiency. A grid cell that can produce, consume, and distribute heat is now referred to as a “heat supplier” and the suitable neighbors receiving heat as “heat receivers”. For each scenario, these were identified and joined as possible sub-areas. This method is visualized in Figure 13.

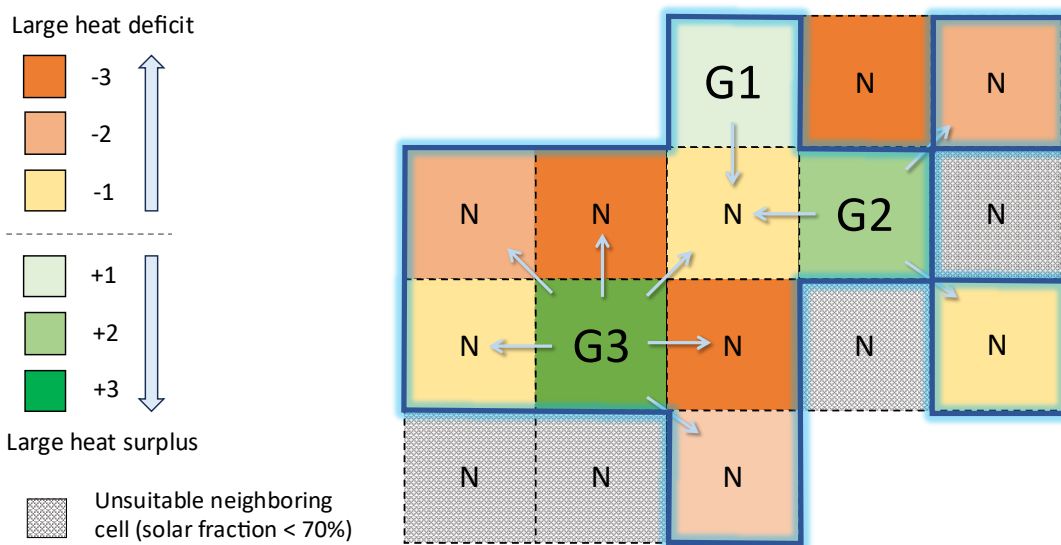


Figure 13: Example of the identification process of sub-areas (here: outlined blue) – Heat suppliers (G1, G2, and G3) shall distribute heat to suitable heat receivers among direct neighbors (N) (here: flow is marked with arrows)

The heat suppliers and receivers were ranked regarding their suitability in which the solar fraction or power gap is the critical factor. An overview of the classification is shown below in Table 10.

Table 10: Classification of LowEx suitability levels (SL) applied to “heat suppliers” and “heat receivers”

		Power gap		
		$\geq 0\%$	$0\% > x \geq -15\%$	$-15\% > x \geq -30\%$
Heat Gap	$\geq 0$ kWh/a	Supplier SL 1 (very high)	Supplier SL 2 (high)	Supplier SL 3 (medium)
	$< 0$ kWh/a	Receiver SL 1 (very high)	Receiver SL 2 (high)	Receiver SL 3 (medium)

#### 4.6. Evaluation of Sub-Areas

To enable the comparison between sub-areas of different scenarios, an evaluation by weighted rating was conducted. Four core criteria had been selected, which were deemed relevant and were also assessable within the defined scope of this study:

- 1) Energy self-sufficiency: How much of the sub-area can be self-sufficient in terms of heating and power?
- 2) Heat security: How secure and reliable would the supply option be?  
How many neighborhoods depend on delivered geothermal energy from others?
- 3) Inclusivity: How much of the district would be covered by LowEx district heating?
- 4) Technical feasibility: How complex would the proposed LowEx heat plan be in terms of technicalities and legal requirements?

These were each given a weighting factor based on its importance. For the first three criteria, the sub-areas were to be measured quantitatively, and the last criteria required a qualitative assessment. These are summarized below in Table 11.

Table 11: Summary of the selected criteria and their weighting factors

<b>Criteria</b>	<b>Formula or Factors</b>	<b>Weighting factor</b>
Energy self-sufficiency	<u>Quantitative</u> : Percentage of heat suppliers and receivers with SL 1 relative to all suitable areas	0.15
Heat security	<u>Quantitative</u> : Percentage of heat suppliers relative to all suitable areas	0.25
Inclusivity	<u>Quantitative</u> : Percentage of all suitable areas relative to all observed areas	0.30
Technical feasibility	<u>Qualitative</u> : BHE configuration (borehole number, depth), number of PV installations, coverage of heating grid	0.30
Total		1.00

A rating scale of 1 (very low) to 5 (very high) was applied in the evaluation. For the quantitative criteria, the rating score was determined based on the result of the calculation. The score was given proportionately to the results, which come in percentages, from 1 (0% - 20%) to 5 (80% to 100%). The given score for each scenario and criteria shall be multiplied by the corresponding weighting factor. The values were summed up to give a total rating score of the sub-areas.

## 5. Results

This chapter consists of results from the technical potential analyses of shallow geothermal energy and solar energy, as well as the outcome of each scenario along with the evaluation of the sub-areas as a potential DH strategy. The complete tables of results, which the presented numbers, diagrams, and figures in this chapter are based on, are found in Appendix A, B, and C.

For greater comprehensibility when referencing, the grid cells are numbered from right to left row by row, starting from 1 at the first grid cell of the first row and ending at 110 at the last grid cell of the last row. These will be referred to as G-1 to G-110 in the current and upcoming chapters.

### 5.1. Shallow Geothermal Energy Potential

#### Potential Areas

The potential areas for BHE installation are displayed in Figure 14. The areas are found across the district with varied distribution, but no grid cell is completely covered by exclusion zones, except for grid cells that only slightly intersect the investigated area and are not completely contained within the boundary, such as G-68 and G-80. In this case, the parts outside the boundary but within the grid cells were not investigated.

The largest potential for BHEs can be seen in the eastern side of the district in G-39, G-52, G-53, and G-54 around the premises of the sports club. These consist of large open spaces and are only intersected by a few trees and smaller structures. Also, BHE potentials are generally found in private gardens and porches, as well as in pavements. The northern region and along the border, as well as parts of the western side, show a large amount of restricting objects, especially buildings, trees, and streets.

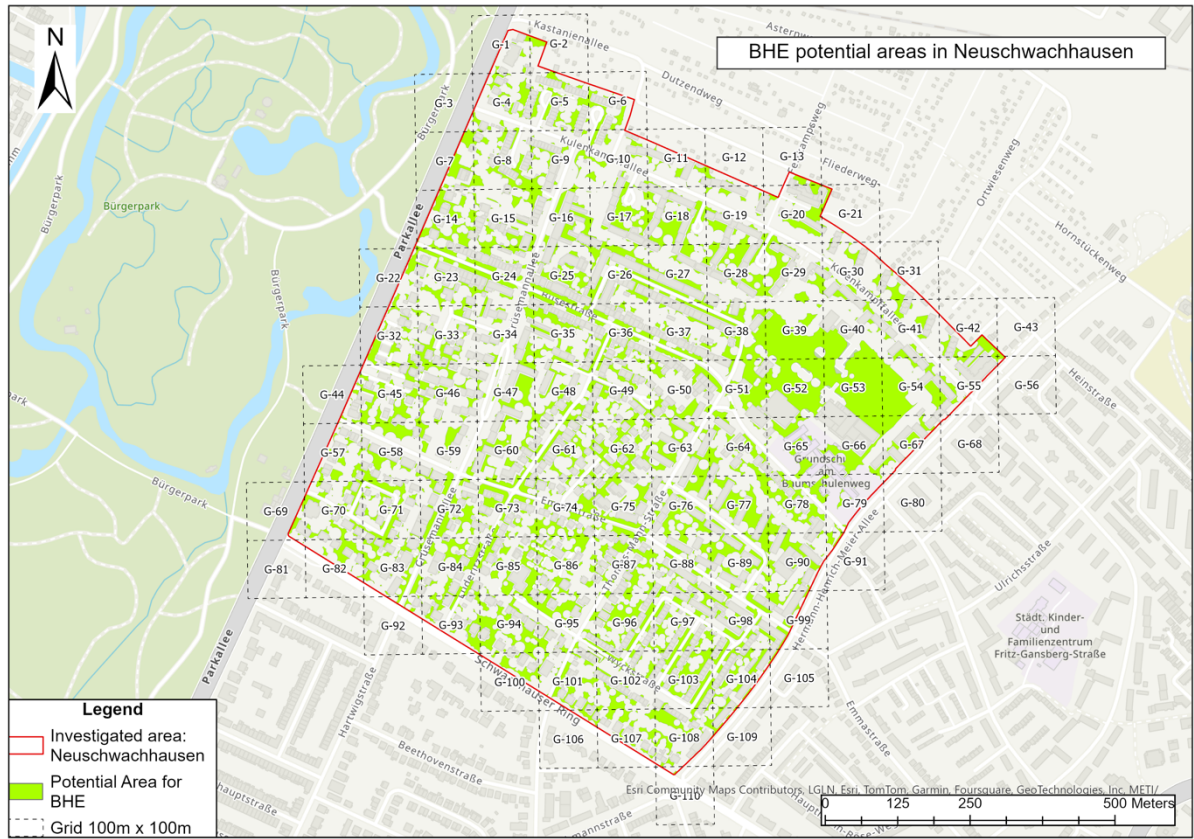


Figure 14: Potential areas for BHEs in Neu-Schwachsen



Figure 15: Close-up view of several of the defined exclusion zones for BHEs (Map: DOP10, © GeoBasis-DE / Landesamt Geoinformation Bremen 2023)

The maximum number of boreholes to be placed within the district is 6,621 for the BHE variant with 100 m depth and 2,240 for that with 300 m depth. Several single boreholes can be found in small polygons with an area of just above 2 m<sup>2</sup>. Figure 16 shows a detailed view of borehole placement of BHEs with 100 m depth and 300 m depth as an example. The alteration in spacing gives a similar reduction on a grid cell level to that of a district level (6,621 boreholes compared to 2,240), for example in G-24 60 boreholes can fit in the former variant compared to 25 boreholes in the latter (reduction = 60%).

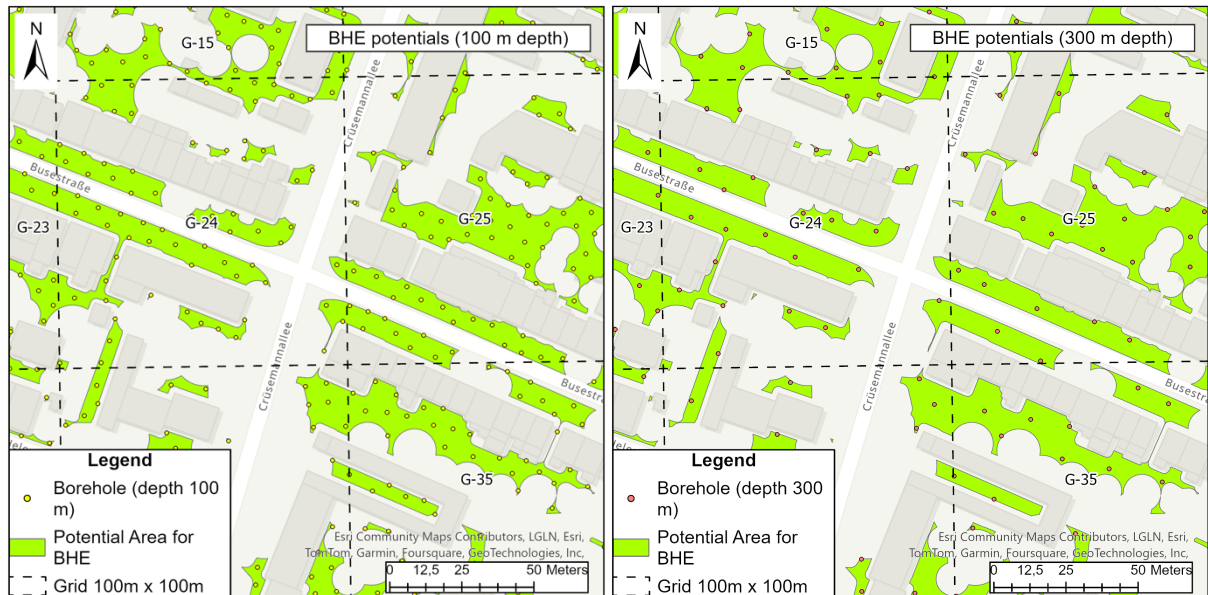


Figure 16: Comparison of possible borehole locations with 100 m depth (left) and 300 m depth (right)

### Simulation Results

A total of 16 simulations were conducted in EED, with 5 simulations each for S-2022, S-2030, and S-2038-a, and one simulation for S-2038-b. The results are presented in Table 12.

Simulations with a higher borehole number reveal lower specific heat potential per borehole. For BHEs in 100 m depth, the heat potential differs by approximately 120 - 150 kWh/a with every 0.1 W/mK change in STC when observed on a singular level. Between simulations for S-2022 and S-2038-a, in which the same borehole number is used, the change from 100 m to 300 m depth increases the heat potential by 3 to 3.6 times despite of the much lower STC in the latter scenario.

Table 12: Simulation results from EED for the scenarios S 2022, S 2030, S 2038-a (depth 100 m) and S 2038-b (depth 300 m).

STC		Depth 100 m, Spacing 6 m					Depth 300 m, spacing 10 m
		1.2 W/mK	1.3 W/mK	1.4 W/mK	1.5 W/mK	1.6 W/mK	0.96 W/mK
S 2038	A	132,000	138,000	143,000	149,000	155,000	246,000
	B	56	56	56	56	56	20
	C	2,357	2,464	2,554	2,661	2,768	12.300
S 2030	A	109,000	114,000	119,000	124,000	128,000	-
	B	42	42	42	42	42	-
	C	2,595	2,714	2,833	2,952	3,048	-
S 2022	A	68,000	71,000	75,000	78,000	81,000	-
	B	20	20	20	20	20	-
	C	3,400	3,550	3,750	3,900	4,050	-

**A** = Maximum base heat load in kWh/a

**B** = Boreholes

**C** = Estimated potential per borehole in kWh/a



Technical potential

The total technical potential for the four scenarios is as follows:

*Table 13: Summary of the total technical potential of shallow geothermal energy*

<b>Scenario</b>	<b>Heat potential in MWh/a</b>
S-2022	6,596
S-2030	11,727
S-2038-a	15,174
S-2038-b	27,552

The results for heat potential are illustrated per grid cell in Figure 17 and Figure 18. The values are classified into 8 groups with intervals of 50,000 kWh/a. In the first scenario (S-2022) with only 30% of the maximum potential used, most of the grid cells have enough potential areas to generate at least 50,000 kWh/a. The highest potential is found in G-53. When maximizing its potential at 100 m depth, the area can provide up to 360,000 kWh/a of geothermal energy, making it the only grid cell showing a maximum potential above 350,000 kWh/a.

The second scenario (S-2030) nearly doubles the total potential, and the highest numbers are seen concentrated around the mentioned area. The impact of the increased area usage from 30% to 70% is also evident (though not as significant) in the southern region of the district.

S-2038-b greatly increases overall geothermal potential in the district. The highest values can be found concentrated in the mid-southern region of the district around G-86, in the mid-western region around G-23, and in the northern half from G-26 to G-53 on the eastern side. The latter region consistently provides the highest energy potential at 528,900 kWh/a. In total, 25 grid cells can now reach heat potentials above 350,000 kWh/a. The median heat potential per grid cell lies at 289,050 kWh/a, almost doubling the value in the 100 m variant (S-2038-a) which lies at 155,571 kWh/a.



Figure 17: Technical potential of shallow geothermal energy in the scenarios S-2022 (top) and S-2030 (bottom) clustered in grid cells



Figure 18: Technical potential of shallow geothermal energy in the scenarios S-2038-a (top) and S-2038-b (bottom) clustered in grid cells

### Method Applicability

The statistical distribution of BHE installations per grid cell (at max. potential) is shown in Figure 19. For the 100 m and 300 m variants, the mean values are 56 and 20 whereas the median values are 64.5 and 23.5, respectively.

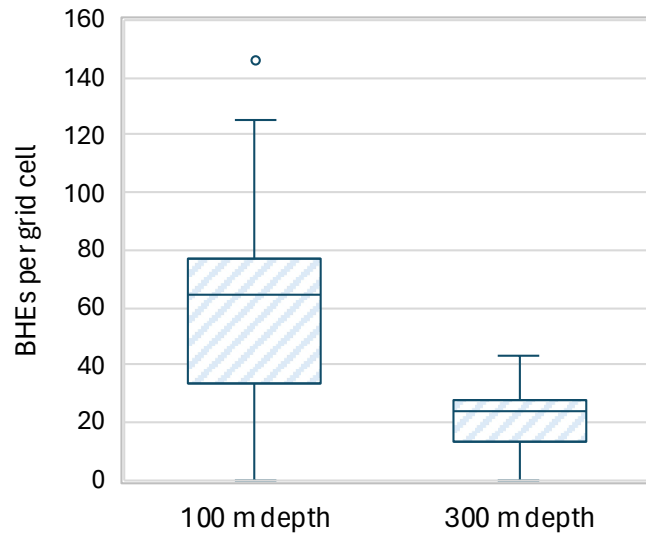


Figure 19: Statistical distribution of BHEs per grid cell in 100 m and 300 m depth

For the applicability test of the method, the selected grid cells are G-53, G-81, G-89, and G-106. The comparison between the test result and the estimated heat potentials in S-2038-a, as presented previously, is displayed in Table 14.

Table 14: Results of the plausibility check compared to the estimated max. potentials in 100 m depth

	<b>G-81</b>	<b>G-106</b>	<b>G-89</b>	<b>G-53</b>
BHE number	1	8	80	146
Estimated heat potential per BHE in kWh/a	2.357	21.179	204.286	359.786
Heat potential per BHE according to test in kWh/a	8.500	44.000	182.000	265.000

The test result shows a much higher heat extraction potential in grid cells G-81 and G-106, in which a few BHEs are simulated, by a factor of 3 to 4 compared to the estimation result in the scenario. In contrast, a lower heat extraction is observed in G-89 and G-53 in which numerous BHEs can be installed. Figure 20 reveals deviations between the two results as well as between the number of BHEs in the grid cell and the overall mean.

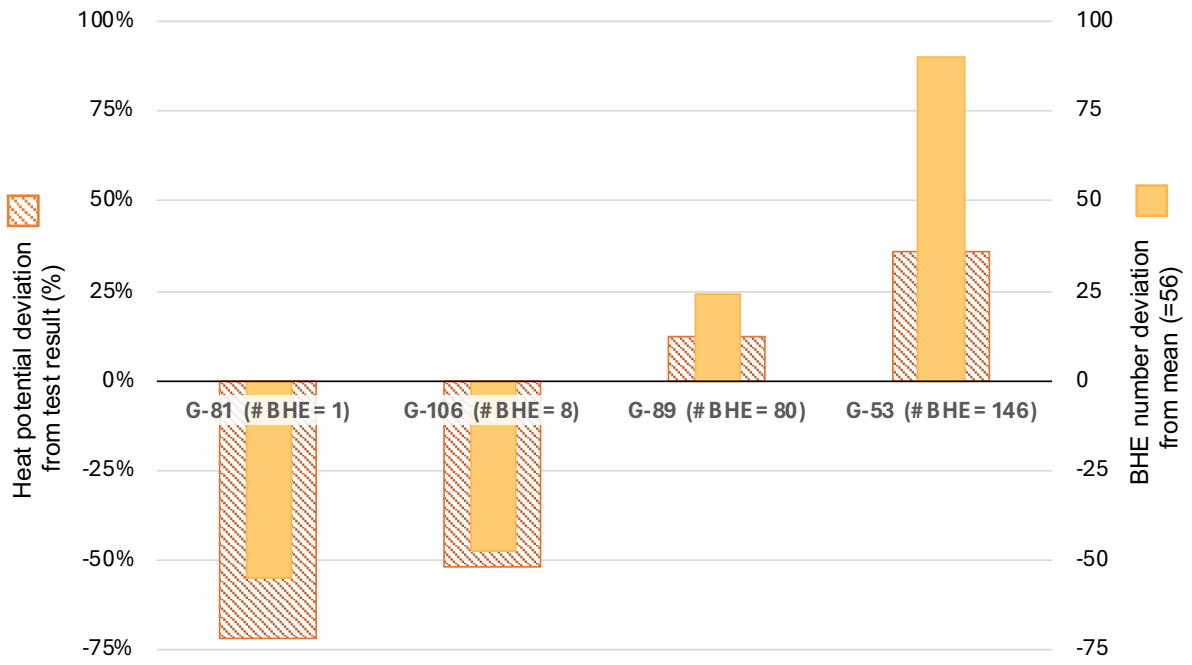


Figure 20: Deviation in sampled grid cells in terms of heat potential and BHE number

## 5.2. Solar Energy Potential

### Simulation Results

Table 15 presents an overview of the 11 simulations in Polysun, each with varying “mean aspect” and “mean slope” as input variables. The resulting energy yield is presented in the last two columns. Pitched roofs are presented in simulations no. 1 to 8, and flat roofs are presented in simulation no. 9. Results from simulations no. 10 and 11 represent the PV modules on solar parking lots.

All pitched roofs within the study area, regardless of aspect, have an average slope of around 31° to 38° in the flatter group (10° - 50°) and 53° to 55° in the steeper group (50° - 90°). The highest energy yield at 188 kWh/m<sup>2</sup>a is achieved by PV on less inclined roofs with SSW orientation (simulation no. 5). On the contrary, PV on pitched roofs with ESE orientation and higher inclination would deliver only 169 kWh/m<sup>2</sup>, which is the lowest out of the roof simulations. Modules facing opposite directions at a low slope, as in the simulations for solar parking lots, deliver yields that differ by 11 kWh/m<sup>2</sup>a. The lowest energy yield overall results from the NE-oriented variant at 155 kWh/m<sup>2</sup>a (simulation no. 11).

*Table 15: Simulation results from Polysun*

Subcategory	Slope	Simulation	Input: mean aspect (°)	Input: mean slope (°)	Energy yield of 10 modules (kWh/a)	Specific energy yield (kWh/m <sup>2</sup> a)
ESE, aspect 90° - 135°	10° - 50°	1	61.3	38.3	2,897	171
	50° - 90°	2	55.7	53.0	2,854	169
SSE, aspect 135° - 180°	10° - 50°	3	42.7	30.5	3,073	182
	50° - 90°	4	41.7	55.1	2,977	176
SSW, aspect 180° - 225°	10° - 50°	5	-27.4	38.1	3,176	188
	50° - 90°	6	-28.8	55.0	3,071	182
WSW, aspect 225° - 270°	10° - 50°	7	-46.8	33.0	3,029	179
	50° - 90°	8	-47.0	52.8	2,933	174
FR, all aspects	< 10°	9	-35.0	35.0	3,127	185
PL, SW	-	10	-40.0	5.0	2,812	166
PL, NE	-	11	140.0	5.0	2,613	155

Out of all the defined “flat roofs”, the average aspect is  $-35^\circ$  for south-west and  $55^\circ$  for south-east orientation. These two groups have orientations that are almost exactly perpendicular to one another. On flat roofs, PV modules could be installed optimally facing any of the two directions. However, the solar irradiation at  $-35^\circ$  is expectedly higher compared to  $55^\circ$  (less deviation from true south at  $0^\circ$ ), hence, the south-west orientation was chosen along with the ideal inclination of  $35^\circ$  for the substructure for all PV installations on flat roofs. This subcategory demonstrates the second-highest yield at  $185 \text{ kWh/m}^2\text{a}$  in comparison to the rest.

### Technical Potentials

The total technical potential for the four scenarios is as follows:

*Table 16: Summary of the total technical potential of solar energy*

	<b>Total capacity</b>	<b>Total energy yield</b>	<b>Specific energy yield</b>
S-2022	4.7 MWp	4,447 MWh/a	941 kWh/kWp
S-2030	9.9 MWp	8,986 MWh/a	912 kWh/kWp
S-2038-a and S-2038-b	10.1 MWp	9,160 MWh/a	908 kWh/kWp

The first scenario provides the lowest possible capacity overall at 4.7 MWp. The value is doubled to 9.9 MWp, then raised slightly to 10.1 MWp in the subsequent scenarios. The order of the annual specific yield is inverted, with 941 kWh/kWp being the highest achieved in the first scenario and 908 kWh/kWp as the lowest shown by the last two scenarios.

The pitched roofs in the district consist mostly of roofs with high PV adequacy (= adequacy level 2) in terms of area. The ones with very high adequacy (= adequacy level 1) make up a smaller proportion, but the difference between the two is less significant when observing the total yield. The roofs could generate 4,447 MWh/a in S-2022 compared to 8,966 MWh/a in S-2030, in which the two adequacy levels are combined. Transforming the identified parking lots to solar parking lots by 2038 could deliver an additional 173 MWh/a, boosting the maximum potential in the district to 9,160 MWh/a.

Figure 21 illustrates the proportion of each subcategory in the district’s total potential. Regardless of adequacy levels, pitched roofs with lower inclination ( $10^\circ - 50^\circ$ ) and an SSW orientation have the largest solar energy potential, followed by those with an ESE orientation and similar inclination. Steeper roofs ( $50^\circ - 90^\circ$ ) overall provide little potential, of which the

lowest can be observed in roofs facing ESE, SSE, and WSW with only very little contribution at below 1%. Less than 5% is delivered by flat roofs.

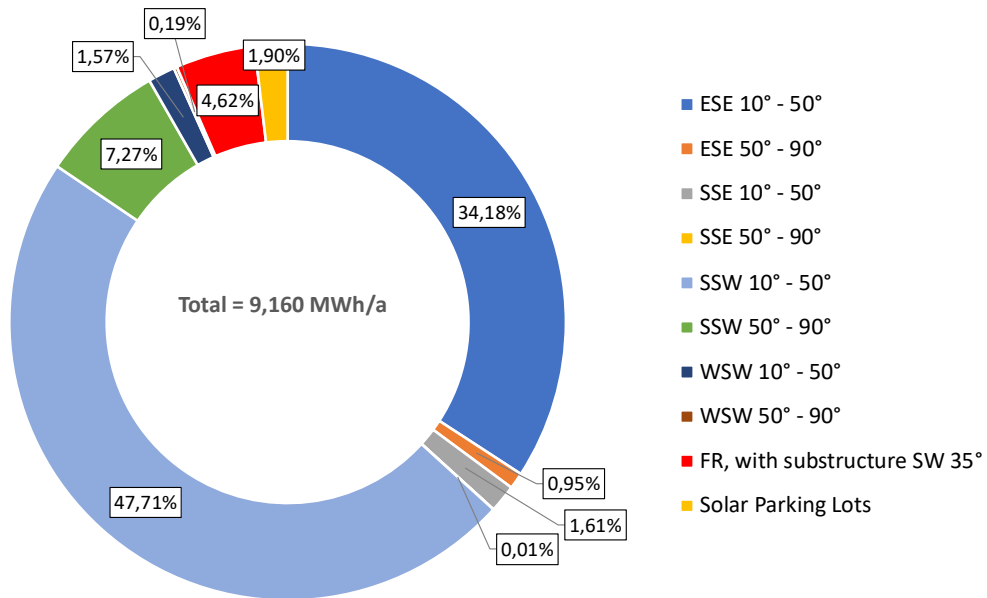


Figure 21: Proportions of PV sub-categories in the total technical potential

The distribution of solar energy potential is displayed in Figure 22 and Figure 23 in equal intervals of 30,000 kWh/a. Using only roofs with very high PV adequacy, as observed in S-2022, shows a fairly uneven distribution of power generation. In all scenarios, the areas with the highest potential are seen in G-25 and G-26 at a maximum of about 213,000 kWh/a and 234,000 kWh/a respectively. This is also noticeable in the central to southern region in the later scenario S-2030, precisely in G-63 and the surrounding neighborhood to the south. Using all suitable roofs, as in S-2030, results in a less sparsed yield distribution. Some concentration can be seen in the upper, central, and southern parts of the district. Out of all the grid cells that are completely contained within the defined boundary, only G-39 and G-53 display solar potential below 30,000 kWh/a.

A median yield of 83,173 kWh/a per grid cell could be achieved by 2038 once the solar parking lots are implemented. All cells would profit equally from this measure by 1,580 kWh/a. This corresponds to only 0.5% of the defined interval shown in the figures, thus the spatial distributions in S-2030 and both scenarios of S-2038, as presented in Figure 22 and Figure 23, do not differ significantly from each other. Nevertheless, class changes are visible in G-16, G-45, G-51 and G-66.



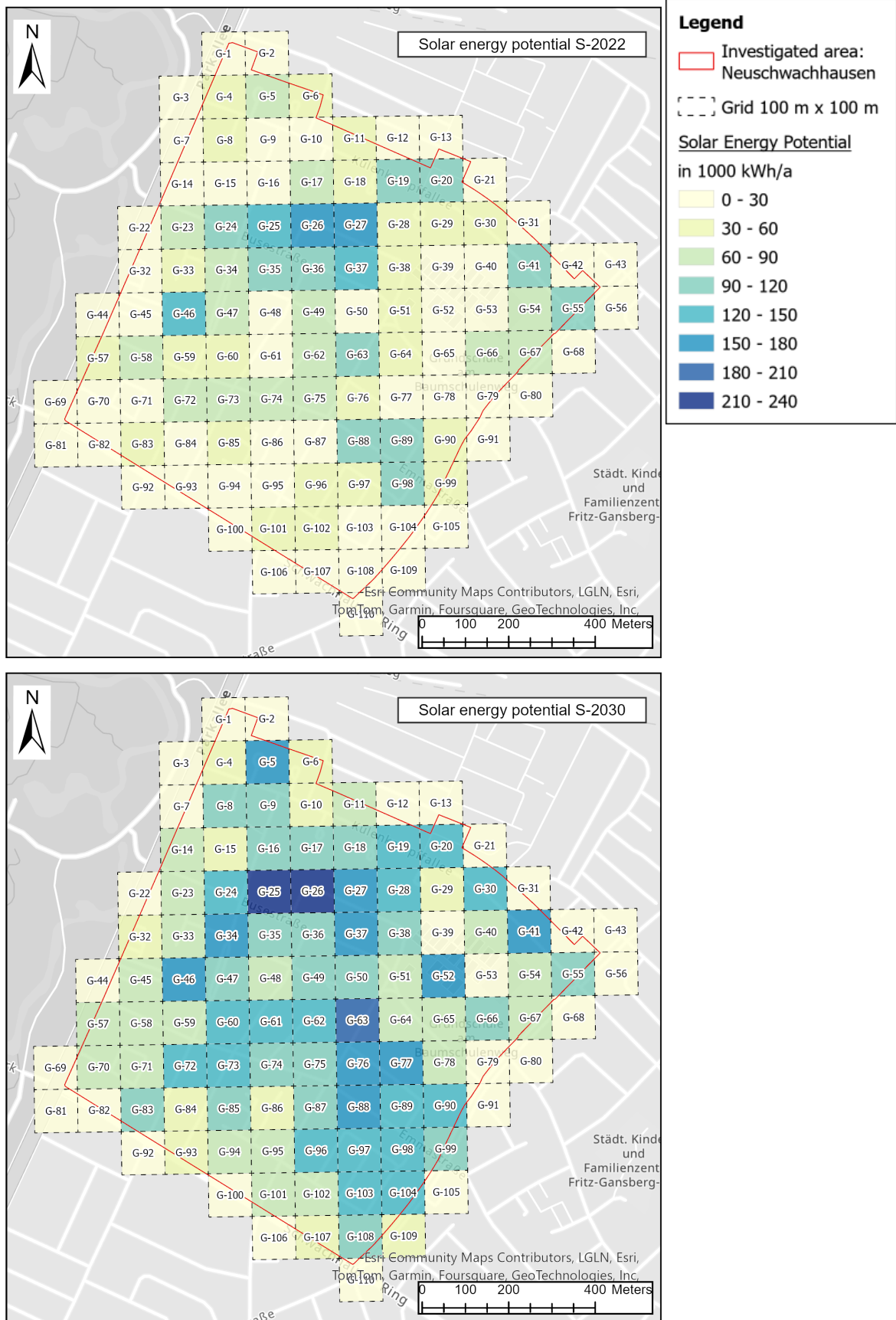


Figure 22: Technical potential of solar energy in S-2022 (top) and S-2030 (bottom) clustered in grid cells

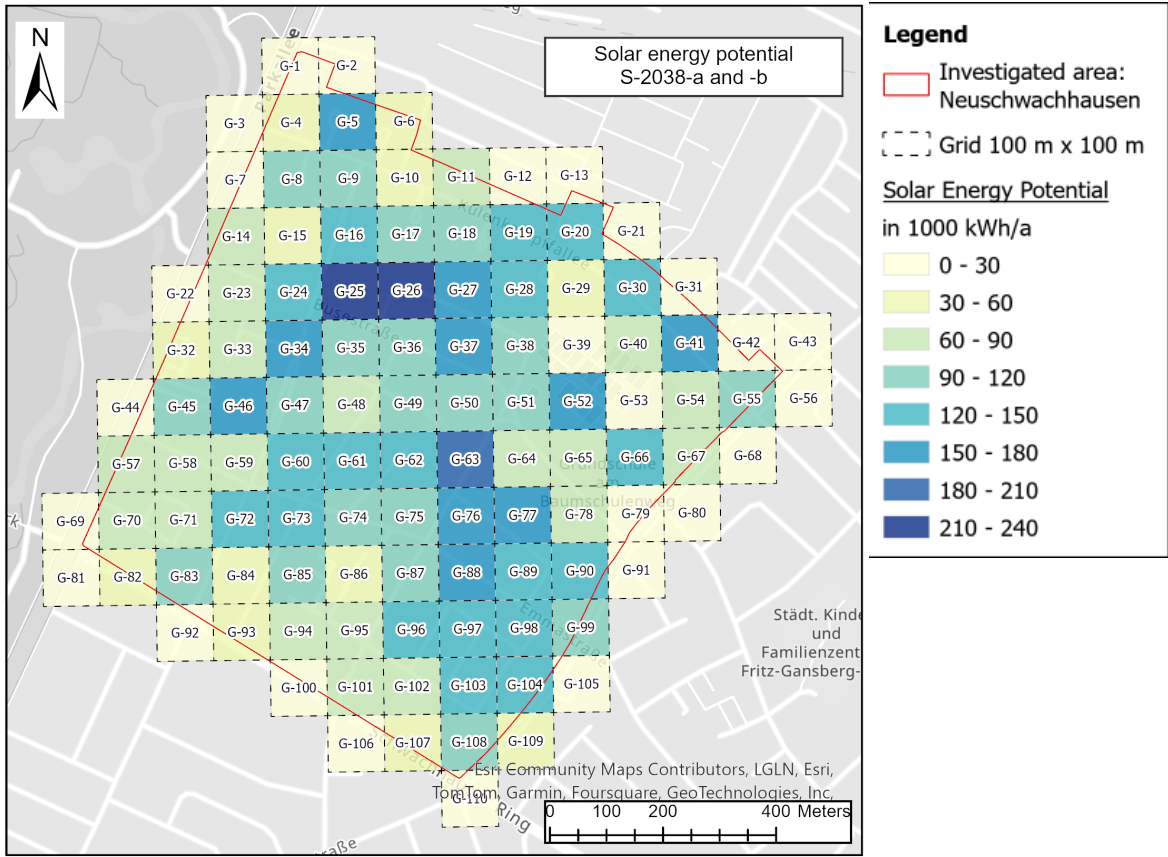


Figure 23: Technical potential of solar energy in S-2038-a and S-2038-b clustered in grid cells

### 5.3. Scenario Outcomes

This subchapter presents the result from the interpolation and clustering of given heat demand data and the consequent power demand. The combined outcome of energy potential and demand and the resulting sub-areas in each scenario are presented as well.

#### 5.3.1. Heat and Power Demand

The heat and power demand observed in the scenarios are as shown below.

*Table 17: Overview of the observed heat and power demand in all scenarios*

<b>Values in MWh/a</b>	<b>S-2022</b>	<b>S-2030</b>	<b>S-2038-a and b</b>
Total heat demand	37,374	28,506	22,706
Total power demand	12,458	9,502	7,569

The decrease from S-2022 to S-2030 is steeper than from S-2030 to S-2038 in both aspects. The interpolation for S-2038 resulted in a total heat demand of 22,706 MWh/a. The power demand here is estimated to be reduced from 12,458 MWh/a as of status quo to 9,502 MWh/a in S-2030, then to 7,569 MWh/a in the S-2038-a and -b. The values in the last two scenarios correspond to 60 - 61% of those in the first.

The clustered heat demand data in all scenarios are shown in Figure 24 and Figure 25. The highest values are most prominent in the northern and southern regions of the district. G-18 shows the highest heat demand at 933,700 kWh/a in S-2022. This number can be reduced to 575.727 kWh/a in S-2038-a and -b. The area with the lowest heat demand is mostly found in the eastern region. A separate figure for power demand is omitted here since power demand is directly proportional to heat demand and the spatial distribution in equal intervals would be identical.



Figure 24: Heat demand distribution in S-2022 (top) and S-2030 (bottom) clustered in grid cells

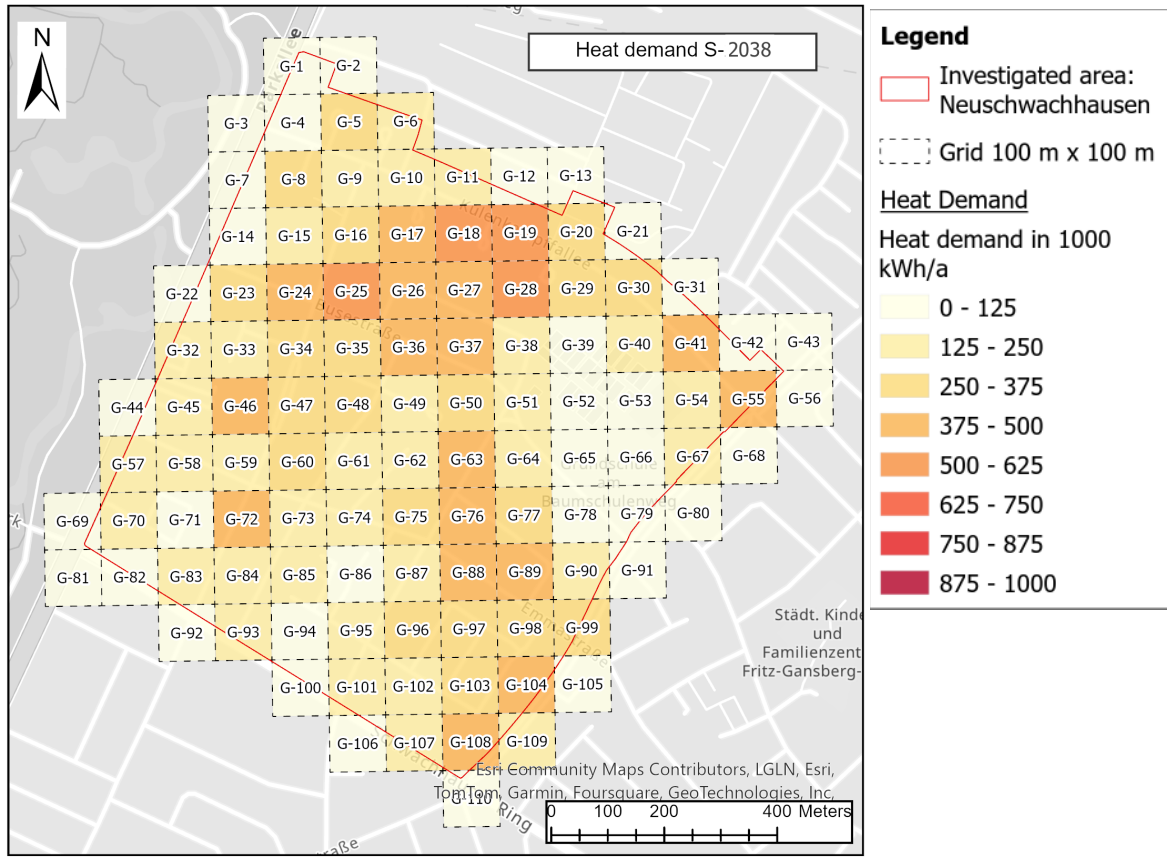


Figure 25: Heat demand distribution in S-2038-a and -b

### 5.3.2. Energy Potential and Demand Gap

As indicated previously, there are several grid cells only intersecting slightly with the study area boundary. These lack sufficient data to be compared with the rest and to be analyzed in terms of sub-area suitability. Therefore, grid cells whose center point does not lie within the border are excluded from here on. The number of observed grid cells is reduced to 84.

The number of grid cells with heat and power surplus is presented in Table 18. S-2022 shows the least number with 5 and 1 for heat and power, respectively. The number rises to 50 and 66 in S-2038-b. The preceding scenario has the largest difference between the two values (= 41) while the first scenario has the lowest (= 4). It is also the only occurrence where the number of heat excess areas surpasses that of power.

Table 18: Number of grid cells with heat and power surplus out of the observed 84 in all scenarios

	S-2022	S-2030	S-2038-a	S-2038-b
Heat surplus	5	9	25	50
Power surplus	1	41	66	66

The distributions of heat and power gap are displayed together in Figure 26 and Figure 27. The heat gap is classified into 10 groups with intervals of 80 kWh/a with the value 320,000 kWh/a set as the observation limit in both heat surplus and deficit. Grid cells with values beyond that in the negative or positive range are considered extreme values and are viewed as similar regardless of the actual number. The proportion of power gap is only shown for those grid cells that lack solar energy potential (power gap < 0%). Grid cells with sufficient potential to cover their demand (power gap  $\geq$  0%) can be distinguished by the missing hatched pattern.

The most prominent outcome in S-2022 is that most areas have large energy potential and demand gaps. Extreme heat deficit (below -320,000 kWh/a) is visible from the northern to the southern part of the district. The largest region with both heat and power deficit is shown in the mid to northern part around G-26. Among those grid cells with extreme deficit, only G-27 and G-20 display a power gap above -30%. Five areas showing heat surplus include the mid-eastern region around G-53, leading with values between 80,000 and 160,000 kWh/a. In the southern region, G-86 is noticeable as the only area with heat surplus.

In S-2030, the defined classes appear to be more evenly distributed. While most areas still show heat deficit, many with extreme values in the previous scenario have now shown significantly more heat potential and even sufficient PV potential. Heat surplus is still found concentrated on the eastern side around G-53. Individual areas, G-86 and G-94, also appear to show energy sufficiency in both heating and power.

Compared to the previous scenario, S-2038-a displays much more distributed areas with heat surplus, though most are below 80,000 kWh/a. These areas all show sufficient PV potential to cover the required power. Overall, a deficit in solar power potential is only apparent in 16 areas with a slight concentration in the north of the district around G-19. Extreme heat surplus is expected in G-53, followed by its neighboring areas G-52 and G-39.

In S-2038-b, all three grid cells can achieve extreme values (above 320,000 kWh/a). Areas in the mid-southern region around G-86 also show a very high heat surplus. While the majority within the district shows enough heat potential to meet the demand, there are 34 areas that do not. The northern neighborhoods around G-18 and G-19, and the far eastern area in G-55 are the areas with the three highest heat deficits at below -240,000 kWh/a. The highest negative at nearly -326,000 kWh/a is apparent in G-19. The two final scenarios differ significantly from each other in terms of heat gap while the power gap remains constant due to the identical conditions for solar energy.

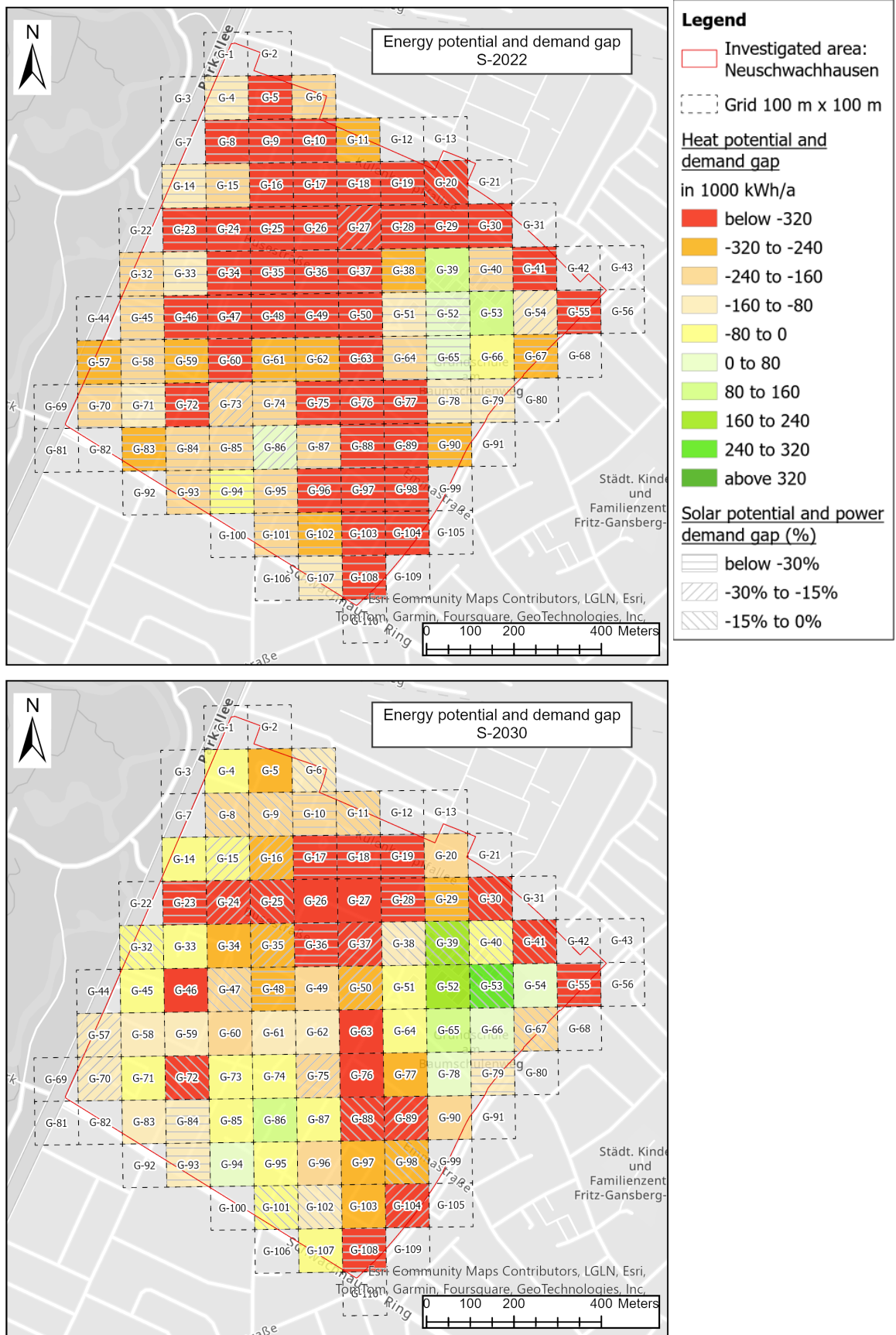


Figure 26: Geothermal potential and heat demand in comparison to solar energy potential and power demand in S-2022 (top) and S-2030 (bottom) clustered in grid cells

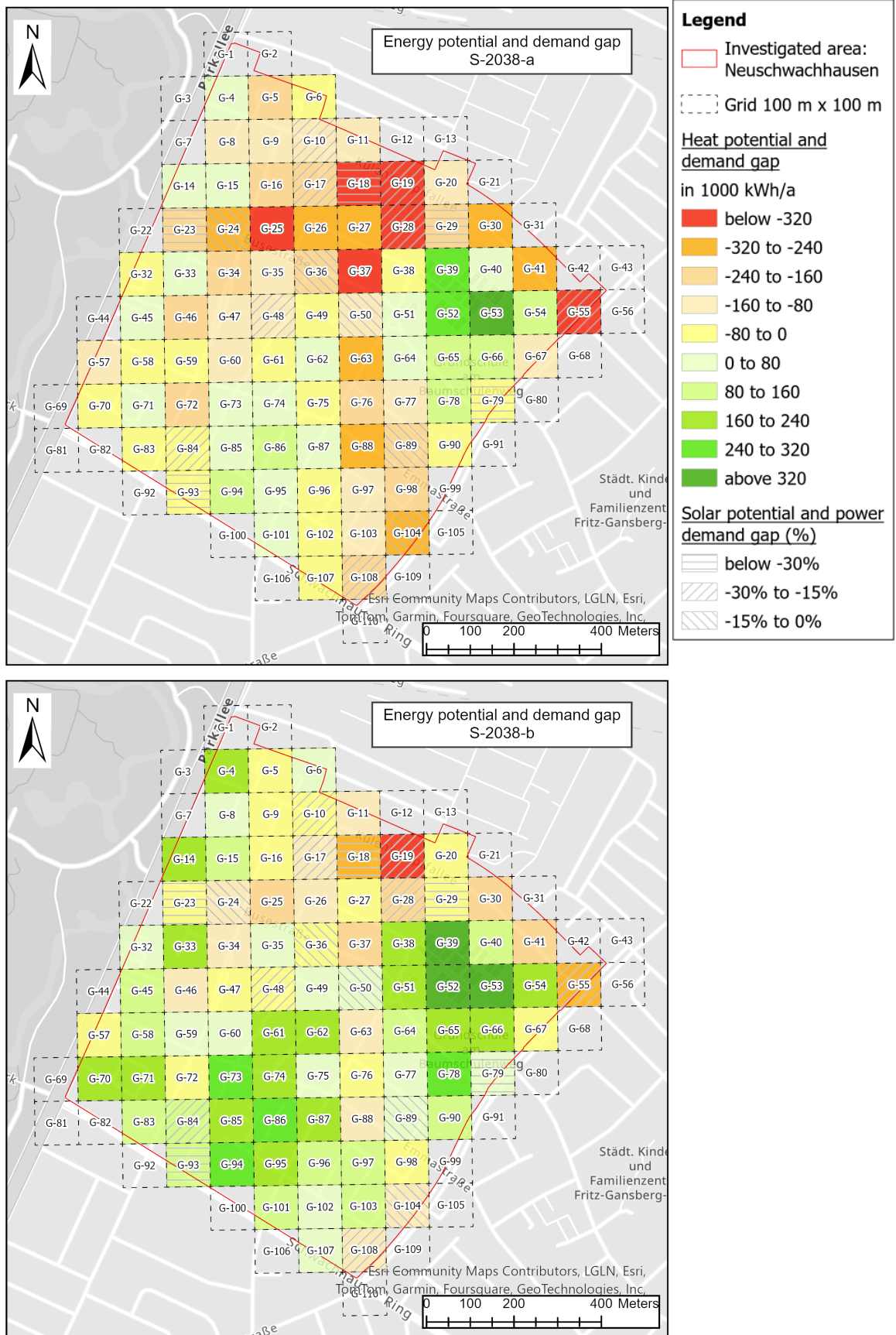


Figure 27: Geothermal potential and heat demand in comparison to solar energy potential and power demand in S-2038-a (top) and S-2038-b (bottom) clustered in grid cells



### 5.3.3. Sub-Areas for LowEx District Heating

Based on the findings presented previously, the suitable sub-areas for LowEx district heating were identified and are depicted in Figure 28 and Figure 29. The potential areas are grouped according to the suitability levels (SL) as “heat supplier” and “heat receiver”.

The first scenario (S-2022) shows four potential neighborhoods as one joint sub-area and one single sub-area. G-39 and G-53 on the eastern side appear to be the only heat suppliers with very high suitability. The neighboring cell G-66, which covers buildings of the sports club, has the most adequate circumstance in this scenario to join as a heat receiver. The single sub-area in the mid-southern region (G-86) requires more power than its own PV system could provide, and so is noted with the SL 3.

Both sub-areas appear to have expanded in S-2030, creating five more suppliers in the mid-eastern region. This remains the strongest in terms of potential for heat generation and distribution. Two neighborhoods with SL 2 have also appeared as suitable heat receivers of G-39. Furthermore, the region around G-86, in which multiple detached and semi-detached houses dominate, appears to have gained several receivers – five of which with SL 1 and one with SL 2. There are no neighborhoods with medium suitability (SL 3) in this scenario.

In scenario S-2038-a, the two separated sub-areas have expanded in opposite directions leaving a “strip” of areas marked unsuitable, which covers dense neighborhoods, from G-37 all the way south to G-108. The only grid cell with SL 3 is G-84 as a heat receiver. In the north-western corner of the district, there are areas covering only a few detached houses with large gardens that are identified as very suitable heat suppliers. However, these sub-areas are disconnected from the rest.

S-2038-b presents many neighborhoods with medium to very high SL, nearly covering the whole district. In this case, these would be joined together to create a large sub-area with a LowEx heating network. Out of the identified potential areas, the two lower categories (SL 2 and SL 3) are only apparent in 5 grid cells each. The northern region of the district around G-18 is the only remaining large area that is deemed unsuitable. The only neighborhood almost completely enclosed by sub-areas is G-29.



Figure 28: LowEx sub-areas in S-2022 (top) and S-2030 (bottom) ranked by their suitability



Figure 29: LowEx sub-areas in S-2038-a (top) and S-2038-b (bottom) ranked by their suitability

### 5.3.4. Evaluation

Applying the evaluation method presented in Chapter 4.6, the sub-areas were assessed according to the four defined criteria. For the first three criteria, the scores were determined quantitatively as presented below.

*Table 19: Numbers for the quantitative evaluation of the sub-areas and the results*

		<b>S-2022</b>	<b>S-2030</b>	<b>S-2038-a</b>	<b>S-2038-b</b>
	Grid cells considered	84	84	84	84
	Number of areas with SL1	8	19	42	60
	Number of suitable areas	9	22	43	67
	Number of suppliers	7	16	30	46
Sub-areas criteria	Energy self-sufficiency	60.0%	84.2%	97.6%	86.3%
	Heat security	60.0%	47.4%	59.5%	65.8%
	Inclusivity	6.0%	22.6%	50.0%	86.9%

The result ranks the large sub-area of S-2038-b as the highest, followed by those of S-2030 and S-2038-a with the same total score, then the smaller sub-areas of S-2022 with the lowest rank. The rating scores given to each scenario are shown as follows in Table 20.

*Table 20: Evaluation of the sub-areas in all scenarios using a scale of 1 (very low) to 5 (very high)*

<b>Criteria</b>	<b>Weighting factor</b>	<b>S-2022</b>	<b>S-2030</b>	<b>S-2038-a</b>	<b>S-2038-b</b>
Energy self-sufficiency	0.15	3	5	5	5
Heat security	0.25	3	3	3	4
Inclusivity	0.30	1	2	3	5
Technical feasibility	0.30	5	4	3	1
<b>Total</b>		<b>3.00</b>	<b>3,30</b>	<b>3,30</b>	<b>3,55</b>

Concerning its energy self-sufficiency, the first scenario (S-2022) is ranked lower with a score of 3 than the other following scenarios with 5. More than 65% of the sub-areas in S-2038-b are heat suppliers, so the scenario (S-2038-b) is expected to have the highest security and reliability in providing geothermal heat with a score of 4. All three preceding scenarios are less secure in this aspect and were equally given a score of 3. The rating score regarding inclusivity increases chronologically with each scenario. The biggest difference is between the last two variants, which shows a leap from 3 to 5 (S-2038-a and S-2038-b).

As the only qualitatively measured criteria, the max. score regarding technical feasibility is attained by the first scenario (S-2022) due to the following circumstances: Here, the heat

suppliers only have a few non-residential structures. The open space would give less complexity in borehole drilling, and with only two heat receivers, hence less heat demand to cover, the potential heating grid can be restricted to only that relatively small region. Overall, there is still relatively little power demand within the defined sub-areas, meaning PV modules would remain limited. The other single-cell sub-area also indicates that the installation of the necessary technologies and pipelines would be much less complicated. With increasing BHE and PV installations and the expanding heating grid, the rating score decreases by 1 for each subsequent scenario until 2038-a before the larger leap by 2 for S-2038-b due to the extension of borehole depth from 100 to 300 m, which requires much more intensive drilling. Hence, the lowest score for technical feasibility is given to the sub-area of the last scenario.

## 6. Discussion

This chapter summarizes and discusses the findings in the context of the defined objectives. The obtained results focusing on the sub-areas are discussed in the following sub-chapter, while the overall proposed workflow is assessed in the next sub-chapter.

### 6.1. LowEx District Heating Strategy

According to the findings on geothermal and solar energy potentials as well as heat demand distribution, the sub-areas for LowEx district heating (DH) are expected to rise gradually in size and number when analyzed from a temporal perspective. The evaluation shows that the optimistic scenario S-2038-b leads in terms of overall quality, meaning that the conditions set here are technically ideal. Therefore, the second research question as stated in Chapter 1.2 is answered: from a technical perspective, Neu-Schwachhausen hosts a great potential of LowEx DH as a heating strategy if circumstances regarding heat demand as well as green energy availability and accessibility improve. The relevant aspects are clarified and discussed in detail in the following.

#### Ideal Conditions for Geothermal Energy

In the deciding criteria “heat security” and “inclusivity”, S-2038-b is rated high compared to the preceding scenario, from which it differs solely by the altered BHE configuration. BHEs at 300 m depth are expected to not only provide a much higher specific heat, as revealed in the simulation results in Chapter 5.1, but to also strengthen and expand the heat grid to numerous areas that were previously deemed unsuitable. It is understood, that expanding the borehole

to 300 meters would increase accessible temperatures by 6 K due to the geothermal gradient (Panteleit et al., 2022; Schiel et al., 2016). The result implies that this would be enough to raise the total potential from 15 MWh/a to 27.5 MWh/a, thereby gaining 25 neighborhoods with heat surplus, despite the expectedly poor STC of 0.96 W/mK. Furthermore, the larger heat potential would support the grid stability and sustainability (here measured as very high “heat security”) as revealed in the evaluation. At times of higher peak loads, the consumers within the sub-areas would be able to rely more on the additional extracted heat, than those with a lower proportion of heat suppliers to receivers. A less stable heat grid would face a greater possibility of supply shortage when seasonally stored heat is insufficient, such as on extremely cold days. This indicates the importance of high-capacity and efficient storage technologies especially under such circumstances, for example the use of reversible heat pumps to store any ambient heat from warmer months underground. Here, integrating a cooling network would perhaps be a good option as well (Cruickshank & Baldwin, 2022). However, the biggest disadvantage of boreholes at such depths is the preparation and installation phase, also summarized as “technical feasibility” in the evaluation. Drilling to a depth of 300 m is subject to technical and legal challenges that currently exist, specifically the additional obligatory approval according to § 7 BBergG and § 12 StandAG.

Furthermore, the geothermal potential analysis confirms that space availability in cities is extremely significant for total heat extraction, which was also acknowledged by Bayer et al. (2019). The challenge in residential districts is proven to be aerial restrictions, especially around buildings and other structures as well as trees. The last factor implies that measures regarding nature conservation would impede climate protection in this aspect as well, which is evident primarily during the installation phase due to the drill machines. With current additional restrictions regarding environmental protection in Neu-Schwachhausen (see Chapter 3), it is difficult to receive a permit to cut and replant trees in another location. Therefore, large open fields, such as around the sports club complex, would contribute greatly as a heat source and are crucial for the LowEx suitability of the neighboring areas. This is evident in S-2022 which, with only 30% of the geothermal potential, presents a sub-area that mostly depends on the heat from the fields. The analysis also demonstrates the importance of efficiently using the available space on and around residential properties – a benefit that typically detached houses have. Free space at row houses is typically restricted to smaller gardens and pavements. This is noticeable in Figure 30, which displays the contrast between neighborhoods that typically show a large geothermal deficit (in G-18 and G-19) and surplus (in G-86 and G-94). It also signifies the benefit of creating a heat network with shared sources that disregards the obligatory distance of 5 m to cadastral boundaries (Panteleit et al., 2022).

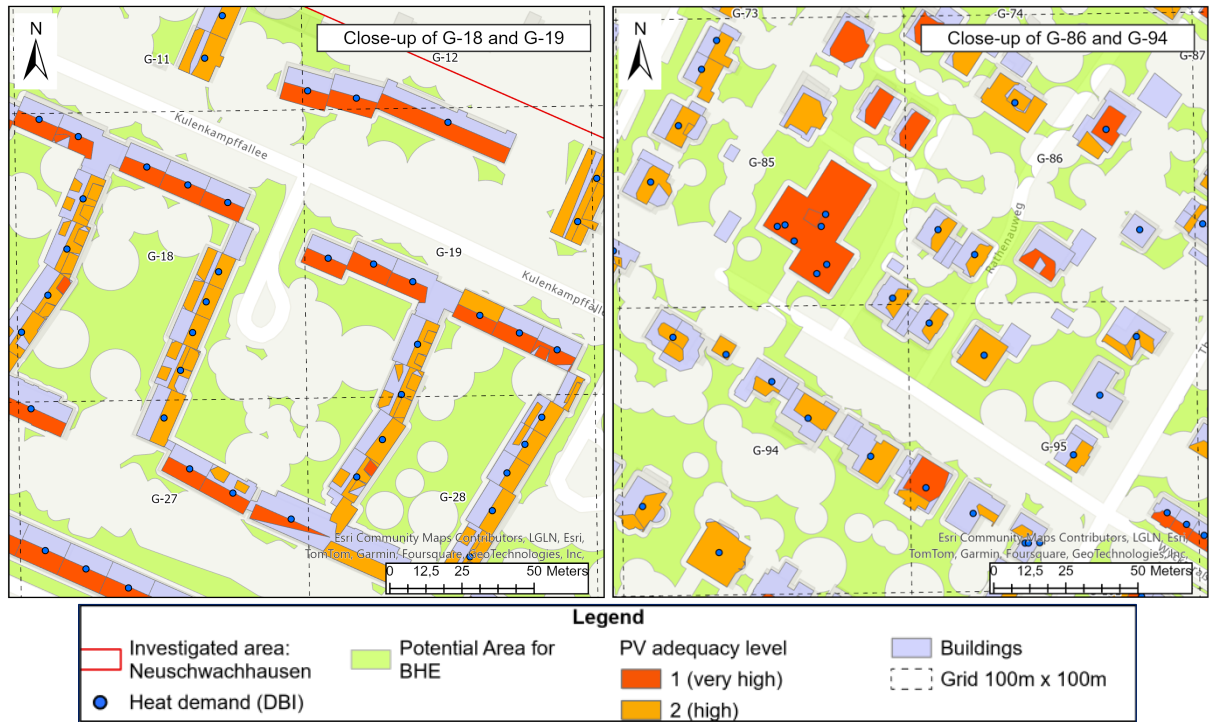


Figure 30: Comparison between densely (left) and sparsely built neighborhoods (right)

### Significance of PV Potential

The solar energy simulations confirmed the importance of optimal aspect and slope. Out of the observed roofs, the dominating roof subcategories are by far those with SSW and ESE orientation and inclination between  $10^\circ - 50^\circ$ . The latter subcategory is the less beneficial of the two since the roofs face away from the optimal south at a greater degree, which negatively impacts the yield (see Chapter 2.2). Buildings with ESE-oriented roofs had mostly been given the PV adequacy level of 2 in the original solar cadastre because of the lower specific yield. Nonetheless, the overall result indicates that its area availability and the resulting power potential should not be overlooked. For example, the densely built row houses in the northern region benefit from this – the combination of SSW and ESE orientation creates two areas (G-25 and G-26) with the highest solar potential energy. Also, in the south-eastern part of the district, Figure 31 shows that PV modules with ESE orientation may even help diminish the power gap, once they come into operation in S-2030. So, the primary focus with PV should be on the usage of SSW and ESE-oriented roofs when pursuing the creation of LowEx sub-areas with a high proportion of SL 1.

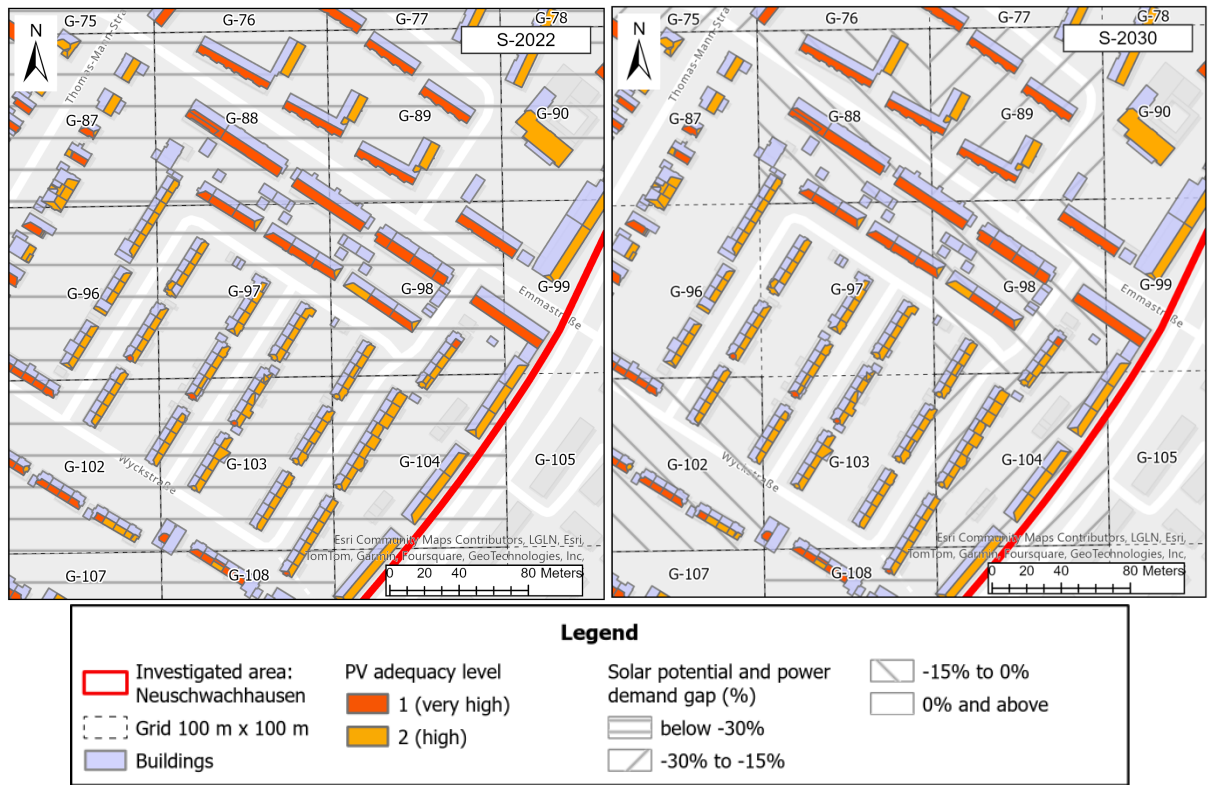


Figure 31: Effect of PV installation on ESE-oriented roofs on the power gap as observed from S-2022 (left) to S-2030 (right)

Consequently, highly efficient modules should be particularly given to ESE-oriented roofs to enhance the specific energy yield. This, while also considering the possibilities for efficient energy storage, would be relevant in realizing the areas of SL 1. Generally, full energy self-sufficiency can be achieved by increasing the self-consumption rate of the PV system, and the number of areas of SL 1 influences the criteria “energy self-sufficiency” in the evaluation. However, the given rating should also be interpreted critically. For example, the sub-areas of S-2022 are rated “medium” in this aspect, solely because the sports complex is identified as “heat suppliers” of SL 1 – though these, in fact, exclusively generate (without consuming) heat due to the lack of consumers within the grid cell. Thus, the bordering residential area (G-66) is the only “true” self-sufficient neighborhood in S-2022 by the arranged definition. This would expand if the potential areas for BHE and PV are used more efficiently like in the next scenarios. Poor energy self-sufficiency indicates a lower degree of climate neutrality overall, especially in the first scenario, since Germany’s power grid in 2022 was still dominated by fossil fuel sources (UBA, 2024a). The correlation between the two aspects should become less conclusive with time, presuming that nationwide power production will have zero-emission by 2045 as targeted in § 3 KSG. So, from this perspective, the sub-areas in S-2038-a and -b are more “climate-friendly” than those in S-2030 despite the same rating score for the criteria “energy self-sufficiency”.



### Challenges

The dilemma between BHE and PV is prominent in densely built areas. Especially small row houses often have gardens that could contain only a few BHEs but have enough roof area for higher yield by PV. In S-2030, many neighborhoods to which such houses belong display a heat potential shortage, yet technically have enough solar energy potential to cover the power demand. This leads to them being excluded as sub-areas if the surrounding neighbors are equally unsuitable, as is the case in the northern and western part of Neu-Schwachhausen until 2030 (compare Figure 26 with Figure 28 in Chapter 5.3).

When observing the impact of solar parking lots, results show it is less significant in terms of specific and total power generation. However, this workflow only gives a very rough estimation according to the average form of the parking lots, while assuming that all installed modules face either south-west or north-east at 5° inclination, which is less ideal for Bremen as explained in Chapter 2.2. Simulation results alone show that these configurations only produce 166 and 155 kWh/a, respectively, per m<sup>2</sup> of module area. A more detailed inspection of each parking lot is required, so that the optimal setup can be selected and a more accurate output examined, as emphasized in the study by Hochreutner et al. (2022). Such a feasibility study is desirable because within an already dense urban space, using every possibility efficiently and cleverly can considerably ease the path to reaching the climate protection goals of Bremen.

The results also underline the significance of heat demand reductions. An example can be seen between S-2030 and S-2038-a or -b. Although the solar parking lots only give a small boost of about 1,500 kWh/a per grid cell, reducing power demand enhances the outcome – thus neighborhoods with “power surplus” are extended from 44 to 61 (see Table 18 in Chapter 5.3.2). This implies that PV is an ideal supplement in modern, energy-efficient buildings as seen in the practical example in Wüstenrot (dena, 2021), hence the significance of building retrofits (BMWK, 2024; Lund et al., 2021) to positively alter the LowEx suitability level of many neighborhoods and achieve optimal sub-areas of high quality. This would be a heavy challenge for the district due to the dominating number of old houses. Further, the measures must be major enough that the energy demand could be reduced to at least 60% of current levels by 2038 based on the scenario outcomes (see Table 17 in Chapter 5.3.1). If only the impact on heating is considered, the reduction should be much greater for 100 m boreholes to be sufficient for most neighborhoods, since excess heat is still only generated in 25 out of 84 observed neighborhoods. Drastically restricting individual heat consumption through other actions would be a necessary addition to extend the inclusivity of the sub-areas in S-2038-a, for instance in cases where 300 m boreholes are not possible.

### Suggested Heating Strategy

The strategy of LowEx DH highly depends on the combination of heat demand reductions and effective use of space for the renewables. Though as partly mentioned, to maximize the inclusivity and self-sufficiency in the district, certain areas should still be provided with higher-efficiency technology. Investing in more powerful modules will become more feasible given the expected decrease in module costs with time (Wirth & ISE, 2023). Also, with heat pumps of higher efficiency, the power demand would automatically decrease – for example, raising merely the SPF from 3 to 4 would decrease the power demand by 24%. Another option would be to not implement LowEx DH and use a central heat pump for those regions. The cost for individual heat pumps could instead be spent on a large-scale heat pump with higher thermal output in total, as it is typically more cost-effective (Averfalk et al., 2021). An appropriate location for the large heat pump as well as the additional output gained, after considering the greater heat transport loss, would need to be identified in another study. Moreover, the potential solar parking lots can be a more effective addition if they are used as a direct supplement to the heat pump. A practical example of such systems is yet to be made.

Some dense neighborhoods with less geothermal potential even with 300 m deep BHEs (e.g. G-18 and G-19) may simply not be suitable for this concept of LowEx DH. An additional heat source such as air source heat pumps or solar thermal collectors might be the solution. Also, buildings with excessive solar energy potential would especially benefit from the thermal collectors, such as in S-2038-a with the highest ratio of power surplus to heat surplus. Instead of having unused valuable roof area, installing these could provide additional heat for buildings with limited geothermal supply, aid ground heat regeneration, and offer valuable seasonal storage when coupled with the BHEs (Cruickshank & Baldwin, 2022), similar to the system in Neckarsulm (dena, 2021). To which extent these alterations may positively impact the sub-areas needs to be explored in a subsequent study. The potential of incorporating wastewater heat, similar to the concept in the Tabakquartier (Justus Grosse, 2023), should be researched as well to support the supply in densely built areas and improve overall heat security.

To conclude, some areas should be prioritized in the planning, including neighborhoods surrounding the sports club complex and those in the southern region with the several detached houses and large gardens. Several areas with lower geothermal potential can benefit much more from the 300 m deep boreholes so the approval procedures should be eased. However, it is important to remember that this represents an ideal situation by excluding the factor “economic feasibility” of the sub-areas. As explained in Chapter 2.3, LowEx DH is less competitive in areas of lower heat demand density, mainly because of the high specific capital costs (Averfalk et al., 2021). Considering the occurring costs for BHE installations alone, which could reach up to 70 €/m (Bockelmann et al., 2019), boreholes with 300 m depth as suggested

in S-2038-b might not be feasible in this magnitude if current financial circumstances do not improve. An option to minimize the costs would be limiting 300 m boreholes to only areas in which the heat extraction at 100 m would be insufficient. Other measures that were discussed require a tremendous amount of costs. This highlights the importance of financial assistance from the local and national government in the form of subsidies and bonuses, such as the support for purchasing heat pumps, building retrofits, and establishing the necessary pipelines offered as part of the new BEG and BEW programs. With the upcoming regulation following the Climate Protection Strategy 2038 that obliges solar parking lots in Bremen, the expensive installation should be partially funded through similar programs – the state of Baden Württemberg gives a good example in this aspect (UMBW, 2024). The necessity is greater in Neu-Schwachhausen since, possibly, the identified parking lots could only deliver a lower specific yield, meaning cost-efficiency must be supported.

To gain more perspective, the identified sub-areas could be compared to the modeled “Suitability Areas” in Bremen (Knies et al., 2024), which indirectly consider possible costs by the linear heat density. This is important since perhaps regions with detached houses and large gardens might be less viable according to the method. Furthermore, the presented sub-areas only give an illustration to roughly answer the question of “where” and “how” while disregarding social factors. In reality, the formation of such joint heat grids may differ since the term “neighborhood” itself is individually defined. Therefore, this proposed heating strategy can be used to assist a more detailed, preliminary study for Neu-Schwachhausen.

## 6.2. Workflow Assessment

The presented workflow is suitable for the first identification and estimation of the technical potentials of shallow geothermal and solar energy within a typical urban district. It gives an overview of the cumulated energy potential and demand in a year, their spatial distribution, and ultimately the possible areas for LowEx district heating. Due to the clustering method, the results can be broadly mapped, making it suitable for scanning larger areas as well. All in all, the first research question of this study, as stated in Chapter 1.2, has been addressed successfully. However, several aspects must be discussed in terms of validity, accuracy, and limitation.

### Geodata

The provided ALKIS data and the solar cadastre of Bremen complement each other well. Discrepancies can yet be found in certain areas, such as roof polygons that do not fit accurately on the building or touch the outline of any building. For instance, a few polygons appear to be

on top of a building according to the aerial photo but lack the building polygon itself. These large discrepancies have been excluded from the analysis by filtering, though it is not guaranteed that there are no other undetected discrepancies that may affect the potential analysis. Likewise, this applies to heat demand, of which the point data in some cases also indicate false coordinates or spatial discrepancies to the building data. Geodata for certain objects should also be collected regionally and made easily accessible for a more precise analysis. For example, as explained in Chapter 2.1, other relevant objects would add restrictions for BHEs but had to be omitted in the study, including existing pipelines of other functionalities, such as the wastewater and rain sewer systems, cables for telecommunication and electrical power. The missing register of private trees and many public trees also likely poses an issue for potential area accuracy. Manual digitization is time-consuming and may lead to falsely registering bushes as trees and vice versa.

Modeled heat demand data that were used to represent the status quo are based on both actual (e.g. building dimensions, census data) and assumed data. The latter includes the estimation of the buildings' energy efficiency class based merely on the building type and construction year (Heinrich et al., 2023), although many of the observed buildings might have already been retrofitted. Therefore, the collection of factual, precise data about the current condition of buildings, especially their energy-efficiency class, is crucial for any research or feasibility study regarding heat supply options.

#### Energy Simulations with EED and Polysun

This study shows that the program EED can be used for a broad estimation of the geothermal energy extraction based on various inputs, including BHE tube type, heat-carrying medium, borehole configuration, depth, soil properties, and heat demand. The program is designed to support BHE field configuration and omits heat pump properties except for the SPF. In this method, the technical potential is directly taken from the maximum heat demand base load which the BHE may legally cover, using ground temperature from modeled data of unclear origin. Precise information at the investigated depth regarding ground temperature, the rock type, STC, moisture content, and porosity are important factors that determine the heat reservoir. Compared to the estimated values in the feasibility study of "Humboldt-Straße" in Bremen (energiekonsens GmbH, 2022), the simulated heat extraction per borehole at 300 m is about 38% less, if a similar SPF is considered. Though in this reference the STC value of the ground is not stated, so perhaps better ground conditions (e.g. higher STC) are found in the area. Real values from examples under similar conditions were not obtainable at the time of this study, but are yet necessary to confirm the plausibility. Sampling at several locations in Neu-Schwachhausen especially for boreholes at 300 m depth is highly recommended. This

could at least improve the STC accuracy in terms of value and distribution since the applied number is only estimated based on modeled data and one sample data up to 100 m depth (see Chapter 4.3.2).

Furthermore, the applicability test shows that the simulation and calculation method, as presented in Chapters 4.3.3 and 4.3.4, tend to under- or overestimate the heat potentials. The intensity increases with higher deviation from the mean number of BHEs per grid cell at max. potential (see Figure 20 on page 42). Fields with more BHEs than average are overestimated to a lesser degree, implying that the interference effect does not increase linearly with more BHE installations and consistent spacing. In this study, the specific heat extraction derives from a simulation based on the mean borehole number. The wider borehole distribution at 100 m than 300 m depth signifies that the former gives a less precise result. More detailed research on the impact of borehole number on geothermal interference is needed to confirm this.

Nonetheless, the interference can be minimized by setting larger borehole spacing. To limit the inaccuracy, it would be best to conduct several simulations for every STC value, each varying in BHE number (e.g. 10, 30, 50, 70). Then, the BHE number of each grid cell can be multiplied with the result that derives from the closest simulation setting, similar to calculating PV potential using sub-categories.

The workflow with Polysun offers the flexibility of choosing a commercially available PV module type. The annual specific yields of PV in all three scenarios fall around the average expected value of 922 kWh/kWp (equals to full load hours in h/a) and none of the total potential reaches above 65% of the technically possible output, given the average daily sunlight of 1545 h/a in Bremen (Wirth & ISE, 2023). This validates the result of the solar energy potential analysis. Nevertheless, the categorization of roofs from the solar cadastre could be expanded for more accurate PV yield estimations, for example, by dividing each aspect category into four sub-categories that vary in slope instead of two. Also, it is essential to consider that the broad estimation on a roof is not based on the number of modules to be installed, but rather on the “technical potential area” and the specific yield per gross area (kWh/m<sup>2</sup>) of the module. Potentials could be miscalculated since the actual total area of a PV array would rarely be the exact size of the roof potential area due to the module’s dimensions. Hence, the suggested method can be applied for a quick PV analysis on a medium to large scale, but this should not replace a second detailed check of the max. module number and a more precise simulated yield because of the variety of slopes and aspects.

#### Ideas for Improvement

It is important to note that the workflow only delivers the total cumulated energy potential and demand in a year, while actual heat demand and energy availability, in particular required solar

power, strongly vary according to season and daytime. Especially peak solar energy production and heat pump output usually show an inversion throughout the year, hence the relevance of energy storage technologies. So expected seasonal fluctuation should be considered in succeeding studies to also understand better which storage technology would be optimal.

In the study, the data and results were clustered using a geographical grid with a resolution of 100 m, but this can be exchanged to adjust the spatial roughness. The resolution should be selected depending on the targeted level of detail, in which the results are expected, as well as the size of the study area and existing neighborhood constellations. The latter is important since social factors may influence the formation of LowEx heat grids, as stated previously. In all GIS tools created for data clustering, the grid should be set as an input parameter to enable free selection. However, certain code modifications may be required if the new grid has a different naming system for the cells' unique polygon ID. An idea to overcome this would be to rename the grid cells from the start (e.g. G-1 to G-110) and use it as the referring ID. This would enable the use of a grid from any source and improve overall GIS automation.

It is foreseeable that the workflow is applicable in all areas of Bremen due to similar topography and existing geodata from the same source. The geodata can also be simply exchanged with more recent findings to update the analysis results. Certain areas in Bremen may have other restricting objects for geothermal extraction, such as archeological monuments, (drinking) water protection sites, and larger water bodies (e.g. the Weser), and so the geodata should be retrieved and integrated into the GIS tool for a more automatized process. The workflow needs further exploration regarding its applicability in other towns and cities. The solar cadastre, heat demand data, and STC vector data are provided specifically for Bremen, therefore some modifications in the GIS and Excel tools would be necessary when examining other places. Finally, integrating the linear heat density as an economic parameter for suitability can enhance the workflow, as applied already in certain studies (Dochev et al., 2018; Knies, 2018).

## 7. Conclusion and Outlook

Bringing the heat transition forward in Germany is impossible without addressing the challenge of providing clean thermal energy in buildings, which contribute largely to the final energy consumption, and thus, GHG emissions. Legal instruments that recently came into effect will hopefully show positive impacts in the coming years and decades, especially in urban areas where the population likely increases while energy demand must be reduced. Nowhere else is space availability for local renewable sources as highly valued, so modern solutions such as urban-integrated technologies and green district heating are favorable. The concerning rate of global warming drives the dynamic of world politics, hence the race to find the optimal strategy and technology for sustainable heating under various circumstances.

This thesis emphasizes the importance of finding local energy sources in densely built districts. When applied widely, shallow geothermal energy up to 300 m below ground may significantly assist in covering a district's heat demand for space and water heating. The enormous potential in open spaces such as green areas and sports fields cannot be ignored. The concept of LowEx DH should generally be enhanced by joining heat sources due to the unequal space availability in residential neighborhoods. The resulting raised power consumption can be alleviated by installing PV on existing roofs and solar parking lots. Highly efficient heat pumps and modules are particularly important in areas with potentials that are insufficient to meet the energy demand. The proposed sub-areas are optimal for LowEx DH if technical quality, such as energy self-sufficiency, is to be achieved. Moreover, it is crucial to implement measures for heat demand reductions largely through building retrofits to realize this strategy effectively. The results cannot replace feasibility studies or technical planning but rather give a different aspect of implementing the heat transition at a district level.

The workflow is developed based on Neu-Schwachhausen but should be ideally applicable to other urban areas. Accuracy of geodata is highly important as these are the foundation of the results. The workflow is made in a way that these can be exchanged for more current data or data for the corresponding district. Perhaps assumptions for the heat demand model should be minimized by collecting actual energy efficiency classes of buildings. Future works can be directed to improve the workflow by advancing automation and adding missing factors, especially base and peak loads to provide energy storage solutions as well as an economic parameter. The impact of adding solar thermal collectors in areas with low geothermal potential can be investigated if a third technology is considered. Another interesting topic would be to integrate the cooling demand given that shallow geothermal energy can profit from the coupling of heating and cooling, and that high temperatures will, unfortunately, more likely occur with time.

## References

- Arbeitsgemeinschaft Fernwärme (AGFW), Der Energieeffizienzverband für Wärme, Kälte und KWK e.V. (2023). *Hauptbericht 2021* [Main Report].
- Averfalk, H., Benakopoulos, T., Best, I., Dammel, F., Engel, C., Geyer, R., Lygnerud, K., & Werner, S. (2021). *Low-Temperature district heating implementation guidebook: Final report of IEA DHC Annex TS2: implementation of Low-Temperature district heating systems*. Fraunhofer Verlag.
- Bayer, P., Attard, G., Blum, P., & Menberg, K. (2019). The geothermal potential of cities. *Renewable and Sustainable Energy Reviews*, 106, 17–30. <https://doi.org/10.1016/j.rser.2019.02.019>
- Bayerisches Landesamt für Umwelt (LfU). (2012). *Merkblatt Nr. 3.7/2—Planung und Erstellung von Erdwärmesonden*.
- Bockelmann, F., Peter, M., & Schlosser, M. (2019). *Energetische und wirtschaftliche Bewertung von Wärmequellen für Wärmepumpen*. Technische Universität Braunschweig.
- Boyle, G. (2012). *Renewable energy: Power for a sustainable future* (Open University, Ed.; 3rd ed). Oxford University Press in association with the Open University.
- Bremen Online. (n.d.). *Chronik für Schwachhausen—Aus der Geschichte*. Retrieved May 5, 2024, from <https://www.bremen.de/leben-in-bremen/wohnen/stadtteile/stadtteilgeschichte-schwachhausen>
- Bremer Energie-Konsens GmbH (energiekonsens GmbH). (2022). *Kaltes Nahwärmenetz in der Humboldtstraße, Bremen Machbarkeitsstudie*. [https://energiekonsens.de/media/pages/media/ddfe06d0dd-1688549390/knw-bre\\_langbericht.pdf](https://energiekonsens.de/media/pages/media/ddfe06d0dd-1688549390/knw-bre_langbericht.pdf)
- Bundesamt für Kartographie und Geodäsie (BKG). (2023). *Geographische Gitter für Deutschland in Lambert-Projektion*. <https://gdz.bkg.bund.de/index.php/default/geographische-gitter-fur-deutschland-in-lambert-projektion-geogitter-inspire.html>
- Bundesministerium für Wirtschaft und Klimaschutz (BMWK). (2024). *Auf einen Blick: Die neue Förderung für den Heizungstausch*. [https://www.energiewechsel.de/KAENEF/Redaktion/DE/Downloads/foerderung-heizungstausch-beg.pdf?\\_\\_blob=publicationFile&v=22](https://www.energiewechsel.de/KAENEF/Redaktion/DE/Downloads/foerderung-heizungstausch-beg.pdf?__blob=publicationFile&v=22)
- Bundesverband der Energie- und Wasserwirtschaft (BDEW). (2023, October 10). *Beheizungsstruktur des Wohnungsbestandes in Deutschland*. <https://www.bdew.de/service/daten-und-grafiken/beheizungsstruktur-wohnungsbestand/>
- Bundesverband der Energie- und Wasserwirtschaft (BDEW) e.V. (2023). *Die Energieversorgung 2022—Jahresbericht*.
- Bundesverband Geothermie. (2021, January 15). *Das größte kalte Nahwärmenetz Deutschlands in Warendorf hat Leuchtturmcharakter*. <https://www.geothermie.de/aktuelles/nachrichten/news-anzeigen/news/baustart-fuer-das-groesste-kalte-nahwaermenetz-deutschlands.html>
- Bundesverband Wärmepumpe (BWP) e. V. (2022). *Wärme- und Kältekonzepte mit Großwärmepumpen*. [https://www.waermepumpe.de/fileadmin/user\\_upload/waermepumpe/08\\_Sonstige/Filedump/BWP\\_A4\\_GrossWP\\_web\\_mail.pdf](https://www.waermepumpe.de/fileadmin/user_upload/waermepumpe/08_Sonstige/Filedump/BWP_A4_GrossWP_web_mail.pdf)



- Christner, D. T. (2022). *Verpflichtende Installation einer Photovoltaikanlage über neu hergestellten Parkplätzen auf Gewerbeflächen – ein Überblick über die gesetzliche Neu- regelung des § 8 Abs. 2 LBauO NRW*. GÖRG Partnerschaft von Rechtsanwälten mbB.
- Cruikshank, C. A., & Baldwin, C. (2022). Sensible thermal energy storage: Diurnal and seasonal. *Storing Energy*.
- Deutscher Wetterdienst (DWD). (2021, February 11). *Sonnenscheindauer: Vieljährige Mittelwerte 1981—2010*.  
[https://www.dwd.de/DE/leistungen/klimadatendeutschland/mittelwerte/sonne\\_8110\\_fest\\_html.html?view=na&publication&nn=16102](https://www.dwd.de/DE/leistungen/klimadatendeutschland/mittelwerte/sonne_8110_fest_html.html?view=na&publication&nn=16102)
- Dickinson, J. S., Buik, N., Matthews, M. C., & Snijders, A. (2009). Aquifer thermal energy storage: Theoretical and operational analysis. *Géotechnique*, 59(3), 249–260.  
<https://doi.org/10.1680/geot.2009.59.3.249>
- Dochev, I., Peters, I., Seller, H., & Schuchardt, G. K. (2018). Analysing district heating potential with linear heat density. A case study from Hamburg. *Energy Procedia*, 149, 410–419.  
<https://doi.org/10.1016/j.egypro.2018.08.205>
- Doubleday, K., Hafiz, F., Parker, A., Elgindy, T., Florita, A., Henze, G., Salvalai, G., Pless, S., & Hodge, B. (2019). Integrated distribution system and urban district planning with high renewable penetrations. *WIREs Energy and Environment*, 8(5), e339. <https://doi.org/10.1002/wene.339>
- European Commission (EC). (2020, September 17). *State of the Union: Commission raises climate ambition* [Press Release]. European Commission.  
[https://ec.europa.eu/commission/presscorner/detail/en/ip\\_20\\_1599](https://ec.europa.eu/commission/presscorner/detail/en/ip_20_1599)
- García Gil, A., Garrido Schneider, E. A., Mejías Moreno, M., & Santamarta Cerezal, J. C. (2022a). Introduction. In A. García Gil, E. A. Garrido Schneider, M. Mejías Moreno, & J. C. Santamarta Cerezal, *Shallow Geothermal Energy* (pp. 1–13). Springer International Publishing.  
[https://doi.org/10.1007/978-3-030-92258-0\\_1](https://doi.org/10.1007/978-3-030-92258-0_1)
- García Gil, A., Garrido Schneider, E. A., Mejías Moreno, M., & Santamarta Cerezal, J. C. (2022b). Shallow Geothermal Systems with Closed-Loop Geothermal Heat Exchangers. In A. García Gil, E. A. Garrido Schneider, M. Mejías Moreno, & J. C. Santamarta Cerezal, *Shallow Geothermal Energy* (pp. 121–180). Springer International Publishing. [https://doi.org/10.1007/978-3-030-92258-0\\_5](https://doi.org/10.1007/978-3-030-92258-0_5)
- García Gil, A., Garrido Schneider, E. A., Mejías Moreno, M., & Santamarta Cerezal, J. C. (2022c). Theoretical Background. In A. García Gil, E. A. Garrido Schneider, M. Mejías Moreno, & J. C. Santamarta Cerezal, *Shallow Geothermal Energy* (pp. 15–69). Springer International Publishing. [https://doi.org/10.1007/978-3-030-92258-0\\_2](https://doi.org/10.1007/978-3-030-92258-0_2)
- Hajto, M., Ruediger Grimm, Goetzl, G., Deinhardt, A., Kaufhold, J., Zschoke, K., Heiermann, M., Bukovska, Z., Černák, R., Janža, M., Kłonowski, M. R., Wiesław Kozdroj, & Špela Gregorin. (2019). *The GeoPLASMA-CE Position paper to foster the use of shallow geothermal in Central Europe, Get Warm with Shallow Geothermal Energy*.  
<https://doi.org/10.13140/RG.2.2.21104.48646>
- Heinrich, P., Steyer, N., Wenzel, T., Lehnert, F., Grube, E., & Bleidießel, M. (2023). *DBI-Ansatz zur Modellierung von Wärmebedarfen*. DBI Gas- und Umwelttechnik GmbH.

- Hochreutener, M., Grüter, D. L., Nikiforos, C., & Konersmann, L. (2022). *Solarstrom auf Parkplatzüberdachungen*. Energie Zukunft Schweiz AG.
- Justus Grosse Real Estate GmbH (Justus Grosse). (2023, May 16). *Wärme aus Abwasser für das Tabakquartier* [Press Release]. Tabakquartier. <https://tabakquartier.com/waerme-aus-abwasser-fuer-das-tabakquartier/>
- Kallert, A., Lamvers, E., & Jae Yu, Y. (2021). *Dena-Studie, Thermische Energiespeicher für Quartiere, Überblick zu Rahmenbedingungen, Marktsituation und Technologieoptionen für Planung, Beratung und politische Entscheidungen im Gebäudesektor* (Deutsche Energie-Agentur GmbH (dena), Ed.).
- Kaushika, N. D., Mishra, A., & Rai, A. K. (2018a). BOS and Electronic Regulations. In N. D. Kaushika, A. Mishra, & A. K. Rai, *Solar Photovoltaics* (pp. 93–104). Springer International Publishing. [https://doi.org/10.1007/978-3-319-72404-1\\_8](https://doi.org/10.1007/978-3-319-72404-1_8)
- Kaushika, N. D., Mishra, A., & Rai, A. K. (2018b). Solar PV Module and Array Network. In N. D. Kaushika, A. Mishra, & A. K. Rai, *Solar Photovoltaics* (pp. 81–92). Springer International Publishing. [https://doi.org/10.1007/978-3-319-72404-1\\_7](https://doi.org/10.1007/978-3-319-72404-1_7)
- Knies, J. (2018). A spatial approach for future-oriented heat planning in urban areas. *International Journal of Sustainable Energy Planning and Management*, 3–30. <https://doi.org/10.5278/IJSEPM.2018.16.2>
- Knies, J., Heinrich, P., Steyer, N., Gerling, Y. E., & Schwarz, T. (2024). *Ein ArcGIS-Pro-Modell zur Ermittlung von Eignungsbereichen für Wärmeversorgungsoptionen am Beispiel der Stadt Bremen*. 29. <https://doi.org/10.26092/ELIB/2640>
- Lund, H., Østergaard, P. A., Nielsen, T. B., Werner, S., Thorsen, J. E., Gudmundsson, O., Arabkoohsar, A., & Mathiesen, B. V. (2021). Perspectives on fourth and fifth generation district heating. *Energy*, 227, 120520. <https://doi.org/10.1016/j.energy.2021.120520>
- Lund, H., Werner, S., Wiltshire, R., Svendsen, S., Thorsen, J. E., Hvelplund, F., & Mathiesen, B. V. (2014). 4th Generation District Heating (4GDH). *Energy*, 68, 1–11. <https://doi.org/10.1016/j.energy.2014.02.089>
- Mansouri Kouhestani, F., Byrne, J., Johnson, D., Spencer, L., Hazendonk, P., & Brown, B. (2019). Evaluating solar energy technical and economic potential on rooftops in an urban setting: The city of Lethbridge, Canada. *International Journal of Energy and Environmental Engineering*, 10(1), 13–32. <https://doi.org/10.1007/s40095-018-0289-1>
- Mathes, K., Berger, T., & Auras, S. (2020). *Stadtteilbericht Schwachhausen 2020*. Ortsamt Schwachhausen / Vahr.
- Ministerium für Umwelt, Klima und Energiewirtschaft Baden-Württemberg (UMBW). (2024, April 25). *Parkplatzüberdachung mit Photovoltaik*. Baden-Württemberg.de. <https://um.baden-wuerttemberg.de/de/energie/informieren-beraten-foerdern/foerderprogramme/foerderprogramm-parkplatz-pv>
- Page, J. (2018). The Role of Solar-Radiation Climatology in the Design of Photovoltaic Systems. In *McEvoy's Handbook of Photovoltaics—Fundamentals and Applications* (Third, pp. 601–631). Joe Hayton.

- Panteleit, B., Ortmann, S., & Langer, S. (2022). *Leitfaden oberflächennahe Geothermie im Land Bremen*. Geologischer Dienst für Bremen (GDFB).
- Sächsische Energieagentur GmbH (SAENA GmbH). (2023). *Leitfaden Photovoltaik—Strom erzeugen und optimal nutzen*.
- Schabbach, T., & Leibbrandt, P. (2021). *Solarthermie: Wie Sonne zu Wärme wird*. Springer Berlin Heidelberg. <https://doi.org/10.1007/978-3-662-59488-9>
- Schiel, K., Baume, O., Caruso, G., & Leopold, U. (2016). GIS-based modelling of shallow geothermal energy potential for CO<sub>2</sub> emission mitigation in urban areas. *Renewable Energy*, 86, 1023–1036. <https://doi.org/10.1016/j.renene.2015.09.017>
- Senatorin für Umwelt, Klima, und Wissenschaft (SUKW). (2019). *Solarkataster Bremen*. <https://www.solarkataster-bremen.de/#s=startscreen>
- Statistisches Landesamt Bremen (SLB). (2024). *Bremer Ortsteilatl*. <https://www.statistik-bremen.de/tabellen/kleinraum/ortsteilatl/atlas.html>
- Stober, I., & Bucher, K. (2020a). Erdwärmesonden. In I. Stober & K. Bucher, *Geothermie* (pp. 75–139). Springer Berlin Heidelberg. [https://doi.org/10.1007/978-3-662-60940-8\\_6](https://doi.org/10.1007/978-3-662-60940-8_6)
- Stober, I., & Bucher, K. (2020b). Geothermische Nutzungsmöglichkeiten. In I. Stober & K. Bucher, *Geothermie* (pp. 39–70). Springer Berlin Heidelberg. [https://doi.org/10.1007/978-3-662-60940-8\\_4](https://doi.org/10.1007/978-3-662-60940-8_4)
- Stober, I., & Bucher, K. (2020c). Thermisches Regime der Erde. In I. Stober & K. Bucher, *Geothermie* (pp. 1–17). Springer Berlin Heidelberg. [https://doi.org/10.1007/978-3-662-60940-8\\_1](https://doi.org/10.1007/978-3-662-60940-8_1)
- swb AG. (n.d.). *Solarkataster Berechnungsgrundlage*. Retrieved May 7, 2024, from <https://www.swb.de/-/media/files/energie/broschueren-und-infomaterial/solarkataster-berechnungsgrundlage.pdf>
- swb AG. (2020). *Der Weg der Wärme in die Zukunft, Langfristige Wärmestrategie für Bremen und Bremerhaven*.
- Taylor, N., & Jäger-Waldau, A. (2020). *Photovoltaics: Technology development report 2020*. Publications Office of the European Union.
- Umweltbetrieb Bremen (UBB). (2023). *Baumkataster/WMS\_Baumkataster\_UBB\_offen (MapServer)*. Baumkataster. [https://gris2.umweltbetriebbremen.de/arcgis/rest/services/Baumkataster/WMS\\_Baumkataster\\_UBB\\_offen/MapServer](https://gris2.umweltbetriebbremen.de/arcgis/rest/services/Baumkataster/WMS_Baumkataster_UBB_offen/MapServer)
- Umweltbundesamt (UBA). (2024a). *Erneuerbare Energien in Deutschland. Daten zur Entwicklung im Jahr 2023*. [https://www.umweltbundesamt.de/sites/default/files/medien/479/publikationen/2024\\_uba\\_hg\\_erneuerbareenergien\\_dt.pdf](https://www.umweltbundesamt.de/sites/default/files/medien/479/publikationen/2024_uba_hg_erneuerbareenergien_dt.pdf)
- Umweltbundesamt (UBA). (2024b). *Emissionen ausgewählter Treibhausgase in Deutschland nach Kategorien in Tsd. T Kohlendioxid-Äquivalenten*. Umweltbundesamt. [https://www.umweltbundesamt.de/sites/default/files/medien/384/bilder/dateien/8\\_tab\\_thg-emikat\\_2024-04-02.pdf](https://www.umweltbundesamt.de/sites/default/files/medien/384/bilder/dateien/8_tab_thg-emikat_2024-04-02.pdf)
- Wetter, C., & Brüggling, E. (2023). *Forschungs- und Entwicklungsprojekte 2022/2023*. FH Münster.
- Wirth, H., & ISE, F. (2023). *Aktuelle Fakten zur Photovoltaik in Deutschland*. Fraunhofer-Institut für Solare Energiesysteme ISE.

## List of Appendices

### Appendix A: Shallow Geothermal Energy, Technical Potential

A-1	S-2022
A-2	S-2030
A-3	S-2038-a
A-4	S-2038-b

### Appendix B: Solar Energy, Technical Potential

B-1	S-2022
B-2	S-2030
B-3	S-2038-a and -b

### Appendix C: Scenario Outcome

C-1	S-2022
C-2	S-2030
C-3	S-2038-a and -b

Appendix A-1: Geothermal Energy, Technical Potential in S-2022

Grid Cell (G-)	BHEs with STC = 1.2 W/mK	BHEs with STC = 1.3 W/mK	BHEs with STC = 1.4 W/mK	BHEs with STC = 1.5 W/mK	BHEs with STC = 1.6 W/mK	Geothermal Tech. Potential (kWh/a)
1	1	4	0	0	0	17,600
2	3	0	0	0	0	10,200
3	0	0	0	0	0	-
4	9	7	0	0	0	55,450
5	19	0	0	0	0	64,600
6	10	0	0	0	0	34,000
7	8	2	0	0	0	34,300
8	20	0	0	0	0	68,000
9	14	0	0	0	0	47,600
10	12	0	0	0	0	40,800
11	8	0	0	0	0	27,200
12	2	0	0	0	0	6,800
13	3	0	0	0	0	10,200
14	24	0	0	0	0	81,600
15	19	0	0	0	0	64,600
16	18	0	0	0	0	61,200
17	19	0	0	0	0	64,600
18	23	0	0	0	0	78,200
19	14	0	0	0	0	47,600
20	16	0	0	0	0	54,400
21	3	0	0	0	0	10,200
22	6	0	0	0	0	20,400
23	20	0	0	0	0	68,000
24	21	0	0	0	0	71,400
25	23	0	0	0	0	78,200
26	24	0	0	0	0	81,600
27	22	0	0	0	0	74,800
28	22	0	0	0	0	74,800
29	17	2	0	0	0	64,900
30	5	8	0	0	0	45,400
31	0	5	0	0	0	17,750
32	17	0	0	0	0	57,800
33	21	0	0	0	0	71,400
34	15	0	0	0	0	51,000
35	22	0	0	0	0	74,800
36	25	0	0	0	0	85,000
37	17	1	0	0	0	61,350
38	12	16	0	0	0	97,600
39	12	24	0	0	0	126,000
40	0	20	0	0	0	71,000
41	0	13	0	0	0	46,150
42	0	10	0	0	0	35,500
43	0	1	0	0	0	3,550
44	4	0	0	0	0	13,600
45	26	0	0	0	0	88,400
46	19	0	0	0	0	64,600
47	20	0	0	0	0	68,000
48	20	2	0	0	0	75,100
49	11	11	0	0	0	76,450
50	8	13	0	0	0	73,350
51	0	24	0	0	0	85,200
52	0	38	0	0	0	134,900
53	0	44	0	0	0	156,200
54	0	31	0	0	0	110,050
55	0	11	0	0	0	39,050
56	0	1	0	0	0	3,550
57	12	0	0	0	0	40,800
58	21	0	0	0	0	71,400

Grid Cell (G-)	BHEs with STC = 1.2 W/mK	BHEs with STC = 1.3 W/mK	BHEs with STC = 1.4 W/mK	BHEs with STC = 1.5 W/mK	BHEs with STC = 1.6 W/mK	Geothermal Tech. Potential (kWh/a)
59	16	0	0	0	0	54,400
60	17	2	0	0	0	64,900
61	10	13	0	0	0	80,150
62	0	28	0	0	0	99,400
63	0	22	0	0	0	78,100
64	0	21	0	0	0	74,550
65	0	15	0	0	0	53,250
66	0	20	0	0	0	71,000
67	0	12	0	0	0	42,600
68	0	0	0	0	0	-
69	4	0	0	0	0	13,600
70	21	0	0	0	0	71,400
71	22	0	0	0	0	74,800
72	20	2	0	0	0	75,100
73	14	15	0	0	0	100,850
74	0	25	0	0	0	88,750
75	0	26	0	0	0	92,300
76	0	21	2	0	0	82,050
77	0	14	13	0	0	98,450
78	0	16	11	0	0	98,050
79	0	3	2	0	0	18,150
80	0	0	0	0	0	-
81	0	0	0	0	0	-
82	10	0	0	0	0	34,000
83	17	2	0	0	0	64,900
84	10	14	0	0	0	83,700
85	0	27	0	0	0	95,850
86	0	22	2	0	0	85,600
87	0	13	12	0	0	91,150
88	0	7	13	0	0	73,600
89	0	0	24	0	0	90,000
90	0	0	17	0	0	63,750
91	0	0	3	0	0	11,250
92	2	1	0	0	0	10,350
93	0	15	0	0	0	53,250
94	0	25	3	0	0	100,000
95	0	11	12	0	0	84,050
96	0	0	29	0	0	108,750
97	0	0	25	2	0	101,550
98	0	0	11	13	0	91,950
99	0	0	6	4	0	38,100
100	0	5	2	0	0	25,250
101	0	0	19	3	0	82,950
102	0	0	11	10	0	80,250
103	0	0	11	14	0	95,850
104	0	0	0	19	0	74,100
105	0	0	0	1	0	3,900
106	0	0	0	2	0	7,800
107	0	0	0	12	2	54,900
108	0	0	0	13	7	79,050
109	0	0	0	4	0	15,600
110	0	0	0	0	1	4,050
<b>Total</b>	<b>850</b>	<b>685</b>	<b>228</b>	<b>97</b>	<b>10</b>	<b>6,595,550</b>

Appendix A-2: Geothermal Energy, Technical Potential in S-2030

Grid Cell (G-)	BHEs with STC = 1.2 W/mK	BHEs with STC = 1.3 W/mK	BHEs with STC = 1.4 W/mK	BHEs with STC = 1.5 W/mK	BHEs with STC = 1.6 W/mK	Geothermal Tech. Potential (kWh/a)
1	1	10	0	0	0	29,738
2	8	0	0	0	0	20,762
3	1	1	0	0	0	5,310
4	21	17	0	0	0	100,643
5	45	0	0	0	0	116,786
6	22	0	0	0	0	57,095
7	20	6	0	0	0	68,190
8	48	0	0	0	0	124,571
9	32	0	0	0	0	83,048
10	27	0	0	0	0	70,071
11	18	0	0	0	0	46,714
12	5	0	0	0	0	12,976
13	7	0	0	0	0	18,167
14	56	0	0	0	0	145,333
15	45	0	0	0	0	116,786
16	43	0	0	0	0	111,595
17	43	0	0	0	0	111,595
18	53	0	0	0	0	137,548
19	33	0	0	0	0	85,643
20	38	0	0	0	0	98,619
21	7	0	0	0	0	18,167
22	13	0	0	0	0	33,738
23	46	0	0	0	0	119,381
24	49	0	0	0	0	127,167
25	53	0	0	0	0	137,548
26	55	0	0	0	0	142,738
27	50	0	0	0	0	129,762
28	52	0	0	0	0	134,952
29	41	4	0	0	0	117,262
30	12	18	0	0	0	80,000
31	0	12	0	0	0	32,571
32	41	0	0	0	0	106,405
33	50	0	0	0	0	129,762
34	36	0	0	0	0	93,429
35	50	0	0	0	0	129,762
36	57	0	0	0	0	147,929
37	40	2	0	0	0	109,238
38	27	37	0	0	0	170,500
39	27	56	0	0	0	222,071
40	0	46	0	0	0	124,857
41	0	29	0	0	0	78,714
42	0	24	0	0	0	65,143
43	0	2	0	0	0	5,429
44	10	0	0	0	0	25,952
45	60	0	0	0	0	155,714
46	45	0	0	0	0	116,786
47	46	0	0	0	0	119,381
48	46	4	0	0	0	130,238
49	26	26	0	0	0	138,048
50	19	29	0	0	0	128,024
51	0	57	0	0	0	154,714
52	0	88	0	0	0	238,857
53	0	102	0	0	0	276,857
54	0	72	0	0	0	195,429
55	0	25	0	0	0	67,857
56	0	1	0	0	0	2,714
57	29	0	0	0	0	75,262

Grid Cell (G-)	BHEs with STC = 1.2 W/mK	BHEs with STC = 1.3 W/mK	BHEs with STC = 1.4 W/mK	BHEs with STC = 1.5 W/mK	BHEs with STC = 1.6 W/mK	Geothermal Tech. Potential (kWh/a)
58	48	0	0	0	0	124,571
59	36	0	0	0	0	93,429
60	40	4	0	0	0	114,667
61	22	30	0	0	0	138,524
62	0	65	0	0	0	176,429
63	0	51	0	0	0	138,429
64	0	49	0	0	0	133,000
65	0	36	0	0	0	97,714
66	0	48	0	0	0	130,286
67	0	28	0	0	0	76,000
68	0	0	0	0	0	-
69	8	0	0	0	0	20,762
70	50	0	0	0	0	129,762
71	51	0	0	0	0	132,357
72	48	5	0	0	0	138,143
73	33	36	0	0	0	183,357
74	0	58	0	0	0	157,429
75	0	60	0	0	0	162,857
76	0	50	4	0	0	147,048
77	0	32	31	0	0	174,690
78	0	36	25	0	0	168,548
79	0	8	4	0	0	33,048
80	0	0	0	0	0	-
81	1	0	0	0	0	2,595
82	23	0	0	0	0	59,690
83	41	6	0	0	0	122,690
84	22	33	0	0	0	146,667
85	0	64	0	0	0	173,714
86	0	51	5	0	0	152,595
87	0	29	28	0	0	158,048
88	0	17	29	0	0	128,310
89	0	0	56	0	0	158,667
90	0	0	41	0	0	116,167
91	0	0	6	0	0	17,000
92	5	2	0	0	0	18,405
93	0	35	0	0	0	95,000
94	0	59	8	0	0	182,810
95	0	25	29	0	0	150,024
96	0	0	67	0	0	189,833
97	0	0	58	5	0	179,095
98	0	0	25	30	0	159,405
99	0	0	13	10	0	66,357
100	0	12	4	0	0	43,905
101	0	0	45	8	0	151,119
102	0	0	25	24	0	141,690
103	0	0	26	33	0	171,095
104	0	0	0	44	0	129,905
105	0	0	0	3	0	8,857
106	0	0	1	5	0	17,595
107	0	0	0	29	4	97,810
108	0	0	0	31	17	143,333
109	0	0	0	8	0	23,619
110	0	0	0	0	2	6,095
<b>Total</b>	<b>1981</b>	<b>1597</b>	<b>530</b>	<b>230</b>	<b>23</b>	<b>11,726,690</b>



Appendix A-3: Geothermal Energy, Technical Potential in S-2038-a

Grid Cell (G-)	BHEs with STC = 1.2 W/mK	BHEs with STC = 1.3 W/mK	BHEs with STC = 1.4 W/mK	BHEs with STC = 1.5 W/mK	BHEs with STC = 1.6 W/mK	Geothermal Tech. Potential (kWh/a)
1	2	14	0	0	0	39,214
2	11	0	0	0	0	25,929
3	1	1	0	0	0	4,821
4	30	24	0	0	0	129,857
5	64	0	0	0	0	150,857
6	32	0	0	0	0	75,429
7	28	8	0	0	0	85,714
8	68	0	0	0	0	160,286
9	46	0	0	0	0	108,429
10	39	0	0	0	0	91,929
11	26	0	0	0	0	61,286
12	7	0	0	0	0	16,500
13	10	0	0	0	0	23,571
14	80	0	0	0	0	188,571
15	64	0	0	0	0	150,857
16	61	0	0	0	0	143,786
17	62	0	0	0	0	146,143
18	76	0	0	0	0	179,143
19	47	0	0	0	0	110,786
20	54	0	0	0	0	127,286
21	10	0	0	0	0	23,571
22	19	0	0	0	0	44,786
23	66	0	0	0	0	155,571
24	70	0	0	0	0	165,000
25	76	0	0	0	0	179,143
26	79	0	0	0	0	186,214
27	72	0	0	0	0	169,714
28	74	0	0	0	0	174,429
29	58	6	0	0	0	151,500
30	17	26	0	0	0	104,143
31	0	17	0	0	0	41,893
32	58	0	0	0	0	136,714
33	71	0	0	0	0	167,357
34	51	0	0	0	0	120,214
35	72	0	0	0	0	169,714
36	82	0	0	0	0	193,286
37	57	3	0	0	0	141,750
38	39	53	0	0	0	222,536
39	39	80	0	0	0	289,071
40	0	65	0	0	0	160,179
41	0	42	0	0	0	103,500
42	0	34	0	0	0	83,786
43	0	3	0	0	0	7,393
44	14	0	0	0	0	33,000
45	85	0	0	0	0	200,357
46	64	0	0	0	0	150,857
47	66	0	0	0	0	155,571
48	66	5	0	0	0	167,893
49	37	37	0	0	0	178,393
50	27	42	0	0	0	167,143
51	0	81	0	0	0	199,607
52	0	125	0	0	0	308,036
53	0	146	0	0	0	359,786
54	0	103	0	0	0	253,821
55	0	36	0	0	0	88,714
56	0	2	0	0	0	4,929
57	41	0	0	0	0	96,643

Grid Cell (G-)	BHEs with STC = 1.2 W/mK	BHEs with STC = 1.3 W/mK	BHEs with STC = 1.4 W/mK	BHEs with STC = 1.5 W/mK	BHEs with STC = 1.6 W/mK	Geothermal Tech. Potential (kWh/a)
58	69	0	0	0	0	162,643
59	52	0	0	0	0	122,571
60	57	5	0	0	0	146,679
61	32	43	0	0	0	181,393
62	0	93	0	0	0	229,179
63	0	73	0	0	0	179,893
64	0	70	0	0	0	172,500
65	0	51	0	0	0	125,679
66	0	68	0	0	0	167,571
67	0	40	0	0	0	98,571
68	0	0	0	0	0	-
69	12	0	0	0	0	28,286
70	71	0	0	0	0	167,357
71	73	0	0	0	0	172,071
72	68	7	0	0	0	177,536
73	47	51	0	0	0	236,464
74	0	83	0	0	0	204,536
75	0	85	0	0	0	209,464
76	0	71	6	0	0	190,286
77	0	45	44	0	0	223,250
78	0	52	36	0	0	220,071
79	0	11	6	0	0	42,429
80	0	0	0	0	0	-
81	1	0	0	0	0	2,357
82	33	0	0	0	0	77,786
83	58	8	0	0	0	156,429
84	32	47	0	0	0	191,250
85	0	91	0	0	0	224,250
86	0	73	7	0	0	197,768
87	0	42	40	0	0	205,643
88	0	24	42	0	0	166,393
89	0	0	80	0	0	204,286
90	0	0	58	0	0	148,107
91	0	0	9	0	0	22,982
92	7	3	0	0	0	23,893
93	0	50	0	0	0	123,214
94	0	84	11	0	0	235,089
95	0	36	41	0	0	193,411
96	0	0	96	0	0	245,143
97	0	0	83	7	0	230,571
98	0	0	36	43	0	206,339
99	0	0	19	14	0	85,768
100	0	17	6	0	0	57,214
101	0	0	64	11	0	192,696
102	0	0	36	34	0	182,393
103	0	0	37	47	0	219,536
104	0	0	0	63	0	167,625
105	0	0	0	4	0	10,643
106	0	0	1	7	0	21,179
107	0	0	0	41	5	122,929
108	0	0	0	44	24	183,500
109	0	0	0	12	0	31,929
110	0	0	0	0	3	8,304
<b>Total</b>	<b>2830</b>	<b>2276</b>	<b>758</b>	<b>327</b>	<b>32</b>	<b>15,173,661</b>

Appendix A-4: Geothermal Energy, Technical Potential in S-2038-b

Grid Cell (G-)	BHEs with STC = 0.96 W/mK	Geothermal Tech. Potential (kWh/a)
1	6	73,800
2	4	49,200
3	0	-
4	23	282,900
5	23	282,900
6	14	172,200
7	12	147,600
8	27	332,100
9	17	209,100
10	17	209,100
11	7	86,100
12	2	24,600
13	4	49,200
14	27	332,100
15	22	270,600
16	23	282,900
17	23	282,900
18	27	332,100
19	17	209,100
20	14	172,200
21	6	73,800
22	8	98,400
23	29	356,700
24	25	307,500
25	27	332,100
26	32	393,600
27	30	369,000
28	26	319,800
29	22	270,600
30	16	196,800
31	6	73,800
32	17	209,100
33	29	356,700
34	17	209,100
35	27	332,100
36	29	356,700
37	23	282,900
38	33	405,900
39	42	516,600
40	20	246,000
41	14	172,200
42	13	159,900
43	1	12,300
44	6	73,800
45	26	319,800
46	21	258,300
47	21	258,300
48	24	295,200
49	26	319,800
50	25	307,500
51	27	332,100
52	38	467,400
53	43	528,900
54	30	369,000
55	13	159,900

Grid Cell (G-)	BHEs with STC = 0.96 W/mK	Geothermal Tech. Potential (kWh/a)
56	1	12,300
57	14	172,200
58	25	307,500
59	17	209,100
60	26	319,800
61	31	381,300
62	31	381,300
63	25	307,500
64	25	307,500
65	18	221,400
66	24	295,200
67	16	196,800
68	0	-
69	2	24,600
70	31	381,300
71	27	332,100
72	28	344,400
73	35	430,500
74	31	381,300
75	27	332,100
76	28	344,400
77	32	393,600
78	31	381,300
79	8	98,400
80	0	-
81	1	12,300
82	11	135,300
83	26	319,800
84	28	344,400
85	30	369,000
86	29	356,700
87	29	356,700
88	24	295,200
89	35	430,500
90	24	295,200
91	4	49,200
92	4	49,200
93	20	246,000
94	33	405,900
95	29	356,700
96	34	418,200
97	36	442,800
98	28	344,400
99	10	123,000
100	12	147,600
101	22	270,600
102	25	307,500
103	35	430,500
104	24	295,200
105	1	12,300
106	5	61,500
107	15	184,500
108	24	295,200
109	6	73,800
110	2	24,600

Appendix B-1: Solar Energy, Technical Potential in S-2022

Grid Cell (G-)	ESE slope 0° - 50°	ESE slope 50° - 90°	SSE slope 10° - 50°	SSE slope 50° - 90°	SSW slope 10° - 50°	SSW slope 50° - 90°	WSW slope 10° - 50°	WSW slope 50° - 90°	S (flat roof) slope of sub-structure 35°	Total potential (kWh/a)
1	-	-	-	-	-	-	-	-	-	-
2	-	-	-	-	-	-	-	-	-	-
3	-	-	-	-	-	-	-	-	-	-
4	-	-	-	-	31,728	-	-	-	-	31,728
5	-	-	-	-	70,424	7,584	-	-	-	78,008
6	-	-	-	-	35,589	-	-	-	-	35,589
7	-	-	-	-	-	-	-	-	-	-
8	-	-	-	-	32,034	-	-	-	-	32,034
9	-	-	-	-	20,586	-	-	-	-	20,586
10	-	-	-	-	25,040	-	-	-	785	25,825
11	-	-	-	-	36,505	-	-	-	-	36,505
12	-	-	-	-	23,499	-	-	-	-	23,499
13	-	-	-	-	-	-	-	-	-	-
14	-	-	-	-	13,979	-	-	-	-	13,979
15	-	-	-	-	-	-	-	-	-	-
16	-	-	-	-	6,295	-	-	-	-	6,295
17	-	-	-	-	74,802	-	-	-	1,482	76,283
18	-	-	-	-	45,228	-	-	-	295	45,523
19	-	-	-	-	97,174	-	-	-	646	97,820
20	-	-	-	-	117,744	-	-	-	-	117,744
21	-	-	-	-	-	-	-	-	-	-
22	-	-	-	-	2,956	-	-	-	-	2,956
23	-	-	-	-	63,433	-	-	-	-	63,433
24	-	-	-	-	89,375	25,321	-	-	762	115,458
25	-	-	-	-	134,338	-	-	-	7,081	141,419
26	-	-	-	-	166,923	-	-	-	1,430	168,353
27	-	-	-	-	161,520	-	-	-	-	161,520
28	-	-	-	-	45,265	-	-	-	571	45,837
29	13,911	-	-	-	21,879	-	-	-	-	35,791
30	-	-	-	-	54,597	-	-	-	-	54,597
31	-	-	-	-	-	-	-	-	-	-
32	-	-	-	-	11,870	-	-	-	-	11,870
33	-	-	-	-	29,736	22,927	-	-	-	52,663
34	-	-	-	-	88,361	-	-	-	-	88,361
35	-	-	-	-	95,871	-	-	-	4,391	100,262
36	-	-	-	-	84,630	4,778	-	-	2,538	91,947
37	-	-	-	-	126,548	8,644	-	-	2,910	138,103
38	-	-	-	-	58,315	-	-	-	-	58,315
39	-	-	-	-	-	-	-	-	-	-
40	-	-	-	-	-	-	-	-	-	-
41	-	-	21,403	-	37,410	-	38,515	-	-	97,327
42	-	-	-	-	-	-	-	-	-	-
43	-	-	-	-	-	-	-	-	-	-
44	-	-	-	-	-	-	-	-	-	-
45	-	-	-	-	26,803	-	-	-	-	26,803
46	-	-	-	-	134,876	-	-	-	-	134,876
47	-	-	-	-	60,842	-	-	-	-	60,842
48	-	-	-	-	12,067	-	-	-	-	12,067
49	-	-	-	-	83,549	-	-	-	-	83,549
50	-	-	-	-	10,864	-	7,338	-	-	18,202
51	-	-	-	-	32,143	-	-	-	15,610	47,753
52	-	-	-	-	-	-	-	-	11,336	11,336
53	-	-	-	-	-	-	-	-	-	-
54	-	-	70,386	-	-	-	-	-	-	70,386
55	35,341	-	-	-	30,231	-	36,719	-	-	102,292
56	-	-	-	-	-	-	-	-	-	-
57	-	-	-	-	6,881	-	-	-	1,015	7,896
58	-	-	-	-	8,986	23,149	-	-	2,620	34,755
59	-	-	-	-	61,414	10,130	-	-	-	71,543
60	-	-	-	-	37,608	-	-	-	-	37,608
61	-	-	-	-	30,263	9,657	-	-	-	39,920
62	-	-	1,802	-	16,160	-	-	-	1,030	18,993
63	-	-	-	-	73,760	-	-	-	-	73,760
64	-	-	-	-	114,341	-	-	-	-	114,341

Grid Cell (G-)	ESE slope 0° - 50°	ESE slope 50° - 90°	SSE slope 10° - 50°	SSE slope 50° - 90°	SSW slope 10° - 50°	SSW slope 50° - 90°	WSW slope 10° - 50°	WSW slope 50° - 90°	S (flat roof) slope of sub-structure 35°	Total potential (kWh/a)
65	-	-	-	-	4,656	-	-	-	-	4,656
66	30,787	-	-	-	-	-	-	-	36,967	67,754
67	32,245	-	-	-	47,423	-	-	-	-	79,668
68	-	-	-	-	-	-	-	-	-	-
69	-	-	-	-	41,162	-	-	-	-	41,162
70	-	-	-	-	14,469	-	-	-	-	14,469
71	-	-	-	-	-	-	-	-	-	-
72	-	-	-	-	7,499	-	-	-	-	7,499
73	-	-	-	-	52,595	20,467	-	-	15,288	88,349
74	-	-	-	-	19,803	53,804	-	-	-	73,607
75	-	-	-	-	43,479	14,231	-	-	3,524	61,234
76	-	-	-	-	40,543	-	-	-	30,243	70,786
77	13,730	-	-	-	27,749	-	-	-	-	41,479
78	-	-	-	-	26,808	-	-	-	-	26,808
79	-	-	-	-	-	-	-	-	-	-
80	-	-	-	-	-	-	-	-	-	-
81	-	-	-	-	-	-	-	-	-	-
82	-	-	-	-	36,941	-	-	-	-	36,941
83	-	-	-	-	1,446	-	-	-	-	1,446
84	-	-	-	-	50,034	-	-	-	-	50,034
85	-	-	-	-	-	-	-	-	-	-
86	-	-	-	-	-	-	-	-	44,888	44,888
87	-	-	-	-	7,555	-	-	-	9,485	17,040
88	-	-	-	-	20,899	7,869	-	-	-	28,768
89	-	-	-	-	113,484	-	-	-	2,462	115,945
90	-	-	-	-	106,362	-	-	-	-	106,362
91	-	-	-	-	-	-	-	-	-	-
92	-	-	-	-	-	-	-	-	-	-
93	-	-	-	-	-	-	-	-	-	-
94	-	-	-	-	2,073	-	-	-	-	2,073
95	-	-	-	-	7,935	-	-	-	-	7,935
96	-	-	-	-	10,153	-	-	-	6,188	16,341
97	-	-	-	-	42,713	6,494	-	-	-	49,206
98	-	-	-	-	48,205	-	-	-	-	48,205
99	-	-	2,840	-	94,640	-	-	-	-	97,479
100	-	-	-	-	-	-	-	-	-	-
101	-	-	-	-	-	7,921	-	-	-	7,921
102	-	-	-	-	35,132	-	-	-	9,587	44,719
103	-	-	-	-	44,822	4,871	-	-	-	49,693
104	-	-	-	-	9,413	2,278	-	-	-	11,691
105	-	-	-	-	-	-	-	-	-	-
106	6,953	-	-	-	34,126	-	-	-	361	41,441
107	-	-	-	-	-	-	-	-	-	-
108	-	-	-	-	29,496	-	-	-	-	29,496
109	-	-	-	-	25,683	-	-	-	-	25,683
110	-	-	-	-	-	-	-	-	-	-
<b>Total</b>	<b>132,967</b>	<b>-</b>	<b>96,430</b>	<b>-</b>	<b>3,691,737</b>	<b>230,125</b>	<b>82,572</b>	<b>-</b>	<b>213,496</b>	<b>4,447,328</b>

Appendix B-2: Solar Energy, Technical Potential in S-2030

Grid Cell (G-)	ESE slope 0° - 50°	ESE slope 50° - 90°	SSE slope 10° - 50°	SSE slope 50° - 90°	SSW slope 10° - 50°	SSW slope 50° - 90°	WSW slope 10° - 50°	WSW slope 50° - 90°	S (flat roof) slope of sub-structure 35°	Total potential (kWh/a)
1	-	-	-	-	-	12,054	-	-	1,153	13,207
2	-	-	-	-	-	-	-	-	-	-
3	-	-	-	-	-	-	-	-	-	-
4	13,038	-	-	-	31,728	-	-	-	911	45,677
5	97,576	-	-	-	70,424	7,584	-	-	-	175,584
6	15,812	-	-	-	35,589	-	-	-	-	51,401
7	-	-	-	-	-	-	-	-	8,449	8,449
8	47,799	-	-	-	44,545	-	-	-	931	93,275
9	58,612	-	-	-	37,151	-	-	-	-	95,763
10	28,826	-	-	-	25,040	-	-	-	785	54,651
11	27,168	-	-	-	36,505	-	-	-	-	63,673
12	-	-	-	-	23,499	-	-	-	-	23,499
13	-	-	-	-	-	-	-	-	-	-
14	19,867	2,616	-	-	24,250	14,452	-	-	-	61,184
15	40,086	-	-	-	10,005	-	-	-	-	50,092
16	112,607	-	-	-	6,295	-	-	-	-	118,901
17	21,541	-	-	-	74,802	-	-	-	4,918	101,261
18	55,168	-	-	-	45,228	-	-	-	4,505	104,901
19	24,963	-	-	-	100,970	-	-	-	6,999	132,932
20	24,185	-	-	-	117,744	-	-	-	-	141,930
21	-	-	-	-	-	-	-	-	-	-
22	11,499	-	-	-	2,956	-	-	-	-	14,455
23	8,413	-	-	-	63,433	6,680	-	-	3,801	82,327
24	2,511	-	-	-	92,816	32,633	-	-	3,117	131,077
25	43,084	-	-	-	149,498	7,179	-	-	13,654	213,415
26	46,440	-	-	-	166,923	5,543	-	-	15,015	233,921
27	12,926	-	-	-	161,520	-	-	-	-	174,446
28	61,410	-	-	-	70,912	-	-	-	4,689	137,011
29	22,464	-	-	-	22,370	-	-	-	6,452	51,286
30	74,145	-	-	-	54,597	-	-	-	-	128,743
31	27,488	-	-	-	-	-	-	-	-	27,488
32	24,263	-	-	-	17,983	14,145	-	-	1,139	57,530
33	16,578	-	-	-	35,054	22,927	-	-	1,761	76,320
34	42,711	-	-	-	113,953	-	-	-	-	156,664
35	-	-	-	-	97,692	6,399	-	-	5,631	109,722
36	14,709	-	-	-	88,942	4,778	-	-	3,050	111,479
37	-	-	-	-	144,203	15,052	-	-	3,514	162,769
38	16,902	-	-	-	71,136	2,541	-	-	-	90,580
39	-	-	-	-	-	-	-	-	-	-
40	-	-	21,100	-	33,539	6,798	-	-	-	61,436
41	56,677	-	21,403	-	37,410	-	38,515	-	-	154,004
42	26,456	-	-	-	-	-	-	-	-	26,456
43	-	-	-	-	-	-	-	-	-	-
44	10,869	-	-	-	10,256	1,573	-	-	-	22,699
45	25,714	4,777	-	-	54,887	-	-	-	4,427	89,806
46	-	-	-	-	160,606	-	-	-	-	160,606
47	44,211	-	-	-	60,842	-	-	-	-	105,054
48	56,144	-	-	-	12,067	16,147	-	-	-	84,357
49	13,767	-	-	-	84,655	2,143	9,828	-	-	110,393
50	34,355	1,701	-	-	50,712	-	7,338	-	3,443	97,550
51	41,785	-	-	-	32,143	-	-	-	15,610	89,538
52	521	-	-	-	145,278	-	-	-	11,336	157,135
53	-	-	-	-	-	-	-	-	523	523
54	-	-	70,386	-	-	-	-	-	-	70,386
55	35,341	-	-	-	30,231	-	36,719	-	-	102,292
56	-	-	-	-	-	-	-	-	-	-
57	33,997	2,090	-	-	6,881	16,497	14,631	10,214	1,015	85,326
58	20,498	-	-	-	16,012	23,149	-	-	2,620	62,278
59	-	-	-	-	71,099	10,130	-	-	-	81,228
60	44,531	-	-	-	43,714	-	-	-	-	88,245
61	71,741	-	-	-	38,332	19,915	-	-	718	130,705
62	46,599	-	1,802	-	53,011	23,268	-	-	1,571	126,252
63	11,126	-	-	-	91,087	21,634	-	-	14,118	137,965
64	76,940	-	-	-	114,341	-	-	-	-	191,281
65	-	-	30,139	-	4,656	-	34,830	-	10,539	80,165

Grid Cell (G-)	ESE slope 0° - 50°	ESE slope 50° - 90°	SSE slope 10° - 50°	SSE slope 50° - 90°	SSW slope 10° - 50°	SSW slope 50° - 90°	WSW slope 10° - 50°	WSW slope 50° - 90°	S (flat roof) slope of sub- structure 35°	Total potential (kWh/a)
66	31,486	790	-	-	-	-	-	-	87,271	119,548
67	33,509	-	-	-	47,423	-	-	-	-	80,932
68	-	-	-	-	-	-	-	-	-	-
69	61,916	-	-	-	41,162	-	-	-	17,584	120,662
70	6,600	-	-	-	14,469	-	-	-	-	21,069
71	9,151	-	-	-	48,875	5,559	-	-	-	63,585
72	15,898	-	-	-	13,600	38,979	-	-	-	68,477
73	42,869	-	-	-	52,595	22,476	-	-	17,372	135,311
74	25,783	-	-	-	19,803	80,292	-	-	-	125,878
75	6,430	3,195	-	-	50,007	22,693	-	6,323	5,378	94,026
76	20,004	-	-	-	40,543	3,413	-	-	30,243	94,203
77	134,463	-	-	-	27,749	-	-	-	-	162,212
78	123,196	-	-	-	26,808	-	-	-	-	150,004
79	-	-	-	-	-	-	-	-	-	-
80	-	-	-	-	-	-	-	-	-	-
81	-	-	-	-	-	-	-	-	-	-
82	67,343	-	-	-	36,941	2,057	-	-	-	106,341
83	-	-	-	-	10,350	18,499	-	-	-	28,848
84	58,430	-	-	-	50,643	-	-	-	1,324	110,397
85	20,695	-	-	-	1,355	19,090	-	-	3,167	44,307
86	50,393	-	-	-	-	-	-	-	44,888	95,281
87	17,031	-	-	-	11,322	-	-	-	12,350	40,703
88	27,272	18,059	-	-	20,899	46,599	-	726	612	114,168
89	40,201	-	-	-	113,484	-	-	-	2,462	156,147
90	14,366	-	-	-	106,362	-	-	-	-	120,728
91	-	-	-	-	-	-	-	-	-	-
92	109,089	11,150	-	-	-	8,262	-	-	-	128,500
93	4,541	-	-	-	-	-	-	-	-	4,541
94	11,832	6,760	-	-	8,144	3,931	-	-	-	30,668
95	27,800	-	-	-	17,246	5,984	-	-	19,759	70,789
96	23,718	-	-	-	22,173	21,325	-	-	14,244	81,459
97	82,033	-	-	840	42,713	14,550	-	-	-	140,136
98	82,646	10,676	-	-	48,205	5,465	-	-	-	146,991
99	26,747	2,737	2,840	-	103,669	-	-	-	-	135,993
100	41,407	-	-	-	-	2,810	-	-	-	44,217
101	-	-	-	-	-	7,921	-	-	-	7,921
102	11,060	-	-	-	35,132	17,625	-	-	9,587	73,404
103	23,031	2,048	-	-	54,280	4,871	1,610	-	-	85,840
104	124,116	-	-	-	9,413	6,168	-	-	-	139,698
105	-	-	-	-	-	-	-	-	-	-
106	18,276	10,959	-	-	47,633	-	-	-	361	77,230
107	6,311	-	-	-	-	-	-	-	-	6,311
108	16,406	9,394	-	-	29,496	2,170	-	-	-	57,465
109	51,116	-	-	-	27,965	11,825	-	-	-	90,906
110	-	-	-	-	-	-	-	-	-	-
<b>Total</b>	<b>3,131,235</b>	<b>86,952</b>	<b>147,670</b>	<b>840</b>	<b>4,369,978</b>	<b>665,784</b>	<b>143,471</b>	<b>17,263</b>	<b>422,998</b>	<b>8,986,190</b>

Appendix B-3: Solar Energy, Technical Potential in S-2038-a and -b

Grid Cell (G-)	ESE slope 0° - 50°	ESE slope 50° - 90°	SSE slope 10° - 50°	SSE slope 50° - 90°	SSW slope 10° - 50°	SSW slope 50° - 90°	WSW slope 10° - 50°	WSW slope 50° - 90°	S (flat roof) slope of sub-structure 35°	Parking Lots (*)	Total potential (**) (kW/h/a)
1	-	-	-	-	-	12,054	-	-	1,153	-	14,788
2	-	-	-	-	-	-	-	-	-	-	-
3	-	-	-	-	-	-	-	-	-	-	-
4	13,038	-	-	-	31,728	-	-	-	911	-	47,258
5	97,576	-	-	-	70,424	7,584	-	-	-	-	177,165
6	15,812	-	-	-	35,589	-	-	-	-	-	52,981
7	-	-	-	-	-	-	-	-	8,449	-	10,029
8	47,799	-	-	-	44,545	-	-	-	931	-	94,855
9	58,612	-	-	-	37,151	-	-	-	-	-	97,344
10	28,826	-	-	-	25,040	-	-	-	785	-	56,231
11	27,168	-	-	-	36,505	-	-	-	-	-	65,253
12	-	-	-	-	23,499	-	-	-	-	-	25,079
13	-	-	-	-	-	-	-	-	-	-	-
14	19,867	2,616	-	-	24,250	14,452	-	-	-	-	62,765
15	40,086	-	-	-	10,005	-	-	-	-	-	51,672
16	112,607	-	-	-	6,295	-	-	-	-	-	120,482
17	21,541	-	-	-	74,802	-	-	-	4,918	-	102,842
18	55,168	-	-	-	45,228	-	-	-	4,505	-	106,482
19	24,963	-	-	-	100,970	-	-	-	6,999	-	134,513
20	24,185	-	-	-	117,744	-	-	-	-	-	143,510
21	-	-	-	-	-	-	-	-	-	-	-
22	11,499	-	-	-	2,956	-	-	-	-	-	16,035
23	8,413	-	-	-	63,433	6,680	-	-	3,801	-	83,908
24	2,511	-	-	-	92,816	32,633	-	-	3,117	-	132,658
25	43,084	-	-	-	149,498	7,179	-	-	13,654	-	214,995
26	46,440	-	-	-	166,923	5,543	-	-	15,015	-	235,501
27	12,926	-	-	-	161,520	-	-	-	-	-	176,027
28	61,410	-	-	-	70,912	-	-	-	4,689	-	138,591
29	22,464	-	-	-	22,370	-	-	-	6,452	-	52,867
30	74,145	-	-	-	54,597	-	-	-	-	-	130,323
31	27,488	-	-	-	-	-	-	-	-	-	29,068
32	24,263	-	-	-	17,983	14,145	-	-	1,139	-	59,110
33	16,578	-	-	-	35,054	22,927	-	-	1,761	-	77,901
34	42,711	-	-	-	113,953	-	-	-	-	-	158,244
35	-	-	-	-	97,692	6,399	-	-	5,631	-	111,303
36	14,709	-	-	-	88,942	4,778	-	-	3,050	-	113,060
37	-	-	-	-	144,203	15,052	-	-	3,514	-	164,349
38	16,902	-	-	-	71,136	2,541	-	-	-	39,368	92,160
39	-	-	-	-	-	-	-	-	-	-	-
40	-	-	21,100	-	33,539	6,798	-	-	-	-	63,017
41	56,677	-	21,403	-	37,410	-	38,515	-	-	-	155,584
42	26,456	-	-	-	-	-	-	-	-	28,852	28,037
43	-	-	-	-	-	-	-	-	-	-	-
44	10,869	-	-	-	10,256	1,573	-	-	-	-	24,279
45	25,714	4,777	-	-	54,887	-	-	-	4,427	-	91,387
46	-	-	-	-	160,606	-	-	-	-	-	162,186
47	44,211	-	-	-	60,842	-	-	-	-	-	106,634
48	56,144	-	-	-	12,067	16,147	-	-	-	-	85,937
49	13,767	-	-	-	84,655	2,143	9,828	-	-	-	111,973
50	34,355	1,701	-	-	50,712	-	7,338	-	3,443	-	99,130
51	41,785	-	-	-	32,143	-	-	-	15,610	82,011	91,119
52	521	-	-	-	145,278	-	-	-	11,336	-	158,716
53	-	-	-	-	-	-	-	-	523	-	2,103
54	-	-	70,386	-	-	-	-	-	-	-	71,966
55	35,341	-	-	-	30,231	-	36,719	-	-	-	103,872
56	-	-	-	-	-	-	-	-	-	-	-
57	33,997	2,090	-	-	6,881	16,497	14,631	10,214	1,015	-	86,907
58	20,498	-	-	-	16,012	23,149	-	-	2,620	-	63,859
59	-	-	-	-	71,099	10,130	-	-	-	-	82,809
60	44,531	-	-	-	43,714	-	-	-	-	-	89,825
61	71,741	-	-	-	38,332	19,915	-	-	718	-	132,286
62	46,599	-	1,802	-	53,011	23,268	-	-	1,571	-	127,832
63	11,126	-	-	-	91,087	21,634	-	-	14,118	-	139,546
64	76,940	-	-	-	114,341	-	-	-	-	-	192,861
65	-	-	30,139	-	4,656	-	34,830	-	10,539	23,613	81,745
66	31,486	790	-	-	-	-	-	-	87,271	-	121,128
67	33,509	-	-	-	47,423	-	-	-	-	-	82,512

(\*) Value is not directly assigned to the corresponding grid cell

(\*\*) Refers to total roof potential + average supplementary power from parking lots (here: 1,580 kWh/a)



Grid Cell (G-)	ESE slope 0° - 50°	ESE slope 50° - 90°	SSE slope 10° - 50°	SSE slope 50° - 90°	SSW slope 10° - 50°	SSW slope 50° - 90°	WSW slope 10° - 50°	WSW slope 50° - 90°	S (flat roof) slope of sub- structure 35°	Parking Lots (*)	Total potential (**) (kWh/a)
68	-	-	-	-	-	-	-	-	-	-	-
69	61,916	-	-	-	41,162	-	-	-	17,584	-	122,242
70	6,600	-	-	-	14,469	-	-	-	-	-	22,650
71	9,151	-	-	-	48,875	5,559	-	-	-	-	65,166
72	15,898	-	-	-	13,600	38,979	-	-	-	-	70,057
73	42,869	-	-	-	52,595	22,476	-	-	17,372	-	136,891
74	25,783	-	-	-	19,803	80,292	-	-	-	-	127,459
75	6,430	3,195	-	-	50,007	22,693	-	6,323	5,378	-	95,607
76	20,004	-	-	-	40,543	3,413	-	-	30,243	-	95,784
77	134,463	-	-	-	27,749	-	-	-	-	-	163,793
78	123,196	-	-	-	26,808	-	-	-	-	-	151,584
79	-	-	-	-	-	-	-	-	-	-	-
80	-	-	-	-	-	-	-	-	-	-	-
81	-	-	-	-	-	-	-	-	-	-	-
82	67,343	-	-	-	36,941	2,057	-	-	-	-	107,922
83	-	-	-	-	10,350	18,499	-	-	-	-	30,429
84	58,430	-	-	-	50,643	-	-	-	1,324	-	111,977
85	20,695	-	-	-	1,355	19,090	-	-	3,167	-	45,887
86	50,393	-	-	-	-	-	-	-	44,888	-	96,862
87	17,031	-	-	-	11,322	-	-	-	12,350	-	42,283
88	27,272	18,059	-	-	20,899	46,599	-	726	612	-	115,748
89	40,201	-	-	-	113,484	-	-	-	2,462	-	157,727
90	14,366	-	-	-	106,362	-	-	-	-	-	122,309
91	-	-	-	-	-	-	-	-	-	-	-
92	109,089	11,150	-	-	-	8,262	-	-	-	-	130,081
93	4,541	-	-	-	-	-	-	-	-	-	6,121
94	11,832	6,760	-	-	8,144	3,931	-	-	-	-	32,248
95	27,800	-	-	-	17,246	5,984	-	-	19,759	-	72,370
96	23,718	-	-	-	22,173	21,325	-	-	14,244	-	83,039
97	82,033	-	-	840	42,713	14,550	-	-	-	-	141,717
98	82,646	10,676	-	-	48,205	5,465	-	-	-	-	148,572
99	26,747	2,737	2,840	-	103,669	-	-	-	-	-	137,573
100	41,407	-	-	-	-	2,810	-	-	-	-	45,797
101	-	-	-	-	-	7,921	-	-	-	-	9,502
102	11,060	-	-	-	35,132	17,625	-	-	9,587	-	74,985
103	23,031	2,048	-	-	54,280	4,871	1,610	-	-	-	87,421
104	124,116	-	-	-	9,413	6,168	-	-	-	-	141,278
105	-	-	-	-	-	-	-	-	-	-	-
106	18,276	10,959	-	-	47,633	-	-	-	361	-	78,810
107	6,311	-	-	-	-	-	-	-	-	-	7,891
108	16,406	9,394	-	-	29,496	2,170	-	-	-	-	59,046
109	51,116	-	-	-	27,965	11,825	-	-	-	-	92,486
110	-	-	-	-	-	-	-	-	-	-	-
<b>Total</b>	<b>3,131,235</b>	<b>86,952</b>	<b>147,670</b>	<b>840</b>	<b>4,369,978</b>	<b>665,784</b>	<b>143,471</b>	<b>17,263</b>	<b>422,998</b>	<b>173,844</b>	<b>9,137,909</b>

(\*) Value is not directly assigned to the corresponding grid cell

(\*\*) Refers to total roof potential + average supplementary power from parking lots (here: 1,580 kWh/a)

## Appendix C-1: Scenario Outcome in S-2022

Grid Cell (G-)	Heat Demand (kWh/a)	Heat Gap (kWh/a)	Power Demand (kWh/a)	Power Gap (kWh/a)	Power Gap in relation (%)	Sub-area Suitability Level (*)
1	126,200	- 108,600	42,067	- 42,067	-100%	n/a
2	-	10,200	-	-	0%	n/a
3	-	-	-	-	0%	n/a
4	148,100	- 92,650	49,367	- 17,638	-36%	0
5	543,000	- 478,400	181,000	- 102,992	-57%	0
6	220,400	- 186,400	73,467	- 37,877	-52%	0
7	42,600	- 8,300	14,200	- 14,200	-100%	n/a
8	425,000	- 357,000	141,667	- 109,633	-77%	0
9	406,900	- 359,300	135,633	- 115,047	-85%	0
10	379,100	- 338,300	126,367	- 100,542	-80%	0
11	283,400	- 256,200	94,467	- 57,962	-61%	0
12	124,400	- 117,600	41,467	- 17,968	-43%	n/a
13	-	10,200	-	-	0%	n/a
14	220,700	- 139,100	73,567	- 59,588	-81%	0
15	247,200	- 182,600	82,400	- 82,400	-100%	0
16	558,600	- 497,400	186,200	- 179,905	-97%	0
17	605,300	- 540,700	201,767	- 125,483	-62%	0
18	933,700	- 855,500	311,233	- 265,710	-85%	0
19	866,900	- 819,300	288,967	- 191,146	-66%	0
20	412,200	- 357,800	137,400	- 19,656	-14%	0
21	-	10,200	-	-	0%	n/a
22	26,800	- 6,400	8,933	- 5,978	-67%	n/a
23	615,000	- 547,000	205,000	- 141,567	-69%	0
24	703,400	- 632,000	234,467	- 119,009	-51%	0
25	873,200	- 795,000	291,067	- 149,648	-51%	0
26	826,000	- 744,400	275,333	- 106,980	-39%	0
27	667,000	- 592,200	222,333	- 60,814	-27%	0
28	834,100	- 759,300	278,033	- 232,197	-84%	0
29	505,300	- 440,400	168,433	- 132,643	-79%	0
30	586,800	- 541,400	195,600	- 141,003	-72%	0
31	112,800	- 95,050	37,600	- 37,600	-100%	n/a
32	246,100	- 188,300	82,033	- 70,164	-86%	0
33	228,500	- 157,100	76,167	- 23,504	-31%	0
34	507,800	- 456,800	169,267	- 80,905	-48%	0
35	537,300	- 462,500	179,100	- 78,838	-44%	0
36	640,000	- 555,000	213,333	- 121,387	-57%	0
37	776,700	- 715,350	258,900	- 120,797	-47%	0
38	384,000	- 286,400	128,000	- 69,685	-54%	0
39	-	126,000	-	-	0%	1
40	256,100	- 185,100	85,367	- 85,367	-100%	0
41	621,200	- 575,050	207,067	- 109,740	-53%	0
42	118,600	- 83,100	39,533	- 39,533	-100%	n/a
43	-	3,550	-	-	0%	n/a
44	157,600	- 144,000	52,533	- 52,533	-100%	n/a
45	310,600	- 222,200	103,533	- 76,730	-74%	0
46	615,800	- 551,200	205,267	- 70,391	-34%	0
47	420,700	- 352,700	140,233	- 79,391	-57%	0
48	520,600	- 445,500	173,533	- 161,467	-93%	0
49	403,900	- 327,450	134,633	- 51,085	-38%	0
50	493,000	- 419,650	164,333	- 146,131	-89%	0
51	218,100	- 132,900	72,700	- 24,947	-34%	0
52	58,000	76,900	19,333	- 7,997	-41%	0
53	-	156,200	-	-	0%	1
54	249,500	- 139,450	83,167	- 12,781	-15%	30
55	754,400	- 715,350	251,467	- 149,175	-59%	0
56	-	3,550	-	-	0%	n/a

(\*) 1 = Supplier, very high; 2 = Supplier, high; 3 = Supplier, medium  
10 = Receiver, very high; 20 = Receiver, high; 30 = Receiver, medium  
n/a = grid cell mostly outside of boundary, not considered as sub-area

Grid Cell (G-)	Heat Demand (kWh/a)	Heat Gap (kWh/a)	Power Demand (kWh/a)	Power Gap (kWh/a)	Power Gap in relation (%)	Sub-area Suitability Level (*)
57	308,100	- 267,300	102,700	- 67,945	-66%	0
58	311,300	- 239,900	103,767	- 32,223	-31%	0
59	308,700	- 254,300	102,900	- 65,292	-63%	0
60	439,800	- 374,900	146,600	- 106,680	-73%	0
61	333,600	- 253,450	111,200	- 92,207	-83%	0
62	362,900	- 263,500	120,967	- 47,207	-39%	0
63	752,700	- 674,600	250,900	- 136,559	-54%	0
64	271,500	- 196,950	90,500	- 49,059	-54%	0
65	20,400	- 32,850	6,800	- 2,144	-32%	0
66	111,800	- 40,800	37,267	30,487	82%	10
67	343,100	- 300,500	114,367	- 34,699	-30%	0
68	-	-	-	-	0%	n/a
69	95,500	- 81,900	31,833	- 17,364	-55%	n/a
70	300,000	- 228,600	100,000	- 100,000	-100%	0
71	207,100	- 132,300	69,033	- 61,534	-89%	0
72	612,100	- 537,000	204,033	- 115,684	-57%	0
73	288,000	- 187,150	96,000	- 22,393	-23%	0
74	298,900	- 210,150	99,633	- 38,399	-39%	0
75	445,900	- 353,600	148,633	- 77,847	-52%	0
76	636,900	- 554,850	212,300	- 170,821	-80%	0
77	547,800	- 449,350	182,600	- 155,792	-85%	0
78	202,400	- 104,350	67,467	- 59,570	-88%	0
79	172,300	- 154,150	57,433	- 57,433	-100%	0
80	-	-	-	-	0%	n/a
81	-	-	-	-	0%	n/a
82	82,800	- 48,800	27,600	- 26,154	-95%	n/a
83	335,300	- 270,400	111,767	- 61,732	-55%	0
84	313,500	- 229,800	104,500	- 104,500	-100%	0
85	313,500	- 217,650	104,500	- 59,612	-57%	0
86	72,400	13,200	24,133	- 7,094	-29%	3
87	288,000	- 196,850	96,000	- 67,232	-70%	0
88	706,300	- 632,700	235,433	- 119,488	-51%	0
89	639,200	- 549,200	213,067	- 106,705	-50%	0
90	366,500	- 302,750	122,167	- 81,004	-66%	0
91	-	11,250	-	-	0%	n/a
92	49,300	- 38,950	16,433	- 16,433	-100%	n/a
93	226,200	- 172,950	75,400	- 73,327	-97%	0
94	168,600	- 68,600	56,200	- 48,265	-86%	0
95	244,800	- 160,750	81,600	- 65,259	-80%	0
96	497,800	- 389,050	165,933	- 116,727	-70%	0
97	563,000	- 461,450	187,667	- 139,462	-74%	0
98	587,700	- 495,750	195,900	- 98,421	-50%	0
99	640,900	- 602,800	213,633	- 176,693	-83%	n/a
100	31,800	- 6,550	10,600	- 2,679	-25%	n/a
101	293,000	- 210,050	97,667	- 52,948	-54%	0
102	385,600	- 305,350	128,533	- 78,840	-61%	0
103	536,300	- 440,450	178,767	- 167,076	-93%	0
104	647,400	- 573,300	215,800	- 215,800	-100%	0
105	-	3,900	-	-	0%	n/a
106	18,800	- 11,000	6,267	- 6,267	-100%	n/a
107	207,800	- 152,900	69,267	- 39,771	-57%	0
108	663,100	- 584,050	221,033	- 195,350	-88%	0
109	311,100	- 295,500	103,700	- 103,700	-100%	n/a
110	-	4,050	-	-	0%	n/a

(\*) 1 = Supplier, very high; 2 = Supplier, high; 3 = Supplier, medium  
10 = Receiver, very high; 20 = Receiver, high; 30 = Receiver, medium  
n/a = grid cell mostly outside of boundary, not considered as sub-area

## Appendix C-2: Scenario Outcome in S-2030

Grid Cell (G-)	Heat Demand (kWh/a)	Heat Gap (kWh/a)	Power Demand (kWh/a)	Power Gap (kWh/a)	Power Gap in relation (%)	Sub-area Suitability Level (*)
1	99,592	- 69,854	33,197	- 19,990	-60%	n/a
2	-	20,762	-	-	0%	n/a
3	-	5,310	-	-	0%	n/a
4	111,294	- 10,651	37,098	8,579	23%	0
5	407,451	- 290,665	135,817	39,767	29%	0
6	163,606	- 106,511	54,535	- 3,134	-6%	0
7	31,875	36,315	10,625	- 2,176	-20%	n/a
8	319,319	- 194,748	106,440	- 13,165	-12%	0
9	303,557	- 220,509	101,186	- 5,422	-5%	0
10	286,531	- 216,460	95,510	- 40,860	-43%	0
11	216,083	- 169,369	72,028	- 8,355	-12%	0
12	94,878	- 81,902	31,626	- 8,127	-26%	n/a
13	-	18,167	-	-	0%	n/a
14	165,055	- 19,722	55,018	6,166	11%	0
15	186,742	- 69,956	62,247	- 12,156	-20%	0
16	425,015	- 313,420	141,672	- 22,770	-16%	0
17	462,347	- 350,752	154,116	- 52,854	-34%	0
18	711,753	- 574,205	237,251	- 132,350	-56%	0
19	661,012	- 575,369	220,337	- 87,405	-40%	0
20	320,373	- 221,754	106,791	35,139	33%	0
21	-	18,167	-	-	0%	n/a
22	20,410	13,328	6,803	7,651	112%	n/a
23	464,029	- 344,648	154,676	- 72,349	-47%	0
24	530,744	- 403,577	176,915	- 45,837	-26%	0
25	661,608	- 524,060	220,536	- 7,121	-3%	0
26	628,128	- 485,390	209,376	24,545	12%	0
27	513,006	- 383,244	171,002	3,444	2%	0
28	637,462	- 502,510	212,487	- 75,477	-36%	0
29	385,302	- 268,040	128,434	- 77,148	-60%	0
30	450,374	- 370,374	150,125	- 21,382	-14%	0
31	86,588	- 54,017	28,863	- 1,375	-5%	n/a
32	186,234	- 79,829	62,078	- 4,548	-7%	0
33	173,472	- 43,710	57,824	18,496	32%	0
34	387,540	- 294,111	129,180	27,484	21%	0
35	403,433	- 273,671	134,478	- 24,755	-18%	0
36	482,604	- 334,675	160,868	- 49,389	-31%	0
37	590,017	- 480,779	196,672	- 33,904	-17%	0
38	293,356	- 122,856	97,785	- 7,206	-7%	20
39	-	222,071	-	-	0%	1
40	200,396	- 75,539	66,799	- 5,362	-8%	20
41	476,849	- 398,135	158,950	- 4,946	-3%	0
42	90,741	- 25,598	30,247	- 3,791	-13%	n/a
43	-	5,429	-	-	0%	n/a
44	118,351	- 92,399	39,450	- 16,752	-42%	n/a
45	233,916	- 78,202	77,972	11,834	15%	0
46	468,659	- 351,873	156,220	4,386	3%	0
47	320,840	- 201,459	106,947	- 1,893	-2%	0
48	394,838	- 264,600	131,613	- 47,256	-36%	0
49	303,753	- 165,705	101,251	9,142	9%	0
50	373,185	- 245,161	124,395	- 26,845	-22%	0
51	166,673	- 11,959	55,558	33,981	61%	10
52	45,965	192,892	15,322	141,814	926%	1
53	-	276,857	-	523	0%	1
54	191,524	3,905	63,841	6,545	10%	1
55	567,975	- 500,118	189,325	- 87,033	-46%	0
56	-	2,714	-	-	0%	n/a

(\*) 1 = Supplier, very high; 2 = Supplier, high; 3 = Supplier, medium  
10 = Receiver, very high; 20 = Receiver, high; 30 = Receiver, medium  
n/a = grid cell mostly outside of boundary, not considered as sub-area

Grid Cell (G-)	Heat Demand (kWh/a)	Heat Gap (kWh/a)	Power Demand (kWh/a)	Power Gap (kWh/a)	Power Gap in relation (%)	Sub-area Suitability Level (*)
57	232,191	- 156,929	77,397	- 15,119	-20%	0
58	235,829	- 111,258	78,610	2,619	3%	0
59	235,081	- 141,652	78,360	9,884	13%	0
60	334,222	- 219,555	111,407	19,298	17%	0
61	251,494	- 112,970	83,831	42,421	51%	0
62	275,507	- 99,078	91,836	46,130	50%	0
63	571,152	- 432,723	190,384	897	0%	0
64	207,212	- 74,212	69,071	8,159	12%	10
65	15,338	82,376	5,113	75,052	1468%	1
66	86,497	43,789	28,832	90,716	315%	1
67	262,193	- 186,193	87,398	- 6,466	-7%	0
68	-	-	-	-	0%	n/a
69	71,720	- 50,958	23,907	- 2,837	-12%	n/a
70	226,731	- 96,969	75,577	- 11,992	-16%	0
71	155,649	- 23,292	51,883	16,594	32%	0
72	467,479	- 329,336	155,826	- 20,515	-13%	0
73	215,188	- 31,831	71,729	54,149	75%	10
74	224,382	- 66,953	74,794	19,232	26%	10
75	337,011	- 174,154	112,337	- 18,134	-16%	0
76	483,118	- 336,070	161,039	1,173	1%	0
77	415,509	- 240,819	138,503	11,501	8%	0
78	149,562	18,986	49,854	35,472	71%	1
79	126,920	- 93,872	42,307	- 42,307	-100%	0
80	-	-	-	-	0%	n/a
81	-	2,595	-	-	0%	n/a
82	61,973	- 2,283	20,658	8,191	40%	n/a
83	256,057	- 133,367	85,352	25,044	29%	0
84	241,610	- 94,943	80,537	- 36,230	-45%	0
85	237,484	- 63,770	79,161	16,120	20%	10
86	56,652	95,943	18,884	21,819	116%	1
87	219,780	- 61,732	73,260	40,908	56%	10
88	546,285	- 417,975	182,095	- 25,948	-14%	0
89	497,253	- 338,586	165,751	- 45,023	-27%	0
90	278,432	- 162,265	92,811	27,851	30%	0
91	-	17,000	-	-	0%	n/a
92	38,080	- 19,675	12,693	- 8,153	-64%	n/a
93	175,565	- 80,565	58,522	- 27,854	-48%	0
94	130,548	52,262	43,516	27,273	63%	1
95	189,919	- 39,895	63,306	18,152	29%	10
96	385,102	- 195,269	128,367	11,769	9%	0
97	438,198	- 259,103	146,066	925	1%	0
98	461,023	- 301,618	153,674	- 17,681	-12%	0
99	491,927	- 425,570	163,976	- 57,634	-35%	n/a
100	24,938	18,967	8,313	- 391	-5%	n/a
101	227,476	- 76,357	75,825	- 2,421	-3%	20
102	297,535	- 155,845	99,178	- 13,338	-13%	0
103	415,463	- 244,368	138,488	1,210	1%	0
104	505,692	- 375,787	168,564	- 40,064	-24%	0
105	-	8,857	-	-	0%	n/a
106	14,572	3,023	4,857	1,454	30%	n/a
107	161,091	- 63,281	53,697	3,768	7%	0
108	516,236	- 372,903	172,079	- 81,173	-47%	0
109	242,654	- 219,035	80,885	- 36,668	-45%	n/a
110	-	6,095	-	-	0%	n/a

(\*) 1 = Supplier, very high; 2 = Supplier, high; 3 = Supplier, medium  
10 = Receiver, very high; 20 = Receiver, high; 30 = Receiver, medium  
n/a = grid cell mostly outside of boundary, not considered as sub-area

### Appendix C-3: Scenario Outcome in S-2038-a and -b

Grid Cell (G-)	Heat Demand (kWh/a)	Heat Gap, S-2038-a (kWh/a)	Heat Gap, S-2038-b (kWh/a)	Power Demand (kWh/a)	Power Gap (kWh/a)	Power Gap in relation (%)	Sub-area Suitability Level, S-2038-a (*)	Sub-area Suitability Level, S-2038-b (*)
1	81,846	- 42,632	- 8,046	27,282	- 12,494	-46%	n/a	n/a
2	-	25,929	49,200	-	1,580	0%	n/a	n/a
3	-	4,821	-	-	1,580	0%	n/a	n/a
4	88,502	41,355	194,398	29,501	17,757	60%	1	1
5	327,928	- 177,071	- 45,028	109,309	67,855	62%	0	10
6	130,517	- 55,088	41,683	43,506	9,476	22%	0	1
7	24,988	60,726	122,612	8,329	1,700	20%	n/a	n/a
8	256,064	- 95,778	76,036	85,355	9,501	11%	0	1
9	211,998	- 103,569	- 2,898	70,666	26,678	38%	0	10
10	230,892	- 138,963	- 21,792	76,964	- 20,733	-27%	0	30
11	174,847	- 113,561	- 88,747	58,282	6,971	12%	0	0
12	76,785	- 60,285	- 52,185	25,595	- 516	-2%	n/a	n/a
13	-	23,571	49,200	-	1,580	0%	n/a	n/a
14	122,292	66,279	209,808	40,764	22,001	54%	1	1
15	150,010	847	120,590	50,003	1,669	3%	1	1
16	344,356	- 200,570	- 61,456	114,785	5,696	5%	0	10
17	375,593	- 229,450	- 92,693	125,198	- 22,356	-18%	0	0
18	575,727	- 396,584	- 243,627	191,909	- 85,427	-45%	0	0
19	534,909	- 424,123	- 325,809	178,303	- 43,790	-25%	0	0
20	251,425	- 124,139	- 79,225	83,808	59,702	71%	0	10
21	-	23,571	73,800	-	1,580	0%	n/a	n/a
22	16,500	28,286	81,900	5,500	10,535	192%	n/a	n/a
23	372,526	- 216,955	- 15,826	124,175	- 40,268	-32%	0	0
24	427,005	- 262,005	- 119,505	142,335	- 9,677	-7%	0	20
25	534,215	- 355,072	- 202,115	178,072	36,924	21%	0	0
26	494,671	- 308,457	- 101,071	164,890	70,611	43%	0	0
27	417,634	- 247,920	- 48,634	139,211	36,815	26%	0	10
28	516,690	- 342,261	- 196,890	172,230	- 33,639	-20%	0	30
29	311,750	- 160,250	- 41,150	103,917	- 51,050	-49%	0	0
30	366,346	- 262,203	- 169,546	122,115	8,208	7%	10	10
31	70,418	- 28,525	3,382	23,473	5,595	24%	n/a	n/a
32	149,897	- 13,183	59,203	49,966	9,145	18%	0	1
33	137,703	29,654	218,997	45,901	32,000	70%	1	1
34	314,817	- 194,603	- 105,717	104,939	53,305	51%	0	10
35	324,091	- 154,377	8,009	108,030	3,272	3%	0	1
36	385,111	- 191,825	- 28,411	128,370	- 15,311	-12%	0	20
37	476,509	- 334,759	- 193,609	158,836	5,513	3%	0	10
38	236,933	- 14,397	168,967	78,978	13,182	17%	10	1
39	-	289,071	516,600	-	1,580	0%	1	1
40	150,471	9,708	95,529	50,157	12,860	26%	1	1
41	387,808	- 284,308	- 215,608	129,269	26,315	20%	10	10
42	73,612	10,174	86,288	24,537	3,499	14%	n/a	n/a
43	-	7,393	12,300	-	1,580	0%	n/a	n/a
44	94,945	- 61,945	- 21,145	31,648	- 7,369	-23%	n/a	n/a
45	186,519	13,838	133,281	62,173	29,214	47%	1	1
46	379,122	- 228,265	- 120,822	126,374	35,812	28%	0	10
47	260,495	- 104,924	- 2,195	86,832	19,802	23%	0	10
48	318,359	- 150,466	- 23,159	106,120	- 20,183	-19%	0	30
49	243,069	- 64,676	76,731	81,023	30,950	38%	10	1
50	299,440	- 132,297	8,060	99,813	- 683	-1%	0	2
51	129,388	70,219	202,712	43,129	47,989	111%	1	1
52	32,655	275,381	434,745	10,885	147,831	1358%	1	1
53	-	359,786	528,900	-	2,103	0%	1	1
54	155,754	98,067	213,246	51,918	20,048	39%	1	1
55	429,426	- 340,712	- 269,526	143,142	- 39,270	-27%	0	0
56	-	4,929	12,300	-	1,580	0%	n/a	n/a
57	186,729	- 90,086	- 14,529	62,243	1,616	3%	0	10

(\*) 1 = Supplier, very high; 2 = Supplier, high; 3 = Supplier, medium  
 10 = Receiver, very high; 20 = Receiver, high; 30 = Receiver, medium  
 n/a = grid cell mostly outside of boundary, not considered as sub-area

Grid Cell (G-)	Heat Demand (kWh/a)	Heat Gap, S-2038-a (kWh/a)	Heat Gap, S-2038-b (kWh/a)	Power Demand (kWh/a)	Power Gap (kWh/a)	Power Gap in relation (%)	Sub-area Suitability Level, S-2038-a (*)	Sub-area Suitability Level, S-2038-b (*)
58	188,825	- 26,182	118,675	62,942	19,867	32%	10	1
59	190,330	- 67,759	18,770	63,443	26,382	42%	10	1
60	269,057	- 122,378	50,743	89,686	42,600	47%	0	1
61	200,777	- 19,384	180,523	66,926	60,907	91%	10	1
62	219,732	9,447	161,568	73,244	66,302	91%	1	1
63	460,601	- 280,708	- 153,101	153,534	39,327	26%	0	10
64	166,690	5,810	140,810	55,563	23,247	42%	1	1
65	11,531	114,148	209,869	3,844	77,901	2027%	1	1
66	68,014	99,557	227,186	22,671	98,457	434%	1	1
67	212,516	- 113,945	- 15,716	70,839	11,674	16%	10	10
68	-	-	-	-	1,580	0%	n/a	n/a
69	57,581	- 29,295	- 32,981	19,194	3,456	18%	n/a	n/a
70	181,313	- 13,956	199,987	60,438	4,728	8%	10	1
71	123,309	48,762	208,791	41,103	28,954	70%	1	1
72	378,422	- 200,886	- 34,022	126,141	10,751	9%	0	10
73	171,464	65,000	259,036	57,155	70,304	123%	1	1
74	177,730	26,806	203,570	59,243	36,363	61%	1	1
75	271,829	- 62,365	60,271	90,610	5,174	6%	10	1
76	389,572	- 199,286	- 45,172	129,857	33,935	26%	0	10
77	335,068	- 111,818	58,532	111,689	39,895	36%	10	1
78	106,461	113,610	274,839	35,487	51,420	145%	1	1
79	78,952	- 36,523	19,448	26,317	- 24,737	-94%	0	0
80	-	-	-	-	1,580	0%	n/a	n/a
81	-	2,357	12,300	-	1,580	0%	n/a	n/a
82	48,403	29,383	86,897	16,134	14,294	89%	n/a	n/a
83	200,358	- 43,929	119,442	66,786	45,191	68%	10	1
84	194,542	- 3,292	149,858	64,847	- 18,960	-29%	30	3
85	179,653	44,597	189,347	59,884	36,977	62%	1	1
86	45,433	152,335	311,267	15,144	27,139	179%	1	1
87	174,517	31,126	182,183	58,172	57,576	99%	1	1
88	441,964	- 275,571	- 146,764	147,321	10,406	7%	0	10
89	402,604	- 198,318	27,896	134,201	- 11,893	-9%	0	2
90	199,383	- 51,276	95,817	66,461	55,781	84%	10	1
91	-	22,982	49,200	-	1,580	0%	n/a	n/a
92	29,890	- 5,997	19,310	9,963	- 3,842	-39%	n/a	n/a
93	139,215	- 16,001	106,785	46,405	- 14,157	-31%	0	0
94	103,969	131,120	301,931	34,656	37,713	109%	1	1
95	150,740	42,671	205,960	50,247	32,792	65%	1	1
96	308,746	- 63,603	109,454	102,915	38,801	38%	10	1
97	352,923	- 122,352	89,877	117,641	30,931	26%	0	1
98	373,157	- 166,818	- 28,757	124,386	13,188	11%	0	10
99	357,081	- 271,313	- 234,081	119,027	- 11,105	-9%	n/a	n/a
100	19,851	37,363	127,749	6,617	2,885	44%	n/a	n/a
101	181,185	11,511	89,415	60,395	14,590	24%	1	1
102	238,942	- 56,549	68,558	79,647	7,773	10%	10	1
103	334,124	- 114,588	96,376	111,375	29,903	27%	0	1
104	407,799	- 240,174	- 112,599	135,933	- 5,852	-4%	0	20
105	-	10,643	12,300	-	1,580	0%	n/a	n/a
106	11,475	9,704	50,025	3,825	4,066	106%	n/a	n/a
107	128,998	- 6,069	55,502	42,999	16,046	37%	10	1
108	390,235	- 206,735	- 95,035	130,078	- 37,592	-29%	0	30
109	191,974	- 160,045	- 118,174	63,991	- 18,194	-28%	n/a	n/a
110	-	8,304	24,600	-	1,580	0%	n/a	n/a

(\*) 1 = Supplier, very high; 2 = Supplier, high; 3 = Supplier, medium  
10 = Receiver, very high; 20 = Receiver, high; 30 = Receiver, medium  
n/a = grid cell mostly outside of boundary, not considered as sub-area